A NOVEL MECHANISM FOR SWITCHING A NEURAL SYSTEM FROM ONE STATE TO ANOTHER

A Dissertation

Presented to the Faculty of the Graduate School

of Cornell University

in Partial Fulfillment of the Requirements for the Degree of

Doctor of Philosophy

by

Chethan Pandarinath

January 2011

A NOVEL MECHANISM FOR SWITCHING A NEURAL SYSTEM FROM ONE STATE TO ANOTHER

Chethan Pandarinath, Ph.D.

Cornell University 2011

The ability to adjust to changing conditions is critical to the functioning of any sensory system. The vertebrate visual system, for example, is well-known for its flexibility – as an animal moves between different environments, the visual system adjusts its processing to match the changing conditions. Though these adjustments have been recognized for years, the mechanisms that underlie them have been unclear. Here we describe a case in which the mechanism could be determined. We investigate a well-known set of adjustments – the adjustments in spatial and temporal processing that accompany the shift from day to night vision. Our findings reveal a novel mechanism in the retina that underlies the adjustment of temporal processing, which may generalize to other networks as well. Further, characterizing these adjustments reveals a previously unknown divergence in the retina's parallel pathways, one that has functional relevance to natural vision.

BIOGRAPHICAL SKETCH

Chethan Pandarinath was born and raised in Roanoke Rapids, North Carolina, where his parents lived for 30 years. He left home at the age of 14 to attend the North Carolina School of Science and Mathematics, where he was surrounded by enthusiastic teachers and talented students with a thirst for knowledge, which cemented his interest in science and engineering. He then attended North Carolina State University, where he was given the freedom to pursue his diverse interests, from electrical and computer engineering, to physics, to the interaction of science, technology, and public policy.

He joined Cornell University in Fall 2003 to pursue a Ph.D. in Electrical and Computer Engineering. While there he became fascinated by the nervous system, which seemed to him far more versatile, complex, and unexplored than any man-made system. He also recognized that several aspects of the nervous system were based around well-known electrical engineering principles, and realized the great potential in understanding this system, that it holds therapeutic promise for many people. He was fortunate enough to get the opportunity to move to Cornell's Weill Medical College campus, where he was able to apply his knowledge of electrical engineering to the study of the nervous system in depth.

To my parents, for their constant love, support, and encouragement.

ACKNOWLEDGEMENTS

First I would like to thank my adviser, Sheila Nirenberg, who has had an immense influence on my scientific career. I am indebted to her for many reasons, but especially for her guidance in demonstrating how problems can be broken down, how science can be effectively communicated, and the importance of focusing on questions with broad impact. I have been constantly amazed and inspired by her tenacity, attention to detail, and ability to think deeply on a broad range of scientific topics, spanning many disciplines.

I sincerely appreciate the contributions of several professors at Cornell and at Weill. I thank Jonathan Victor for his help and advice on several aspects of our collaborative projects. I also thank Bruce Land for his instruction and mentorship during my time in Ithaca, and credit him for sparking my interest in embedded systems.

I appreciate the support of the members of my committee, especially Tony Reeves, for encouraging me to pursue a cross-disciplinary research topic, and for helping me navigate the hurdles involved.

I owe many fellow graduate students for making the whole experience much more enjoyable. There are far too many to name, but I need to especially thank Milind, Eric, Ganesh, Kamal, Gus, Sandeep, Ankit, Naola, Sarah, and Illya. I appreciate the counsel, support, and friendship I've enjoyed from Ben, Alex, and Ashwin. I also appreciate the discussions with and help I've received from my labmates, especially Tanya, Zack, and Jason.

Most importantly, I thank my family, whose unrelenting support and encouragement provide constant motivation and inspiration. My parents have always been exceptional role models. They have taught me the value of education and determination. I especially thank them for impressing on me the importance of putting others before one's self. I will be satisfied if I can become one-tenth as good of a human being as either of them. My brother has also been a huge positive influence in my life, more than I ever give him credit for, and I really appreciate his constant guidance. And of course, I am forever indebted to Tara, whose continual support has allowed me to believe in myself when I couldn't find any reason to. She has helped me through challenge after challenge, always providing love and encouragement. Her kindness and generosity is always an inspiration, and I love her deeply.

TABLE OF CONTENTS

Biographical Sketch iii
Dedication iv
Acknowledgements v
Table of Contents vi
List of Figures vii

1 Introduction.....1

1.1 The adjustment of spatial integration to day and night conditions 2

1.2 Coupling as a mechanism to turn a cell class on or off.....4

1.3 The interaction between the adjustment of temporal processing and the retina's parallel pathways.....5

2 Ganglion cell adaptability: Does the coupling of horizontal cells play a role?.....7

2.1 Introduction 8

2.2 Results 10

2.2.1 Ganglion cells from wild-type and Cx57-deficient mice showed the same shift in spatial tuning 11

2.2.2 Ganglion cells from wild-type and Cx57-deficient mice had the same surround size.....16

2.2.3 Spatial tuning was similar in behaving wild-type and Cx57-deficient mice.....18

2.2.4 Verification with dopamine 21

2.2.5 Blocking the feedback from horizontal cells to photoreceptors altered spatial tuning 23

2.3 Discussion.....25
2.4 Materials and Methods.....30
2.4.1 Animals.....30
2.4.2 Extracellular recordings of ganglion cell responses.....30
2.4.3 Light stimulation.....31
2.4.4 Pharmacology.....32
2.4.5 Data analysis.....33
2.4.6 Behavioral tests using a virtual optokinetic system, light intensities35
2.5 Acknowledgements.....37
3 A novel mechanism for switching a neural system from one state to another.....50
3.1. Introduction.....51
3.2. Results.....53
3.3. Discussion.....62
3.3.1 Estimating the extent to which input resistance can be reduced by coupling.....65
3.3.2 Linking a behavior to a neural mechanism.....68
3.3.3 Potential alternative models for the shift toward low temporal frequencies.....68
3.3.4 Relation of Cx57 to spatial processing in the dark- and light-adapted conditions.....71
3.3.5 Coupling as a mechanism to produce synchrony.....72
3.4. Methods.....73
3.4.1 Animals.....73

3.4.2 The degree of horizontal cell coupling and light intensity 73
3.4.3 The relation of horizontal cell input resistance to coupling for scotopic versus photopic conditions and for wild type versus knockout animals. 74
3.4.4 Behavioral testing using a virtual optokinetic system 76
3.4.5 Stimulating and recording ganglion cell responses 77
3.4.6 Data Analysis 78
3.4.7 Filtered predator movies.....80
3.5 Acknowledgements.....80
4 Symmetry breakdown in the ON and OFF pathways of the retina at night: functional implications 112
4.1 Introduction 113
4.2 Materials & Methods 115
4.2.1 Experiments 115
4.2.2 Data Analysis 117
4.2.3 Animals.....120
4.3 Results 121
4.4 Discussion.....135
4.4.1 Functional implications of the differences in visual processing 137
4.4.2 Relating the differential filtering properties of ON and OFF ganglion cells to retinal circuitry 140
4.5 Acknowledgements.....141

LIST OF FIGURES

Figure 2.1 Dye coupling was abolished in Cx57-deficient mice. 11
Figure 2.2 Ganglion cells from wild-type and Cx57-deficient mice showed the same shift in spatial tuning. 13
Figure 2.3 The distributions of surround sizes were the same for both genotypes. 17
Figure 2.4 Visual performance, measured as contrast sensitivity, was the same for both genotypes. 20
Figure 2.5 The shift produced by dopamine was the same for both genotypes. 22
Figure 2.6 The shift produced by cobalt was the same for both genotypes. ...24
Figure 2.7 Quality of Difference of Gaussians fits 38
Figure 2.8 Shifts in spatial tuning following dopamine and cobalt application, presented as average tuning curves. 39
Figure 2.9 Horizontal cell length constants in the Cx57-deficient mice are significantly reduced. 40

Figure 3.1 The visual system undergoes a shift in integration time as it shifts from daylight to nightlight (photopic to scotopic) conditions. 54
Figure 3.2 The circuit that controls visual integration time can be shifted from one state to another by a change in the gap junction coupling of one of its cell classes. 56

Figure 3.3 When horizontal cell coupling is prevented, the shift to long integration times is impaired at both the behavioral level and the ganglion cell level. 60
Figure 3.4 The selective disadvantage of a Cx57 gene loss. 66
Figure 3.5 The frequency response difference between the rods and cones lies in the high frequencies, not the low. 81
Figure 3.6 Measured photoreceptor responses at increasing levels of light adaptation. 85
Figure 3.7 Modeled photoreceptor responses at increasing levels of light adaptation. 88
Figure 3.8 Modeled ganglion cell responses at increasing levels of light adaptation. 91
Figure 3.9 The visual system undergoes a shift in integration time as it shifts from day to night (photopic to scotopic) conditions. 102
Figure 3.10 The circuit that controls visual integration time can be shifted from one state to another by a change in the gap junction coupling of one of its cell classes. 103
Figure 3.11 When coupling is prevented, the shift to long integration times is impaired at both the behavioral level and the ganglion cell level. 104

Figure 4.1 ON and OFF cells show similar temporal frequency tuning in response to sine wave gratings under photopic conditions. 122
Figure 4.2 Frequency tuning of ON and OFF cells diverges under scotopic conditions. 124

Figure 4.3 ON and OFF cells show similar temporal response properties to white noise under photopic conditions. 126
Figure 4.4 The divergence under scotopic conditions was also observed for the white noise stimulus. 127
Figure 4.5 Under photopic conditions, it is possible to decode across the entire range of temporal frequencies using responses of ON or OFF cells. 130
Figure 4.6 Under scotopic conditions, there is a divergence in performance – ON cells perform better at low frequencies, while OFF cells perform better at high.....132
Figure 4.7 At low light levels, increments become harder to discriminate than decrements of equal magnitude, due to asymmetries in the Poisson distribution. 134
Figure 4.8 Decrements can be detected more readily than increments, and the asymmetry is an accelerating function of contrast. 146
Figure 4.9 All individual ON cell grating responses, tuning curves, and confusion matrices for both light conditions. 148
Figure 4.10 All individual OFF cell grating responses, tuning curves, and confusion matrices for both light conditions. 150
Figure 4.11 Responses in the scotopic condition are driven by the rod bipolar pathway. 153
Figure 4.12 Recovery of responses in the photopic condition was specific to OFF responses.....154

CHAPTER 1

Introduction

A fundamental property of the nervous system is its ability to adjust to different conditions. As an animal moves from one environment to another, the system adjusts itself to accommodate these new conditions. E.g., as it moves into an environment with new stimuli, it shifts its attention; if the stimuli are low contrast, it adjusts its contrast sensitivity; if the signal-to-noise ratio is low, it changes its spatial and temporal integration properties. These adjustments have been well described at the behavioral level – and are clearly critical to our functioning – but how the brain makes these adjustments has yet to be determined.

Here we study the ability of the nervous system to adjust, using the mammalian visual system as our model. We investigate a well-known set of adjustments that occur in visual processing – the changes in spatial and temporal processing that accompany the shift from bright to dark environments, such as the shift from day to night. These adjustments serve presumably to optimize information transmission in each condition: during the day, photons are abundant, and the visual system is a powerful spatial and temporal pattern analyzer; at night, however, photons become limiting, which causes signal to noise ratios to decrease. The system compensates for this decrease by adjusting its spatial and temporal integration properties. It integrates its input over a larger area – both in space, and in time – to allow the transmission of a more reliable signal.

How the visual system performs these adjustments has remained unclear. A large body of evidence, though, points to the retina as the starting point, since the changes are detectable at the level of the retinal ganglion cells (RGCs), the output cells of the retina. What remain to be determined are the mechanisms that allow the retina to have this flexibility.

1.1 The adjustment of spatial integration to day and night conditions

In the first study, presented in Ch. 2, we probe the mechanisms underlying the adjustment of spatial integration to day and night. The extent of a ganglion cell's spatial integration is dependent on its receptive field organization. Most ganglion cell receptive fields consist of two components: a center and a surround, which respond oppositely to light. These components involve multiple mechanisms. The center response is thought to result from signaling from photoreceptors to bipolar cells to ganglion cells. The origin of the surround response, however, is more controversial. Early reports suggested that it was generated in the outer retina, by horizontal cells (HCs). More recently, studies have indicated that mechanisms in the inner retina also contribute – namely, mechanisms involving amacrine cells. The relative contribution of these two cell types to the ganglion cell's receptive field surround – and their involvement in the adjustment of spatial integration between day and night conditions – remains unclear.

Here we test a long-standing hypothesis: that the adjustment to day and night is mediated by changes at the level of horizontal cells, specifically, changes in coupling among these cells. Horizontal cells are coupled by gap

junctions, and it's well-known that this coupling is light dependent. When light levels are high (e.g. during the day), the gap junctions close, and there is little coupling. When light levels are low (e.g. at night), the gap junctions open, and the cells become strongly coupled. Since horizontal cells are known to contribute to the ganglion cell's surround, the hypothesis is that the change in HC coupling between day and night causes a change in the ganglion cell's surround, thereby adjusting spatial integration between the two conditions.

To test whether the changes in coupling play a role, we use a transgenic mouse line in which HC coupling was abolished – these mice lack the gap-junction protein responsible for HC coupling. If coupling were the dominant mechanism for the adjustment of spatial integration, then mice lacking coupling should be unable to adjust with the shift from day to night conditions. We compare spatial integration under these conditions between normal and transgenic mice, both at the level of the mouse's behavior (using visual psychometric measurements in an optomotor task), and at the level of the retina's output (using extracellular recordings from retinal ganglion cells). Our measurements show that mice lacking HC coupling make the same adjustment of spatial integration as normal mice. These results demonstrate that the coupling and uncoupling of horizontal cells does not play a dominant role in the adjustment of spatial integration between day and night.

At first glance, it might seem surprising that preventing changes in horizontal cell coupling – which affects lateral signaling in the retina – has no effect on ganglion cell spatial integration. However, what these results suggest is that inner retinal circuits dominate, at least for the problem of adjusting

spatial integration to day and night conditions. Whatever spatial effects occur when the horizontal cells change from the coupled to the uncoupled state are effectively swamped by stronger circuit actions that occur in the inner retina.

1.2 Coupling as a mechanism to turn a cell class on or off

The results of Ch. 2 indicate that the changes in horizontal cell coupling are not critical for the adjustment of spatial processing. This raises the intriguing question of what function the changes in coupling actually serve. One possibility is that they act as a means to adjust temporal integration, rather than spatial integration.

This hypothesis is the subject of the second study, presented in Ch. 3. We test whether the changes in HC coupling between day and night serve to shift the visual system toward longer integration times. The proposal is as follows: as discussed previously, during the day, the gap junctions between HCs are closed, and there is little coupling. At night, the gap junctions open, and extensive coupling ensues. Since coupling shunts incoming current, the idea is that the extensive coupling causes a strong shunting of horizontal cell current, effectively silencing the HCs. Because horizontal cells play a key role in shaping the integration of visual signals – they provide negative feedback to photoreceptors, which cuts the photoreceptor's integration time short – the hypothesis is that silencing these cells makes integration time longer.

This proposal suggests a novel mechanism for allowing a neural network to adjust its processing – that a network can be shifted from one state to another by a change in the gap junction coupling of one of its cell classes.

The change in coupling provides a means to raise or lower the activity of the cell class, and thereby change the network's behavior. Since gap-junction coupled networks are present throughout the brain, this mechanism has the potential to underlie other behavioral adjustments as well.

To test this hypothesis, we again use the transgenic mouse line in which HC coupling has been abolished. If the hypothesis is correct, then mice lacking coupling should be unable to shift to long integration times in the night condition. Our results show that the hypothesis held: in the transgenic mice, the shift to long integration times was blocked completely at the behavioral level, and almost completely at the ganglion cell level. These results demonstrate a new, simple, and potentially generalizable mechanism for how networks can rapidly adjust themselves to changing environmental demands.

1.3 The interaction between the adjustment of temporal processing and the retina's parallel pathways

In Chapters 2 and 3, we probe the mechanisms that give the retina the flexibility to adjust its processing. Finally, in Ch. 4, we investigate how the adjustment of processing affects the information ultimately conveyed by the retina. Specifically, we study the interaction between the adjustment of temporal processing and the retina's parallel information channels.

Information is conveyed by the retina through multiple parallel channels, and we focus on one of the most well-known examples: the ON and OFF pathways. Most retinal ganglion cells can be divided into these two broad classes: ON cells, which respond to increments of light, and OFF cells, which

respond to decrements. Traditionally, these cell classes have been thought of as “equal and opposite,” that is, they respond to the same features of the visual scene, just with opposite polarity. Recent studies have shown, however, that the two pathways carry at least partially different information, but the functional significance of these differences for visual processing is not well understood.

Here we show that, surprisingly, ON and OFF cells show a substantial difference in the adjustment of temporal processing to day and night conditions, and that this difference confers a functional advantage. First we characterize their temporal responses under daylight conditions, and find that the two classes are largely symmetric – that is, their responses differ in sign, but their temporal characteristics are similar. However, at night, we find that the two classes diverge – ON cells signal better to low temporal frequencies, while OFF cells signal better to high. We then demonstrate that this divergence corresponds to an asymmetry in the physical world, one produced by the Poisson nature of photon capture. At low light levels, the limits placed by quantal fluctuations affect increments and decrements in an asymmetric manner – increments become more difficult to detect than decrements of equal magnitude. Thus, in order to send a reliable signal in the dark, ON cells must integrate their input over a longer period of time than OFF cells, consistent with the observation that ON cells selectively shift toward low temporal frequencies. These results show a novel divergence in the retina’s parallel pathways, and describe its potential value for processing visual information.

CHAPTER 2

Ganglion cell adaptability: Does the coupling of horizontal cells play a role?

Karin Dedek[1], Chethan Pandarinath[2], Nazia M. Alam[3], Kerstin Wellershaus[4], Timm Schubert[1], Klaus Willecke[4], Glen T. Prusky[3], Reto Weiler[1], and Sheila Nirenberg[2]

[1] Dept. of Neurobiology, University of Oldenburg, D-26111 Oldenburg, Germany

[2] Dept. of Physiology and Biophysics, Weill Medical College of Cornell University, New York, New York 10021, United States of America

[3] Canadian Centre for Behavioural Neuroscience, The University of Lethbridge, Lethbridge, Alberta, Canada

[4] Institute of Genetics, University of Bonn, D-53117 Bonn, Germany

Abstract

Background. The visual system can adjust itself to different visual environments. One of the most well known examples of this is the shift in spatial tuning that occurs in retinal ganglion cells with the change from night to day vision. This shift is thought to be produced by a change in the ganglion cell receptive field surround, mediated by a decrease in the coupling of horizontal cells. *Methodology / Principal Findings.* To test this hypothesis, we used a transgenic mouse line, a connexin57-deficient line, in which horizontal

cell coupling was abolished. Measurements, both at the ganglion cell level and the level of behavioral performance, showed no differences between wild-type retinas and retinas with decoupled horizontal cells from connexin57-deficient mice. *Conclusion / Significance.* This analysis showed that the coupling and uncoupling of horizontal cells does not play a dominant role in spatial tuning and its adjustability to night and day light conditions. Instead, our data suggest that another mechanism, likely arising in the inner retina, must be responsible.

2.1 Introduction

Spatial tuning is a fundamental feature of retinal ganglion cells. It allows the detection of spatial patterns on multiple scales (Enroth-Cugell and Robson, 1966). Some cells, for example, are tuned to low spatial frequencies and allow the detection of large spatial patterns. Others are tuned to high spatial frequencies and permit the resolution of fine details (reviewed in (Shapley and Lennie, 1985)).

A ganglion cell's sensitivity to spatial patterns is a function of its receptive field organization. Most ganglion cell receptive fields consist of two components, a center and a surround that respond oppositely to light (Barlow, 1953; Kuffler, 1953). What tunes a ganglion cell to a particular spatial scale are the sizes of these two components and their relative strengths (Shapley and Lennie, 1985; Rodieck and Stone, 1965; Sinclair et al., 2004).

Though the organization of the ganglion cell receptive field has been known for decades, the mechanisms that generate it are not completely understood. The center response is thought to result from vertical signaling

from photoreceptors to bipolar cells to ganglion cells. The origin of the surround response, however, is controversial. Early reports suggested that it was generated by horizontal cells (Werblin and Dowling, 1969; Kaneko, 1970) which appear to act through two pathways: feedback inhibition to photoreceptors (Naka and Witkovsky, 1972; Mangel, 1991) and feedforward inhibition to bipolar cells (Yang and Wu, 1991; Fahey and Burkhardt, 2003). More recent studies, however, indicate a contribution from amacrine cells (Sinclair et al., 2004; Cook and McReynolds, 1998; Bieda and Copenhagen, 1999; Taylor 1999; Flores et al., 2001) which also employ two distinct pathways: direct input to ganglion cells (Cook and McReynolds, 1998; Bieda and Copenhagen, 1999; Flores et al., 2001) and feedback signaling onto bipolar cell terminals (Flores et al., 2001). The relative contributions of these four different surround-generating mechanisms are unclear and remain a subject of much discussion (Sinclair et al., 2004; Cook and McReynolds, 1998; Taylor 1999; Flores et al., 2001; Roska et al., 2000).

A key aspect of the discussion concerns one of the most intriguing features of spatial tuning – its adjustability. It is well known that the spatial tuning can adjust itself in the face of different visual environments (Barlow et al., 1957; Smirnakis et al., 1997). The most well known example is the shift in tuning that occurs when the retina moves from the dark-adapted to the light-adapted state (from night to day vision) (Barlow et al., 1957; Enroth-Cugell and Shapley, 1973; Maffei et al., 1971; Smith 1973). It has long been proposed that this shift is caused by a change in the ganglion cell receptive field surround, mediated by a change in the coupling of horizontal cells (Mangel

and Dowling, 1985). This conjecture arose because this coupling is known to vary with ambient light intensity (Baldridge and Ball, 1991; Tornqvist et al., 1988; Xin and Bloomfield, 1999).

To test this hypothesis, we used a transgenic mouse line, a Connexin57-deficient line, in which horizontal cell coupling is more than 99% abolished, as measured by dye-transfer (Fig. 2.1; (Hombach et al., 2004; Shelley et al., 2006)). *Connexin57* (*Cx57*), a gene that encodes a gap junction protein, is exclusively expressed in retinal horizontal cells, so no other cell classes are affected (Hombach et al., 2004), making this mouse line a powerful model to very selectively address this question.

The results showed that the coupling and uncoupling of horizontal cells does not play a critical role in spatial tuning, that is, it does not substantially contribute to the mechanism that controls the changes in spatial tuning that occur with the switch from night to day vision. We tested this both at the level of ganglion cell performance, using spatial tuning curves and center-surround measurements, and at the level of behavioral performance, using visual psychometric measurements. This analysis provides strong evidence that another mechanism has to be responsible.

2.2 Results

Our aim was to test the hypothesis that changes in horizontal cell coupling play a role in ganglion cell spatial tuning, in particular, in the shift in tuning that occurs when animals move from daytime to nighttime viewing conditions. For that purpose we used a Cx57-deficient mouse line, generated in a C57BL/6

background, and compared it to wild-type C57BL/6 mice, in which horizontal cell coupling was unperturbed (Fig. 2.1). In both mouse lines, spatial tuning and its adjustability were evaluated at the ganglion cell level and the level of behavioral performance.

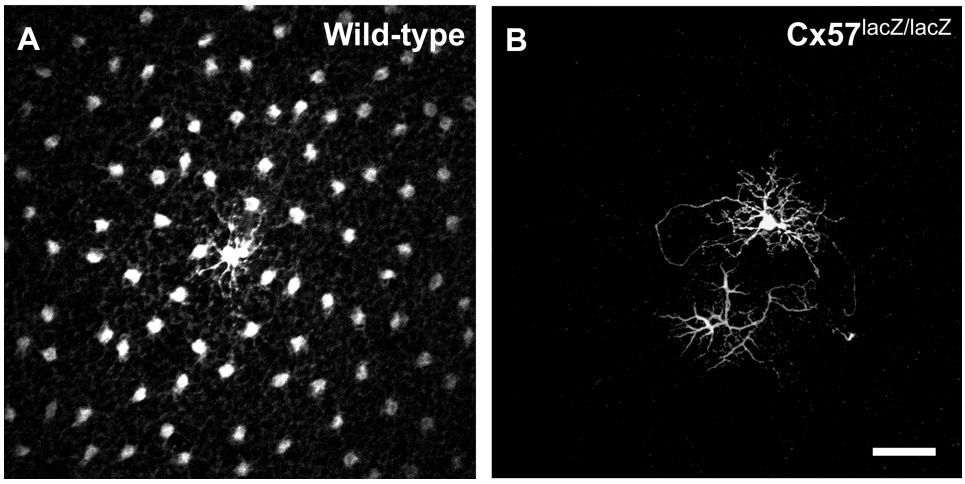

Figure 2.1 Dye coupling was abolished in Cx57-deficient mice.

(**A**) Neurobiotin-injected horizontal cells from wild-type mice showed extensive coupling. Note that coupling extended beyond the borders of the image. In total, 182 horizontal cells were coupled to this cell. (**B**) Horizontal cell from a Cx57-deficient mouse, injected under the same conditions. Coupling was abolished in these mice. Similar results have been shown before (Hombach et al., 2004; Shelley et al., 2006). Scale bar, 50 μm.

2.2.1 Ganglion cells from wild-type and Cx57-deficient mice showed the same shift in spatial tuning

To evaluate ganglion cell spatial tuning, standard methods were used (Enroth-Cugell and Robson, 1966; Sinclair et al., 2004; Campbell and Robson, 1968; Stone and Pinto, 1993). Briefly, drifting sine wave gratings of different spatial frequencies were projected onto the retina, and ganglion cell responses were recorded extracellularly. A spatial tuning curve for each cell was then generated by Fourier analyzing the responses and plotting the amplitude of the fundamental as a function of spatial frequency. To assess the adjustability of spatial tuning, the gratings were presented at two different light intensities, one scotopic, one photopic (see *Methods* for intensities).

Consistent with studies performed in other species (Enroth-Cugell and Robson, 1966; Bisti et al., 1977; Muller and Dacheux, 1997), wild-type mouse retinal ganglion cells showed a shift in spatial tuning when the light level was changed from scotopic to photopic. Specifically, the weight of the ganglion cells' tuning curves shifted from low toward higher spatial frequencies. Representative examples are shown in Fig. 2.2A; Fig. 2.2B shows the mean for all 196 cells in the dataset.

Figure 2.2 Ganglion cells from wild-type and Cx57-deficient mice showed the same shift in spatial tuning.

(**A**, **D**) Representative ganglion cell responses from wild-type (**A**) and Cx57-deficient (**D**) mice to drifting sine wave gratings presented at two different light intensities: scotopic, grey, and photopic, blue. See *Methods*, for light intensities, expressed in both $\mu W/cm^2$ and photoisomerizations. Responses were normalized to the maximum firing rate. Each cell's tuning curve is presented at the right. (**B**, **E**) Average tuning curves (mean ± SEM) for all cells from wild-type (**B**) and Cx57-deficient (**E**) retinas, measured at the scotopic (grey) and the photopic (blue) light intensities. (**C**, **F**) Distribution of the center of mass values for all cells from wild-type (**C**) and Cx57-deficient (**F**) retinas measured at the scotopic (grey) and the photopic (blue) light intensities. No significant difference was observed between the two genotypes for the scotopic condition ($p > 0.35$, $n = 196$ cells for wild-type, $n = 161$ for Cx57-deficient, *KS* test) or the photopic condition ($p > 0.18$, $n = 196$ for wild-type, $n = 161$ for Cx57-deficient, *KS* test).

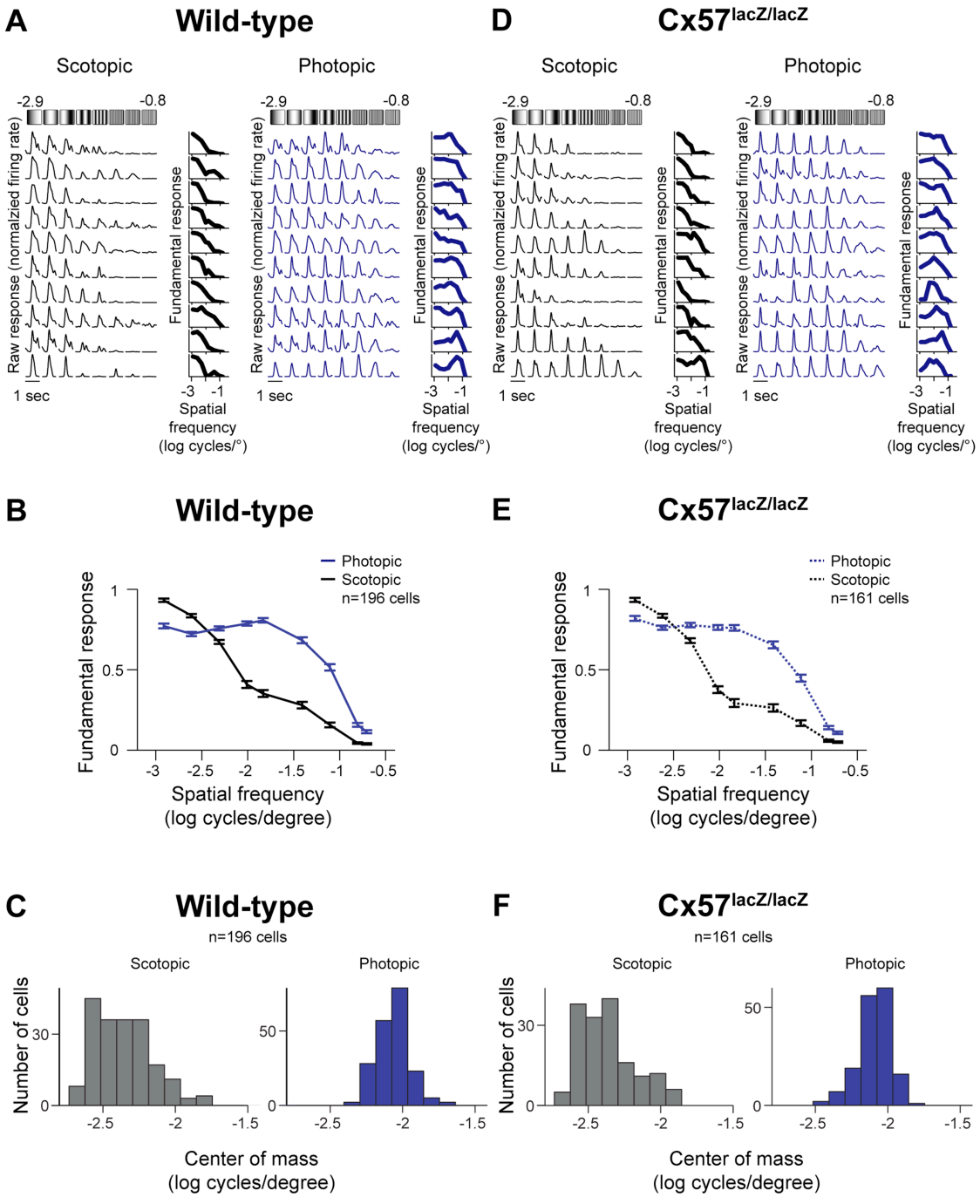
A
Wild-type
Scotopic
Photopic
-2.9
-0.8
Raw response (normalzied firing rate)
Fundamental response
1 sec
-3
-1
Spatial frequency (log cycles/°)
D
Cx57lacZ/lacZ
B
Wild-type
Photopic
Scotopic
n=196 cells
Fundamental response
Spatial frequency (log cycles/degree)
E
Cx57lacZ/lacZ
n=161 cells
C
Wild-type
n=196 cells
Number of cells
Center of mass (log cycles/degree)
F
Cx57lacZ/lacZ
n=161 cells

To quantify the shift, a center of mass analysis was performed, following (Sinclair et al., 2004). At each light level, the center of mass of each tuning curve was calculated, and the distribution of center of mass values was plotted (Fig. 2.2C). This analysis showed a very statistically significant difference between the two distributions [$p < 10^{-4}$, *Kolmogorov-Smirnov (KS)* test]; the mean center of mass value for the photopic condition was nearly twice the spatial frequency of the mean center of mass value for the scotopic condition.

To test whether changes in horizontal cell coupling play a role in mediating this shift, we compared the tuning curves produced by Cx57-deficient retinas, that is, retinas in which the horizontal cell coupling was reduced by > 99%, with those from the normal, wild-type retinas. If changes in the coupling play a role, then there should be no shift in the Cx57-deficient retinas. The results showed that this was not the case. Just as in the wild-type retinas, the tuning curves from the Cx57-deficient mice were weighted towards low spatial frequencies in the scotopic light condition and toward high spatial frequencies in the photopic light condition. Representative examples are shown in Fig. 2.2D; for each cell, the left column shows the tuning curve at the scotopic light level and the right column shows the tuning curve for the same cell at the photopic light level. Fig. 2.2E shows the mean tuning curves for all 161 cells in the dataset. When the shift was quantified using the center of mass analysis (Fig. 2.2F), the results showed no significant difference between the tuning curves from the Cx57-deficient and normal, wild-type retinas ($p > 0.35$, *KS* test, comparing the distribution of center of mass values

from the Cx57-deficient retinas taken at the scotopic light level with the same from the wild-type retinas, and $p > 0.18$, comparing the distribution of center of mass values from the Cx57-deficient retinas taken at the photopic light level with the same from the wild-type retinas).

In summary, these results show that retinas with coupled and uncoupled horizontal cell networks undergo the same shift in spatial tuning when light levels change from scotopic to photopic conditions.

2.2.2 Ganglion cells from wild-type and Cx57-deficient mice had the same surround size

The center of mass analysis shows that the spatial tuning curves undergo a shift with the change in light intensity, but it does not show where in the curves the shift occurs. Because the shift could be caused by any change in the center/surround organization of the ganglion cell receptive field (Shapley and Lennie, 1985; Rodieck, 1965; Sinclair and Nirenberg, 2001), we tested specifically whether it was due to a change in the surround, as expected from previous studies in other species (Barlow et al., 1957; Muller and Dacheux, 1997). To test this, we fit the tuning curves to a standard receptive field model, a difference of Gaussians model (Sinclair et al., 2004; Enroth-Cugell et al., 1983), and measured surround size. Consistent with the studies in other species (Barlow et al., 1957; Muller and Dacheux, 1997), the receptive fields showed no surrounds at the scotopic light level (> 80% of cells were better fit by a single Gaussian, see Materials and Methods), but gained surrounds in photopic light with a mean surround size of 972 ± 78 μm (n = 147) (Fig. 2.3A).

Thus in the wild type, the observed shift in the spatial tuning curves upon light intensity increase was accompanied by a gain of surround (see (Rodieck, 1965; Croner and Kaplan, 1995) for detailed quantitative analysis of how center and surround parameters affect spatial tuning curves; for further discussion, see (Sinclair et al., 2004)).

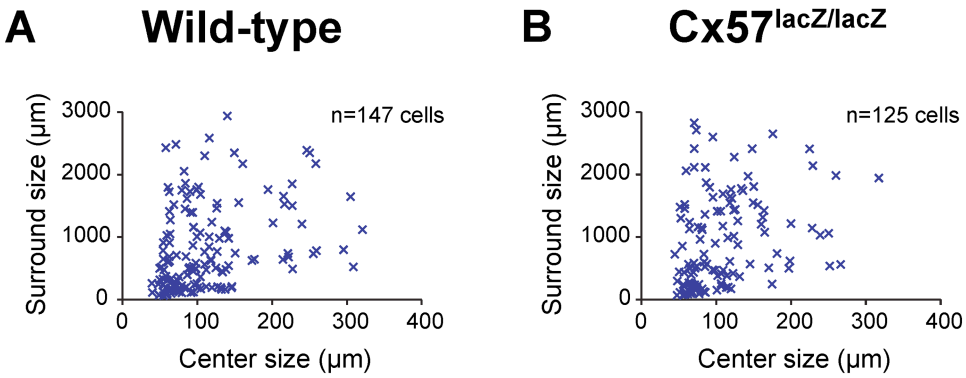

Figure 2.3 The distributions of surround sizes were the same for both genotypes.

Ganglion cells from (**A**) wild-type and (**B**) Cx57-deficient mice ($p > 0.64$, $n = 147$ for wild-type, $n = 125$ for Cx57-deficient, *t*-test) had the same surround sizes [measured only at the photopic level, as there is little or no surround at the scotopic level for both genotypes (see text and *Methods*)].

To test whether changes in the coupling of horizontal cells play a critical role in mediating this gain, we compared ganglion cell surround sizes from Cx57-deficient retinas with those from wild-type retinas. If changes in the coupling play a strong role, then surround sizes should be different in the two

genotypes. Our results indicate that this was not the case. As in the wild-type retinas, ganglion cells from the Cx57-deficient retinas showed no surrounds at the scotopic light level and gained surrounds in photopic light (Fig. 2.3B), and there was no significant difference in the surround size (mean surround size in the Cx57-deficient retinas was 1022 ± 76 μm, $n = 125$, compared to 972 ± 78 μm, $n = 147$ in the wild-type retina, $p > 0.64$, *t*-test).

In sum, ganglion cells from wild-type mice showed a shift in the weight of the spatial tuning curves when the ambient light was increased from scotopic to photopic levels. This shift was associated with a gain in surround size. Ganglion cells from Cx57-deficient mice showed essentially the same behavior (no statistically significant difference), providing further evidence that the coupling and uncoupling of horizontal cells is not the critical mechanism that underlies the change in spatial tuning that occurs with different light intensities.

2.2.3 Spatial tuning was similar in behaving wild-type and Cx57-deficient mice

To assess the role of horizontal cell coupling in spatial tuning on a larger scale, we compared the behavioral performance in spatial pattern detection for wild-type and Cx57-deficient mice using psychometric measurements. For this purpose we used a virtual optokinetic system that allowed a rapid analysis of visual thresholds in freely moving mice (Prusky et al., 2004; Douglas et al., 2005). Animals from both genotypes were presented with drifting sine wave gratings of decreasing contrast to determine contrast sensitivity at a given grating spatial frequency. Since the optokinetic task is not suitable to test

visual performance in the low spatial frequency range, only gratings that had a spatial frequency of at least 0.05 cycles/degree were presented.

As shown before in the mouse and other species (Bisti et al., 1977; Abdeljalil et al., 2005; Benedek et al., 2003), in wild-type mice, contrast sensitivity was lower under scotopic than under photopic conditions. At the higher light intensity, the mice needed less contrast to track the grating (Fig. 2.4A). If horizontal cell coupling does not control spatial tuning at the behavioral level, then performance on this task for the Cx57-deficient and wild-type mice should not differ. This was indeed the case (Fig. 2.4B). Performance was not significantly different between the wild-type and Cx57-deficient animals under both scotopic ($p > 0.5$, *t*-test, Bonferroni corrected) and photopic ($p > 0.1$, *t*-test, Bonferroni corrected) light conditions. Note that the behavioral measurements shown in Figure 2.4 are threshold measurements, rather than averages, following (Prusky et al., 2004; Douglas et al., 2005). With these measurements, animals are pushed to their best performance, which reduces animal-to-animal variability that arises from unrelated causes (e.g., differences in learning or inattention).

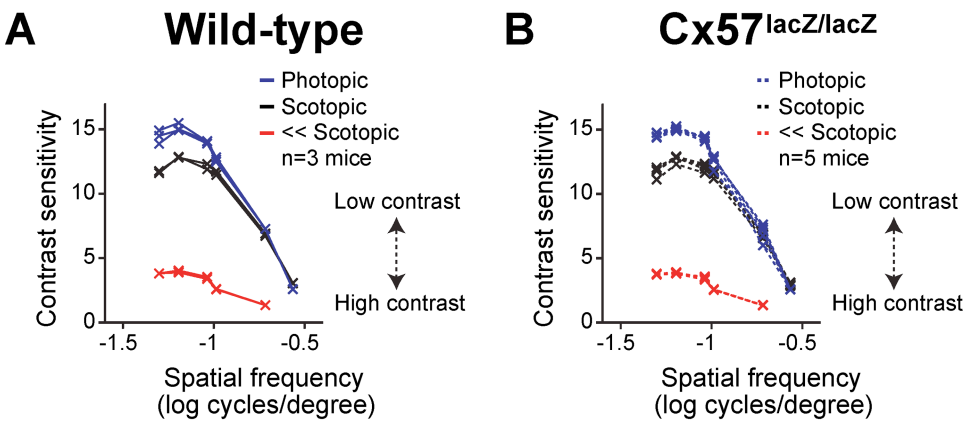

Figure 2.4 Visual performance, measured as contrast sensitivity, was the same for both genotypes.

For (**A**) wild-type and (**B**) Cx57-deficient mice, measurements were taken at three different light intensities: *blue*, photopic, *black*, scotopic, *red*, low scotopic; see *Methods* for all light intensities ($p > 0.25$, low scotopic: $p > 0.5$, scotopic: $p > 0.1$, photopic, *t*-test, Bonferroni corrected). Contrast sensitivity in all mice showed an increase in amplitude and a broadening of spatial frequency profile with increases in light intensity. Note that these are threshold measurements, rather than averages, as described in (Prusky et al., 2004; Douglas et al., 2005). With these measurements, animals are pushed to their best performance, which reduces animal-to-animal variability that arises from unrelated causes (e.g., differences in learning or inattention).

To push the system further, we repeated the psychometric measurements at a much lower light level (4.5 orders of magnitude lower; see *Methods* for all light intensities). At this intensity, contrast sensitivity was much

lower and had a smaller profile than at the intensities used before (Fig. 2.4A, red line). However, behavioral performance from mice lacking horizontal cell coupling was the same as in wild-type mice (Fig. 2.4A,B). Thus, at all the light intensities tested (again, see *Methods* for all intensities) contrast sensitivity between wild-type and Cx57-deficient mice was not significantly different ($p > 0.25$, *t*-test, Bonferroni corrected).

2.2.4 Verification with dopamine

To further assess the result that the coupling of horizontal cells does not play a strong role in ganglion cell spatial tuning, we perturbed horizontal cell networks with the neuromodulator dopamine. Dopamine has been shown to affect ganglion cell receptive fields and therefore the spatial tuning of ganglion cells (Jensen and Daw, 1984; Jensen and Daw, 1986) although there is some disagreement about this (Vigh and Witkovsky, 1999). The mechanism by which it acts is not known since dopamine operates at multiple sites within the retina, but the most widely hypothesized mechanism involves actions on the coupling and uncoupling of horizontal cells (Hampson et al., 1994; He et al., 2000; Teranishi et al., 1983). If dopamine's effects on ganglion cell spatial tuning are mediated through changes in horizontal cell coupling, then its actions should be different in Cx57-deficient versus wild-type mice. We tested this under photopic conditions (note that the coupling in wild-type retinas even under photopic conditions is still higher by a factor of at least 100 compared to the 99% abolished Cx57-knockout (Shelley et al., 2006)), and our results showed that this was not the case. Consistent with expectation (Shelley et al.,

2006; Witkovsky and Dearry, 1992; Wang and Mangel, 1996), dopamine (100 μM) applied to wild-type retinas produced a shift in the weight of the ganglion cell tuning curves toward higher spatial frequencies (Fig. 2.5A, $p < 0.0011$, *KS* test; data are also presented as average tuning curves in *Appendix* Fig. 2.8A). When the same concentration of dopamine was applied to Cx57-deficient mice, the same shift was observed (Fig. 2.5B), $p < 0.0016$, *KS* test). When the two shifts were compared, there was no statistically significant difference ($p > 0.77$, *KS* test). Since the shift in ganglion cell spatial tuning occurred in the Cx57-deficient mice, it has to be mediated by a process other than a change in horizontal cell coupling.

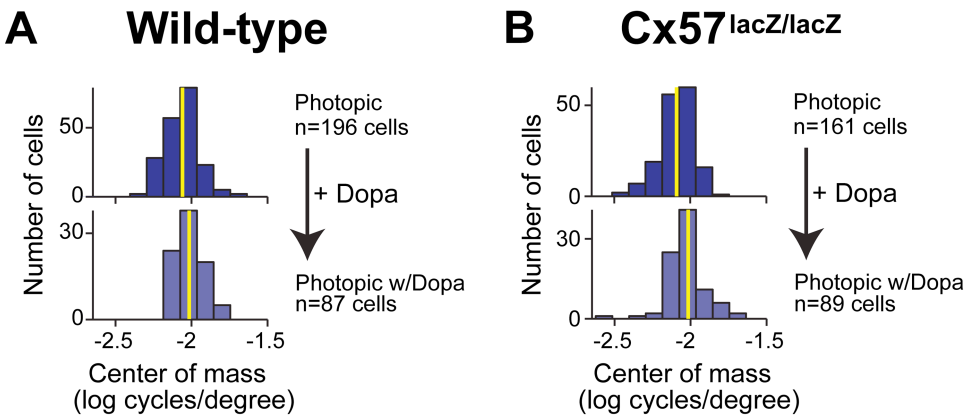

Figure 2.5 The shift produced by dopamine was the same for both genotypes.

For (**A**) wild-type and (**B**) Cx57-deficient retinas, the center of mass values showed a shift in tuning towards higher spatial frequencies with the addition of dopamine ($p < 0.0011$ for wild type, $n = 196$ control, $n = 87$ dopamine; $p < 0.0016$ for Cx57-deficient, $n = 161$ control, $n = 89$ dopamine, *KS* test*).*

Yellow lines indicate the mean of the distributions to clarify the shift. There were no significant differences between the two genotypes ($p > 0.16$ without dopamine, $n = 196$ wild-type, $n = 161$ Cx57-deficient; $p > 0.77$ with dopamine, $n = 87$ wild-type, $n = 89$ Cx57-deficient, *KS* test).

2.2.5 Blocking the feedback from horizontal cells to photoreceptors altered spatial tuning

Since our experiments did not show a role for the coupling of horizontal cells in ganglion cell spatial tuning and its adjustability, the question arises whether horizontal cells contribute to ganglion cell spatial tuning at all in the mouse. Horizontal cells provide negative feedback to cone photoreceptors (Wang and Mangel, 1996) which has been shown in other species to play a role in the organization of ganglion cell receptive fields (Mangel, 1991; Yang and Wu, 1991; Vigh and Witkovsky, 1999; McMahon et al., 2004; Xia and Nawy S, 2003). Feedback can be blocked with cobalt at submillimolar levels (100 μM). At this concentration, feedforward signaling from cones to horizontal cells is intact (Packer and Dacey, 2002), but negative feedback from horizontal cells to cones is attenuated (Vigh and Witkovsky, 1999; Kamermans et al., 2001). As with dopamine, we tested the effect of cobalt under photopic conditions. If horizontal cell feedback is involved in spatial tuning, then tuning should be shifted towards lower spatial frequencies in the presence of cobalt compared to control conditions. Indeed, this was the case (Fig. 2.6). As expected (Mangel, 1991), application of 100 μM cobalt to the wild-type retina led to a shift in spatial tuning towards lower spatial frequencies (Fig. 2.6A, $p < 2\text{x}10^{-5}$,

KS test (data are also presented as average tuning curves in *Appendix* Fig. 2.8b). In line with previous reports from other species (Vigh and Witkovsky, 1999; McMahon et al., 2004), this indicates that negative feedback from horizontal cells to photoreceptors contributes to the spatial tuning of ganglion cells. In Cx57-deficient mice, application of cobalt led to the same shift in spatial tuning (Fig. 2.6B, $p < 0.0019$, *KS* test) in a way that was not significantly different from its effect in wild-type mice ($p > 0.66$, *KS* test). This indicates that feedback was intact in Cx57-deficient mice.

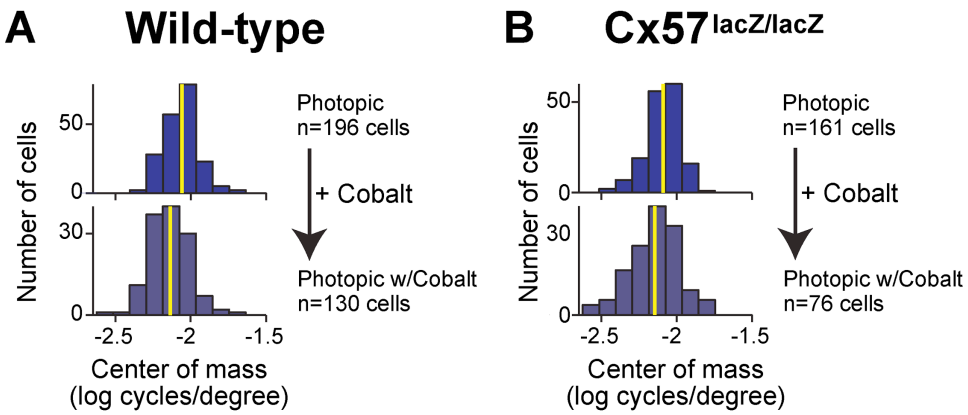

Figure 2.6 The shift produced by cobalt was the same for both genotypes.

For (**A**) wild-type and (**B**) Cx57-deficient retinas, the center of mass values showed a shift in tuning towards lower spatial frequencies with the addition of cobalt ($p < 2\text{x}10^{-5}$ for wild type, $n = 196$ control, $n = 130$ cobalt; $p < 0.0019$ for Cx57-deficient, $n = 161$ control, $n = 76$ cobalt, *KS* test*).* Yellow lines indicate the mean of the distributions to clarify the shift. There were no significant differences between genotypes ($p > 0.16$ without cobalt, $n = 196$ wild-type,

$n = 161$ Cx57-deficient; $p > 0.66$ with cobalt, $n = 130$ wild-type, $n = 76$ Cx57-deficient, *KS* test).

Note that, even when horizontal cell coupling was abolished and horizontal cell feedback was inhibited, spatial tuning under photopic conditions was shifted towards higher spatial frequencies than under scotopic conditions (compare Fig. 2.6B with Fig. 2.2F, $p < 10^{-4}$, *KS* test). This suggests that either cobalt does not completely block horizontal cell feedback in the mouse or that processes in the inner retina must be contributing to spatial tuning.

2.3 Discussion

Numerous studies have shown, at the behavioral level, that the visual system can adjust itself to different visual environments (Smith, 1973; Blakemore et al., 1969; Cavonius and Robbins, 1973; Greenlee et al., 1991). One of the most well known examples of this is the shift in spatial frequency sensitivity that occurs with the change from night (scotopic) to day (photopic) vision (Bisti et al., 1977; Benedek et al., 2003; DeValois and DeValois, 1990). This shift serves presumably as an information-optimizing strategy: at night, i.e., under photon-limited conditions, where the signal-to-noise ratio is low, the visual system is better served by integrating over a large area, so it shifts its tuning toward low spatial frequencies. During the day, when photons are not limiting, the system is better served by integrating over smaller areas, so it can resolve image details; in this case, the shift is toward high spatial frequencies (reviewed in (Atick and Redlich, 1992; van Hateren, 1992)).

How the visual system performs this shift is not clear. A large body of evidence, though, points to the retina as the starting point since the shift is detectable at the level of the ganglion cells (Barlow et al., 1957; Maffei et al., 1971; Muller and Dacheux, 1997). What remains to be determined is the mechanism that confers this on the cells. The most likely candidate is a change in the surround component of the ganglion cell's receptive field, as it is the surround that shapes the amplitude of the ganglion cell's response at low spatial frequencies. Changes in surround size cause the cell to shift its response toward or away from low spatial frequencies (see (Rodieck, 1965; Croner and Kaplan, 1995; Sinclair et al., 2004) for detailed quantitative analysis of how center and surround parameters affect the shape of the ganglion spatial tuning curve).

A long-standing proposal for how surround size might change with different light levels is that it might do so through a change in the gap junctional coupling of horizontal cells. The rationale for this hypothesis is that the extent of horizontal cell coupling is dependent on ambient light intensity (Baldridge and Ball, 1991; Tornqvist et al., 1988; Xin and Bloomfield, 1999). Thus, a change in horizontal cell coupling can serve as a natural knob for adjusting surround size and, therefore, the spatial tuning of the ganglion cells.

Here we tested this proposal. We used the mouse as a model system. We first measured ganglion cell spatial tuning at scotopic and photopic light levels in wild-type animals. As expected, the tuning shifted from low to high spatial frequencies as light intensities were increased from a lower to a higher level. We then measured the spatial tuning in Cx57-deficient mice in which

horizontal cell coupling was reduced by > 99%. If horizontal cell coupling plays a critical role in the adjustability of ganglion cell spatial tuning, then the shift from low to high spatial frequencies should be abolished. Our results indicated that it was not (Fig. 2.2). The shift from low to high spatial frequencies was essentially identical to that observed in wild-type mice. Direct measurements of ganglion cell surround size then confirmed this: If horizontal cell coupling plays a major role in the adjustability of ganglion cell surround size, then the shift from “no surround” to “small surround” should be abolished. It wasn’t. The shift was essentially identical to that observed in the wild type (Fig. 2.3). Finally, behavior measurements provided further confirmation. No difference in spatial tuning sensitivity was observed between the Cx57-deficient and wild-type animals (Fig. 2.4).

These results thus provide strong evidence that changes in the coupling of horizontal cells is not a dominant mechanism for controlling the spatial tuning of ganglion cells. Most significantly, it does not appear to be a critical player in the adjustability of the tuning that occurs with changes from night to day vision. Other processes must dominate. Our measurements with dopamine confirmed this: dopamine’s effects on the spatial tuning of ganglion cells could not have been mediated by a change in horizontal cell coupling since dopamine led to the same shift in spatial tuning in Cx57-deficient mice as in wild type, at least under photopic conditions (Fig. 2.5). This raises the idea that dopamine’s dominant effects with respect to spatial tuning are on other retinal pathways e.g., affecting other electrically coupled networks in the retina (Vaney, 1991), most likely amacrine cell networks (Urschel et al., 2006).

In sum, with the aid of a *Connexin57* knock out, we were able to test the long-standing hypothesis that the coupling and uncoupling of horizontal cells serves as a critical knob for adjusting spatial tuning to different light conditions, i.e., to night versus day conditions. The results show that this hypothesis, at least as it currently stands, must be rejected. The evidence for rejection is extremely strong because the same result presented itself at multiple levels – that is, when changes in horizontal cell coupling were prevented, as was the case in the knock out, the shift in spatial tuning that occurs when the retina moves from night to day proceeded normally – as measured at the level of both ganglion cell performance and whole animal behavioral performance. Thus, changes in horizontal cell coupling cannot be the critical mechanism that underlies this shift.

At first glance, it might seem surprising that preventing the changes in horizontal cell coupling – an act that affects lateral signaling in the retina – had no significant effect on ganglion cell spatial tuning, but this result can be reconciled with the many recent reports that this tuning is shaped by more than one set of circuits – that is, it is shaped by circuits in both the outer and inner retina (Sinclair et al., 2004; Cook and McReynolds, 1998; Taylor, 1999; Flores et al., 2001; Roska et al., 2000; McMahon et al., 2004). What the results of our experiments suggest is that inner retinal circuits dominate – at least for the problem of adjusting spatial tuning to different light conditions. Whatever occurs when the horizontal cells change from the uncoupled to the coupled state is effectively swamped by stronger circuit actions that occur in the inner retina.

This raises the intriguing question of what the changes in horizontal cell coupling are for. One possibility is that they serve to facilitate signal detection in the time domain, rather than the space domain. A change in horizontal cell coupling, because it is a change in the state of a potential shunt (Smith, 1995), would be expected to affect both spatial and temporal signal detection. If its effects on spatial signal detection are redundant to those produced by the inner retina, then losing the coupling would have minimal effect on spatial processing. If its effects on *temporal* signal detection are not redundant, then losing it should affect temporal processing. This work thus creates a new hypothesis for the function of the horizontal cell coupling – that it serves to improve signal-to-noise ratios in the time domain, and, therefore, may be a key player in temporal processing.

Finally, for the sake of completeness, we conclude by stating that we can't completely rule out the possibility that there is another connexin that links horizontal cells. However, if one exists, the likelihood that it contributes substantially to horizontal cell coupling is very small. The reason we state this is that the effects of knocking out Cx57 on horizontal cell coupling are maximal or near maximal, as measured by changes in both dye coupling and horizontal cell length constant. Dye coupling, using neurobiotin, is nearly abolished (>99% abolished) (Hombach et al., 2004; Shelley et al., 2006), and horizontal cell length constants are significantly reduced (Shelley et al., 2006), with a reduction greater than that produced by dopamine application, which also reduces horizontal cell coupling (the hierarchy of length constant reduction is shown in *Appendix* Fig. 2.9). With respect to receptive field evaluations:

horizontal cell length constants in the knockout are on average 50 μm, with the mean dendritic tree diameter for individual horizontal cells at 100 μm (Shelley et al., 2006). Taken together, these data provide strong evidence that Cx57 is the primary, or exclusive, mediator of horizontal cell coupling, and that eliminating its ability to function provides a strong test for the role of horizontal cell coupling in retinal processing.

2.4 Materials and Methods

2.4.1 Animals

For generation of the *Cx57-lacZ* mouse line, part of the coding region of the *Cx57* gene was deleted and replaced with the *lacZ* reporter gene (Hombach et al., 2004). Cx57-deficient mice ($Cx57^{lacZ/lacZ}$) and wild-type controls aged 2 to 4 months were used for all experiments. After each recording, the genotype of the retina was confirmed with staining for β-galactosidase activity and PCR as described (Hombach et al., 2004). All experiments were conducted in accordance with the institutional guidelines for animal welfare.

2.4.2 Extracellular recordings of ganglion cell responses

The isolated mouse retina was placed on a flat array of 64 microelectrodes as described (Sinclair et al., 2004) and bathed in oxygenated Ringer's solution at room temperature. Recordings were made from central retina as described previously (Sinclair et al., 2004; Nirenberg et al., 2001). Briefly, spike trains were recorded using a Plexon Instruments Multichannel Neuronal Acquisition

Processor (Dallas, TX). A custom made time-voltage window discriminator that captured distinct waveforms served to sort spikes on-line into individual units.

2.4.3 Light stimulation

An overhead projector (EIKI OHP-4100, Rancho Santa Margarita, CA) in combination with a liquid crystal display panel (Panasonic PT-L104, Secaucus, NJ) was used to deliver visual stimuli. Neutral density filters attenuated the stimulus intensity to the desired scotopic and photopic light levels. The scotopic intensity was 0.0066 $\mu W/cm^2$; the photopic was 0.21 $\mu W/cm^2$. Following (Nirenberg et al., 2001), and using the spectrum of our monitor, also available in (Nirenberg et al., 2001), these radiometric units can be converted to photoreceptor equivalent photons/μm^2/s: The scotopic intensity converts to 52.5 rod-equivalent photons/μm^2/s and 60 M-cone-equivalent-photons/μm^2/s, the photopic, to 1670 rod-equivalent-photons/μm^2/s and 1900 M-cone-equivalent-photons/μm^2/s. This gives a rate of 32.5 R*/rod/s and 21 R*/M-cone/s for scotopic, and 1120 R*/rod/s, and 650 R*/M-cone/s for photopic, assuming an effective collecting area (i.e., collecting area/funneling factor) from (Lyubarsky et al., 2004; Lyubarsky et al., 1999) of 0.67 μm^2 for rods and 0.34 μm^2 for cones. Note that the emphasis here is on rods and M-cones, as UV pigments are not significantly stimulated with the displays presented in this paper.

As mentioned in the *Introduction* and *Results*, these light levels were chosen to bring out the shift in spatial tuning that occurs as the retina moves from night to day vision, as shown in Fig. 2.2, and to span the range where

changes in horizontal cell coupling are maximal or near maximal, as observed in both mouse (Shelley, Personal communication) and rabbit (Xin and Bloomfield, 1999, Figs. 5 and 9). The scotopic and photopic light levels are also consistent with the levels reported for the mouse rod and cone regimes, as assessed using rod saturation measurements, by (Dodd, 1998).

All stimuli used white light (for spectrum, see (Nirenberg et al., 2001)) and consisted of random flicker, flashes and gratings. To measure receptive field properties of ganglion cells, we used drifting sine wave gratings with 8 different spatial frequencies ranging from $10^{-2.9}$ to $10^{-0.8} = 0.0012$ to 0.155 cycles/degree in three directions. Each spatial frequency and direction was presented for 30 cycles, with a temporal frequency of 1 Hz. The 24 combinations of spatial frequency and direction were randomly interleaved. Measurements always started at the scotopic light intensity. After increasing the light intensity, a series of flashes was run which was followed by a random flicker stimulus to adapt the retina for 20 min before the grating stimulus was started. For the experiments involving drugs (dopamine and cobalt), the drugs were applied during this adaptation time.

2.4.4 Pharmacology

All chemicals were purchased from Sigma (St. Louis, MO). Cobalt and dopamine were dissolved in oxygenated Ringer's solution and were delivered to the retina by continuous perfusion.

2.4.5 Data analysis

Spatial frequency analysis was done using standard methods (Sinclair et al., 2004). Briefly, the spatial tuning of each ganglion cell was evaluated using its responses to drifting sine wave gratings of varying spatial frequency and direction (8 spatial frequencies, 3 directions, see above). For each grating, the first harmonic of the response was calculated. The first harmonic, $R(\mathbf{k})$, with $\mathbf{k} = (k_x, k_y)$ as the two-dimensional spatial frequency, was computed as follows:

$$R(\mathbf{k}) = \left| \frac{2\pi}{\omega} \frac{1}{N_c} \sum_j \exp\left[-i\omega t_j(\mathbf{k}) \right] \right|,$$

where $\omega = 2\pi$ radians/s is the temporal frequency of the drifting sine wave grating; N_c is the number of cycles (30 in our experiments); and $t_j(\mathbf{k})$ is the time of the jth spike produced by a grating with the spatial frequency $\mathbf{k}$. Tuning curves, which give $R(\boldsymbol{k})$ as a function of $\boldsymbol{k}$, were then plotted.

To determine the mean of each cell's spatial tuning curve, the center of mass (CM) of the curve was calculated as:

$$CM = \frac{\sum_k R(\mathbf{k}) \log \mathbf{k}}{\sum_k R(\mathbf{k})}.$$

To determine the center-surround receptive field parameters for each cell, the cells' tuning curves were fit with the standard difference-of-Gaussians model. The model linearly combines the profiles of a tall and narrow Gaussian representing the center and a short and shallow Gaussian of opposite sign

representing the surround (see (Sinclair et al., 2004; Enroth-Cugell et al., 1983); we followed (Sinclair et al., 2004) directly). The model is based on seven parameters; to determine the values of the parameters that give the best fit to the curve, the mean squared error between $R(\mathbf{k})$ and the response predicted by the model $\hat{R}(\mathbf{k})$ was minimized, using a brute force exploration of initial conditions to find the global minimum. $\hat{R}(\mathbf{k})$ was calculated as:

$$\hat{R}(\mathbf{k}) = \left[A_c^2(\mathbf{k}) + A_s^2(\mathbf{k}) - 2A_c(\mathbf{k})A_s(\mathbf{k})\cos\phi\right]^{1/2},$$

where

$$A_c = F_c \exp\left[-\frac{1}{2}\sigma_+^2(k_x\cos\theta - k_y\sin\theta)^2 - \frac{1}{2}\sigma_-^2(k_x\sin\theta + k_y\cos\theta)^2\right]$$

is the strength of the center response, σ_+ and σ_- the major and minor radii of the center (assumed to be asymmetric, based on (Sinclair et al., 2004)), θ its orientation, and

$$A_s = F_s \exp\left[-\frac{1}{2}\sigma_s^2(k_x^2 + k_y^2)\right]$$

is the strength of the surround response, where σ_s (assumed to be symmetric, also based on (Sinclair et al., 2004)) is the size of the surround, and ϕ the phase angle associated with the different delays between the center and surround response. The mean squared error between $R(\mathbf{k})$ and $\hat{R}(\mathbf{k})$, denoted χ^2, is given by:

$$\chi^2 = \sum_k (R(\mathbf{k}) - \hat{R}(\mathbf{k}))^2 .$$

Goodness of fit was then measured by r^2, the fraction of the variance explained by the model, where $r^2 = 1 - \chi^2 / \mathrm{Var}[R(\mathrm{k})]$. Following (Sinclair et al., 2004), only cells whose r^2 values were > 0.6 were included in the dataset. (For visualization of the quality of an r^2 value of 0.6, a hierarchy of fits from $r^2 > 0.9$ to $r^2 < 0.6$ is shown in *Appendix* Fig. 2.7.) Also following (Sinclair et al., 2004), for each parameter, only parameter values that were within 3 standard deviations of the mean for that parameter were included.

Receptive fields with no surrounds: At scotopic light levels, ganglion cell receptive fields showed no surrounds, that is, the best fit, as measured by r^2 was a single Gaussian; no increase in r^2 of more than 0.05 was achieved by including a second Gaussian. >80% of cells at scotopic light levels fell into this category. For a clear demonstration that the single Gaussian was the better fit, see Figure 2.2: As shown in panels B and E, as well as in panels A and C, most (>80%) of the tuning curves at scotopic light levels (black curves) are monotonically decreasing; this is consistent with a fit to a single Gaussian.

2.4.6 Behavioral tests using a virtual optokinetic system, light intensities

Responses were measured using the Prusky/Douglas virtual optokinetic system (Prusky et al., 2004; Douglas et al., 2005). Briefly, the animal, which was freely moving, was placed in a virtual reality chamber, a virtual cylinder,

that projects a vertical sine wave grating. A video camera, situated above the animal, provided live video feedback of the testing arena. The walls of the cylinder were kept a constant distance from the animal's head, "clamping" the spatial frequency of the grating. On each trial, the cylinder was centered on the mouse's head. A drifting grating of a pre-selected spatial frequency at 100% contrast appeared, and the mouse was assessed for tracking behavior for a few seconds. Grating contrast was systematically reduced until no tracking response was observed. The data were then evaluated by fitting the animal's response to steps of decreasing contrast to a logistic function (a psychometric function) using psignifit, version 2.5.6 for Matlab, which implements the maximum-likelihood method described by (Wichmann and Hill, 2001). The animal's contrast threshold for each spatial frequency was taken as the 50% point of the fitted curve. Contrast was calculated from the gratings luminances on the screen: (Lmax – Lmin)/(Lmax + Lmin). Contrast sensitivity is the reciprocal of the threshold. Significance testing was performed for each light level using *t*-tests with Bonferroni correction for multiple comparisons.

Light intensities for the behavior experiments were measured in cd/m^2 using a luminance meter (Minolta, model LS-100). Three were used: 17.9 cd/m^2 0.6 cd/m^2 and 1.8 $x10^{-5}$ cd/m^2. Following (Lyubarsky et al., 2004), which provides a conversion from cd/m^2 to photoreceptor-equivalent photons/μm^2 for mouse, and adjusting for pupil size as in (Lucas, 2003, Figs. 2 and 3), these intensities cover the same range as those used in the recording chamber: 1640 rod-equivalent-photons/μm^2/s (0.5 mm^2 pupil area), 350 rod-equivalent-photons/μm^2/s (fully dilated pupil) to < 0.1 rod-equivalent-photons/μm^2/s. Note

that mice have substantial vision at very low light levels (see (Saszik et al., 2002, Figs. 2 and 3) (ERGs) and (Umino et al., 2008, Fig. 7) (optomotor responses)).

2.5 Acknowledgements

We thank Adam L. Jacobs for helpful discussions and Jennifer Shelley for critical comments on the manuscript.

APPENDIX

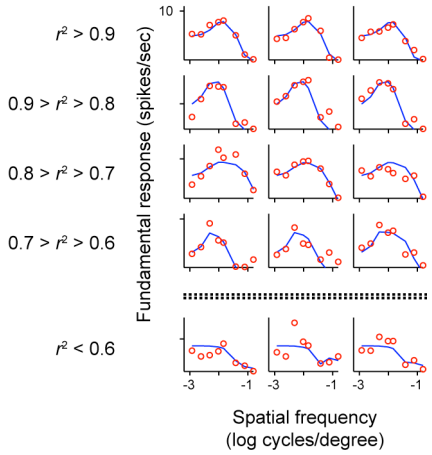

Figure 2.7 Quality of Difference of Gaussians fits

As indicated in the main text (*Methods*), for quality control, and for consistency with previous work (Sinclair et al., 2004), only fits with r^2 values > 0.6 were used. To provide intuition for the quality of an r^2 value of > 0.6, a series of fits from $r^2 > 0.9$ to $r^2 < 0.6$ is shown. A natural breakdown begins below 0.6. Data are plotted on semi-log plots; *red dots* indicate cells' responses, *blue curves* indicate fits.

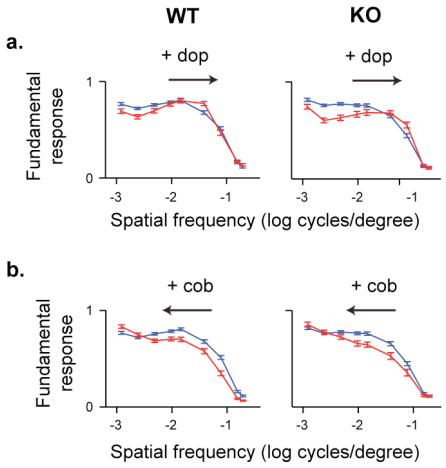

Figure 2.8 Shifts in spatial tuning following dopamine and cobalt application, presented as average tuning curves.

In the main text, the shifts were presented as center-of-mass distributions; that is, we took each cell's tuning curve, measured its center of mass and presented the distribution of center of mass values for all cells in the data set (see Figs. 2.5 and 2.6). For the interested reader, we show here the shifts as average tuning curves (mean ±SEM). Consistent with the center of mass analysis, where all significance tests are presented, dopamine causes a shift to the right for both genotypes, and cobalt causes a shift to the left for both genotypes. *Blue* indicates no drug; *red* indicates drug.

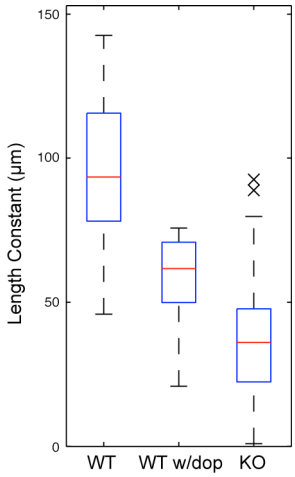

Figure 2.9 Horizontal cell length constants in the Cx57-deficient mice are significantly reduced.

As indicated in the main text, the evidence that knocking out Cx57 blocks horizontal cell coupling is that dye spread (neurobiotin) is >99% abolished, and horizontal cell length constants are significantly reduced, with the reduction greater than that produced by dopamine application, which also reduces horizontal cell coupling (Hampson et al., 1994; He et al., 2000; Teranishi et al., 1983). Here we show the hierarchy of horizontal cell length constant reduction for the three conditions: wild-type, wild-type with dopamine, and Cx57 knockout. For each condition, *red lines* indicate the median, *blue boxes* indicate the upper and lower quartiles; *black lines* indicate the data ranges. *Black x*'s indicate two outliers. For comparison, mean horizontal cell dendritic tree diameter is 100 μm (Shelley et al., 2006).

REFERENCES

1. Enroth-Cugell C, Robson J (1966) The contrast sensitivity of retinal ganglion cells of the cat. J Physiol 187: 517-552.

2. Shapley R, Lennie P (1985) Spatial frequency analysis in the visual system. Annu Rev Neurosci 8: 547-583.

3. Barlow H (1953) Summation and inhibition in the frog's retina. J Physiol 119: 69-88.

4. Kuffler S (1953) Discharge patterns and functional organization of mammalian retina. J Neurophysiol 16: 37-68.

5. Rodieck R, Stone J (1965) Analysis of receptive fields of cat retinal ganglion cells. J Neurophysiol 28: 832-849.

6. Sinclair J, Jacobs A, Nirenberg S (2004) Selective ablation of a class of amacrine cells alters spatial processing in the retina. J Neurosci 24: 1459-1467.

7. Werblin F, Dowling J (1969) Organization of the retina of the mudpuppy, Necturus maculosus. II. Intracellular recording. J Neurophysiol 32: 339-355.

8. Kaneko A (1970) Physiological and morphological identification of horizontal, bipolar and amacrine cells in goldfish retina. J Physiol 207: 623-633.

9. Naka K, Witkovsky P (1972) Dogfish ganglion cell discharge resulting from extrinsic polarization of the horizontal cells. J Physiol 223: 449-460.

10. Mangel S (1991) Analysis of the horizontal cell contribution to the receptive field surround of ganglion cells in the rabbit retina. J Physiol 442: 211-234.

11. Yang X, Wu S (1991) Feedforward lateral inhibition in retinal bipolar cells: input-output relation of the horizontal cell-depolarizing bipolar cell synapse. Proc Natl Acad Sci U S A 88: 3310-3313.

12. Fahey P, Burkhardt D (2003) Center-surround organization in bipolar cells: symmetry for opposing contrasts. Vis Neurosci 20: 1-10.

13. Cook P, McReynolds J (1998) Lateral inhibition in the inner retina is important for spatial tuning of ganglion cells. Nat Neurosci 1: 714-719.

14. Bieda M, Copenhagen D (1999) Sodium action potentials are not required for light-evoked release of GABA or glycine from retinal amacrine cells. J Neurophysiol 81: 3092-3095.

15. Taylor W (1999) TTX attenuates surround inhibition in rabbit retinal ganglion cells. Vis Neurosci 16: 285-290.

16. Flores-Herr N, Protti D, Wässle H (2001) Synaptic currents generating the inhibitory surround of ganglion cells in the mammalian retina. J Neurosci 21: 4852-4863.

17. Roska B, Nemeth E, Orzo L, Werblin F (2000) Three levels of lateral inhibition: A space-time study of the retina of the tiger salamander. J Neurosci 20: 1941-1951.

18. Barlow H, Fitzhugh R, Kuffler S (1957) Change of organization in the receptive fields of the cat's retina during dark adaptation. J Physiol 137: 338-354.

19. Smirnakis S, Berry M, Warland D, Bialek W, Meister M (1997) Adaptation of retinal processing to image contrast and spatial scale. Nature 386: 69-73.

20. Enroth-Cugell C, Shapley R (1973) Adaptation and dynamics of cat retinal ganglion cells. J Physiol 233: 271-309.

21. Maffei L, Fiorentini A, Cervetto L (1971) Homeostasis in retinal receptive fields. J Neurophysiol 34: 579-587.

22. Smith RA, Jr (1973) Luminance-dependent changes in mesopic visual contrast sensitivity. J Physiol 230: 115-135.

23. Mangel S, Dowling J (1985) Responsiveness and receptive field size of carp horizontal cells are reduced by prolonged darkness and dopamine. Science 229: 1107-1109.

24. Baldridge W, Ball A (1991) Background illumination reduces horizontal cell receptive-field size in both normal and 6-hydroxydopamine-lesioned goldfish retinas. Vis Neurosci 7: 441-450.

25. Tornqvist K, Yang X, Dowling J (1988) Modulation of cone horizontal cell activity in the teleost fish retina. III. Effects of prolonged darkness and dopamine on electrical coupling between horizontal cells. J Neurosci 8: 2279-2288.

26. Xin D, Bloomfield S (1999) Dark- and light-induced changes in coupling between horizontal cells in mammalian retina. J Comp Neurol 405: 75-87.

27. Hombach S, Janssen-Bienhold U, Söhl G, Schubert T, Büssow H, et al. (2004) Functional expression of connexin57 in horizontal cells of the mouse retina. Eur J Neurosci 19: 2633-2640.

28. Shelley J, Dedek K, Schubert T, Feigenspan A, Schultz K, et al. (2006) Horizontal cell receptive fields are reduced in connexin57-deficient mice. Eur J Neurosci 23: 3176-3186.

29. Campbell F, Robson J (1968) Application of Fourier analysis to the visibility of gratings. J Physiol 197: 551-566.

30. Stone C, Pinto L (1993) Response properties of ganglion cells in the isolated mouse retina. Vis Neurosci 10: 31-39.

31. Bisti S, Clement R, Maffei L, Mecacci L (1977) Spatial frequency and orientation tuning curves of visual neurones in the cat: effects of mean luminance. Exp Brain Res 27: 335-345.

32. Muller J, Dacheux R (1997) Alpha ganglion cells of the rabbit retina lose antagonistic surround responses under dark adaptation. Vis Neurosci 14: 395-401.

33. Rodieck R (1965) Quantitative analysis of cat retinal ganglion cell response to visual stimuli. Vision Res 5: 583-601.

34. Sinclair J, Nirenberg S (2001) Characterization of neuropeptide Y-expressing cells in the mouse retina using immunohistochemical and transgenic techniques. J Comp Neurol 432: 296-306.

35. Enroth-Cugell C, Robson J, Schweitzer-Tong D, Watson A (1983) Spatio-temporal interactions in cat retinal ganglion cells showing linear spatial summation. J Physiol 341: 279-307.

36. Croner LJ, Kaplan E (1995) Receptive fields of P and M ganglion cells across the primate retina. Vision Res 35: 7-24.

37. Prusky G, Alam N, Beekman S, Douglas R (2004) Rapid quantification of adult and developing mouse spatial vision using a virtual optomotor system. Invest Ophthalmol Vis Sci 45: 4611-4616.

38. Douglas R, Alam N, Silver B, McGill T, Tschetter W, et al. (2005) Independent visual threshold measurements in the two eyes of freely moving rats and mice using a virtual-reality optokinetic system. Vis Neurosci 22: 677-684.

39. Abdeljalil J, Hamid M, Abdel-Mouttalib O, Stéphane R, Raymond R, et al. (2005) The optomotor response: a robust first-line visual screening method for mice. Vision Res 45: 1439-1446.

40. Benedek G, Benedek K, Kéri S, Letoha T, Janáky M (2003) Human scotopic spatiotemporal sensitivity: a comparison of psychophysical and electrophysiological data. Doc Ophthalmol 106: 201-207.

41. Jensen R, Daw N (1984) Effects of dopamine antagonists on receptive fields of brisk cells and directionally selective cells in the rabbit retina. J Neurosci 4: 2972-2985.

42. Jensen R, Daw N (1986) Effects of dopamine and its agonists and antagonists on the receptive field properties of ganglion cells in the rabbit retina. Neuroscience 17: 837-855.

43. Vigh J, Witkovsky P (1999) Sub-millimolar cobalt selectively inhibits the receptive field surround of retinal neurons. Vis Neurosci 16: 159-168.

44. Hampson E, Weiler R, Vaney D (1994) pH-gated dopaminergic modulation of horizontal cell gap junctions in mammalian retina. Proc Biol Sci 255: 67-72.

45. He S, Weiler R, Vaney D (2000) Endogenous dopaminergic regulation of horizontal cell coupling in the mammalian retina. J Comp Neurol 418: 33-40.

46. Teranishi T, Negishi K, Kato S (1983) Dopamine modulates S-potential amplitude and dye-coupling between external horizontal cells in carp retina. Nature 301: 243-246.

47. Witkovsky P, Dearry A (1992) Functional roles of dopamine in the vertebrate retina. Prog Ret Res 10: 247-292.

48. Wang Y, Mangel S (1996) A circadian clock regulates rod and cone input to fish retinal cone horizontal cells. Proc Natl Acad Sci U S A 93: 4655-4660.

49. Baylor D, Fuortes M, O'Bryan P (1971) Receptive fields of cones in the retina of the turtle. J Physiol 214: 265-294.

50. McMahon M, Packer O, Dacey D (2004) The classical receptive field surround of primate parasol ganglion cells is mediated primarily by a non-GABAergic pathway. J Neurosci 24: 3736-3745.

51. Xia Y, Nawy S (2003) The gap junction blockers carbenoxolone and 18beta-glycyrrhetinic acid antagonize cone-driven light responses in the mouse retina. Vis Neurosci 20: 429-435.

52. Packer O, Dacey D (2002) Receptive field structure of H1 horizontal cells in macaque monkey retina. J Vis 2: 272-292.

53. Kamermans M, Fahrenfort I, Schultz K, Janssen-Bienhold U, Sjoerdsma T, et al. (2001) Hemichannel-mediated inhibition in the outer retina. Science 292: 1178-1180.

54. Blakemore C, Campbell F (1969) On the existence of neurones in the human visual system selectively sensitive to the orientation and size of retinal images. J Physiol 203: 237-260.

55. Cavonius C, Robbins D (1973) Relationships between luminance and visual acuity in the rhesus monkey. J Physiol 232: 239-246.

56. Greenlee M, Georgeson M, Magnussen S, Harris J (1991) The time course of adaptation to spatial contrast. Vision Res 31: 223-236.

57. DeValois RL, DeValois KK (1990) Spatial Vision. New York: Oxford University Press.

58. Atick JJ, Redlich AN (1992) What does the retina know about natural scenes? Neural Computation 4: 196-210.

59. van Hateren J (1992) A theory of maximizing sensory information. Biol Cybern 68: 23-29.

60. Vaney D (1991) Many diverse types of retinal neurons show tracer coupling when injected with biocytin or Neurobiotin. Neurosci Lett 125: 187-190.

61. Urschel S, Höher T, Schubert T, Alev C, Söhl G, et al. (2006) Protein kinase A-mediated phosphorylation of connexin36 in mouse retina results in decreased gap junctional communication between AII amacrine cells. J Biol Chem 281: 33163-33171.

62. Smith R (1995) Simulation of an anatomically defined local circuit: the cone-horizontal cell network in cat retina. Vis Neurosci 12: 545-561.

63. Nirenberg S, Carcieri S, Jacobs A, Latham P (2001) Retinal ganglion cells act largely as independent encoders. Nature 411: 698-701.

64. Lyubarsky AL, Daniele LL, Pugh EN (2004) From candelas to photoisomerizations in the mouse eye by rhodopsin bleaching in situ and the light-rearing dependence of the major components of the mouse ERG. Vision Res 44: 3235-3251.

65. Lyubarsky AL, Falsini B, Pennesi ME, Valentini P, Pugh ENJ (1999) UV- and midwave-sensitive cone-driven retinal responses of the mouse: a possible phenotype for coexpression of cone photopigments. J Neurosci 19: 445-455.

66. Shelley J, Personal communication.

67. Dodd RL (1998) The role of arrestin and recoverin in signal transduction by retinal rod photoreceptors. PhD dissertation, Stanford University, Palo Alto CA, 153-165.

68. Wichmann F, Hill N (2001) The psychometric function: I. Fitting, sampling, and goodness of fit. Percept Psychophys 63: 1293-1313.

69. Lucas RJ (2003) Diminished pupillary reflex at high irradiances in melanopsin-knockout mice. Science 299: 245-247.

70. Saszik SM, Robson, JG, Frishman, LJ (2002) The scoptopic threshold response of the dark-adapted electroretinogram of the mouse. J. Physiol. 543: 899-916.

71. Umino Y, Solessio E, Barlow, RB (2008) Speed, spatial, and temporal tuning of rod and cone vision in mouse. *J. Neurosci.* 28: 189-198.

CHAPTER 3

A novel mechanism for switching a neural system from one state to another

Chethan Pandarinath, Illya Bomash, Jonathan Victor, Glen Prusky,
Wayne Tschetter, Sheila Nirenberg

Department of Physiology and Biophysics, Weill Medical College of Cornell University, New York, NY 10065

Abstract

An animal's ability to rapidly adjust to new conditions is essential to its survival. The nervous system, then, must be built with the flexibility to adjust, or shift, its processing capabilities on the fly. To understand how this flexibility comes about, we tracked a well-known behavioral shift, a visual integration shift, down to its underlying circuitry, and found that it is produced by a novel mechanism – a change in gap junction coupling that can turn a cell class on and off. The results showed that the turning on and off of a cell class shifted the circuit's behavior from one state to another, and, likewise, the animal's behavior. The widespread presence of similar gap junction-coupled networks in the brain suggests that this mechanism may underlie other behavioral shifts as well.

3.1. Introduction

The nervous system has an impressive ability to self-adjust – that is, as it moves from one environment to another, it can adjust itself to accommodate the new conditions. For example, as it moves into an environment with new stimuli, it can shift its attention (Desimone and Duncan, 1995; Maunsell and Treue, 2006; Reynolds and Heeger, 2009); if the stimuli are low contrast, it can adjust its contrast sensitivity (Shapley and Victor, 1978; Ohzawa et al., 1982; Bonin et al., 2006); if the signal-to-noise ratio is low, it can change its spatial and temporal integration properties (Peskin et al., 1984; De Valois and De Valois, 1990). These shifts are well described at the behavioral level – and are clearly critical to our functioning – but how the nervous system is able to produce them is not clear. How is it that a network can change the way it processes information on the fly?

In this paper, we describe a case where it was possible to obtain an answer. It is a simple case, but one of the best-known examples of a behavioral shift – the shift in visual integration time that occurs as an animal switches from daylight to nightlight conditions (reviewed in De Valois and De Valois, 1990). In daylight conditions, when photons are abundant, and the signal-to-noise ratio is high, the visual system is shifted toward short integration times. In nightlight conditions, when photons are limited, and the signal-to-noise ratio is low, the system shifts toward long integration times. (See *Appendix 1* for why the shift involves a network action, rather than a simple switch from cones to rods.)

Here we propose a hypothesis for how the shift takes place – it involves a change in gap-junction coupling among the horizontal cells of the retina. The idea is as follows: Horizontal cells are well-known to be coupled by gap junctions, and the coupling is light-dependent (Dong and McReynolds, 1991; Xin and Bloomfield, 1999; Weiler et al., 2000). When light levels are high, the gap junctions close, and there is little coupling. When light levels are low, the gap junctions open, and extensive coupling ensues. Since coupling shunts current, the idea is that the extensive coupling causes a shunting of horizontal cell current, effectively taking the horizontal cells out of the system. Since horizontal cells play a key role in shaping integration time – they provide feedback to photoreceptors that keeps integration time short (Baylor et al., 1971; Kleinschmidt and Dowling, 1975; Dowling, 1987) – taking these cells out of the system makes integration time longer.

This hypothesis raises a new, and potentially generalizable idea – that a neural network can be shifted from one state to another by changing the gap-junction coupling of one of its cell classes. The coupling can act as a means to take a cell class out of a network, and by doing so, change the network's behavior. (For more on generalization, including the time scale of the coupling changes, see *Discussion*.)

We tested the hypothesis using transgenic mice that cannot undergo this coupling (Hombach et al., 2004; Shelley et al., 2006; Dedek et al., 2008). They lack the horizontal cell gap-junction gene, and, as a result, their horizontal cells get locked into the uncoupled state (Hombach et al., 2004; Shelley et al., 2006; Dedek et al., 2008). If the hypothesis is correct, these

animals should not be able to undergo the shift to long integration times. Our results show that the hypothesis held: the shift was blocked completely at the behavioral level, and almost completely at the physiological (i.e., ganglion cell) level.

In sum, we tracked a behavioral change down to the neural machinery that implements it. This revealed a new, simple, and potentially generalizable, mechanism for how networks can rapidly adjust themselves to changing environmental demands.

3.2. Results

Fig. 3.1 gives the starting point for these experiments. It indicates that a) the model system we are using, the mouse, shows the shift in visual integration time observed in other species (Kelly, 1961; van Nes et al., 1967; De Valois and De Valois, 1990; Umino et al., 2008) (Fig. 3.1A), and b) the part of the nervous system responsible for the shift, or at least a large part of it, is the retina, since the shift is readily detectable at the level of the retinal ganglion cells (Fig. 3.1B). The shift at the behavioral level was measured using a standard optomotor task, where the stimuli were drifting sine wave gratings of different temporal frequencies. The shift at the ganglion cell level was measured using three different stimuli: drifting sine wave gratings of different temporal frequencies, a white noise stimulus, and a natural scene stimulus. As indicated in all the panels of the figure, there is a shift from short integration times to long, that is, from high temporal frequencies to low ($p<10^{-3}$, *t*-test

comparing the centers of mass of the frequency response curves for the night (scotopic) condition with those for the day (photopic) condition).

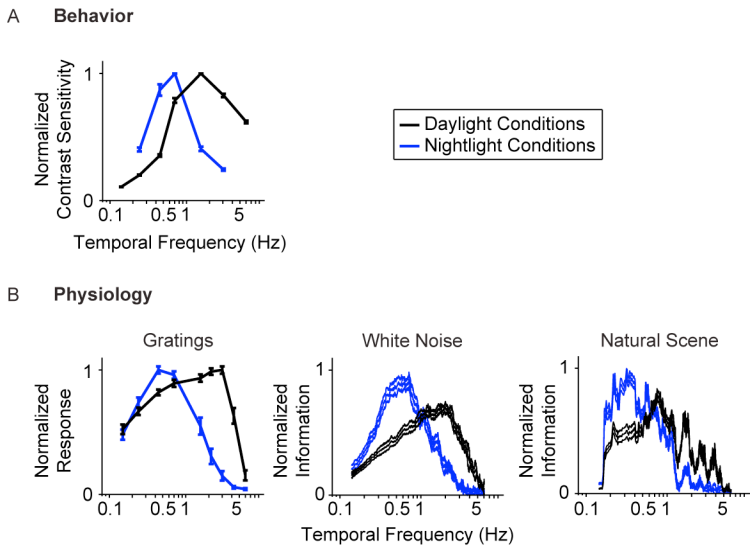

Figure 3.1 The visual system undergoes a shift in integration time as it shifts from daylight to nightlight (photopic to scotopic) conditions.

In daylight conditions, the system favors short integration times (high temporal frequencies); in nightlight conditions, it favors long integration times (low temporal frequencies). See *Methods* for light intensities for the two conditions. (**A**) The shift, measured at the behavioral level using drifting grating stimuli. (**B**) The shift, measured at the ganglion cell level, using three different kinds of stimuli: drifting gratings, white noise, and natural scenes. Behavioral performance was measured as contrast sensitivity, averaged across animals, and peak-normalized (*n*=5, mean ± SEM). Ganglion cell performance in (**B**, *left*) was measured as first harmonic response, averaged across cells, and

peak normalized; ganglion cell performance in (**B**, *middle and right*) was measured as information, normalized for equal area (n=20, mean ± SEM).

Fig. 3.2 shows the proposed model for how the shift is generated. It builds on the well-established front-end circuit that shapes visual integration time (Baylor et al., 1971; Kleinschmidt and Dowling, 1975; Dowling, 1987) (Fig. 3.2A). The circuit contains three cell classes – photoreceptors, bipolar cells and horizontal cells – and operates, briefly, as follows: the photoreceptors send signals forward to both the bipolar and horizontal cells. The bipolar cells continue to send signals forward, while the horizontal cells send signals back onto the photoreceptors. The horizontal cell feedback shapes the photoreceptors' integration time[1] (Baylor et al., 1971; Kleinschmidt and Dowling, 1975; Dowling, 1987).

[1] The integration time of the photoreceptor refers to the length of time over which it responds to light (i.e., the width of the impulse response).

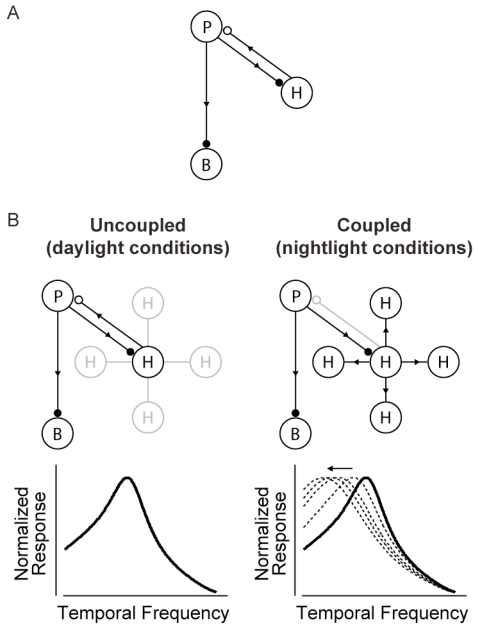

Figure 3.2 The circuit that controls visual integration time can be shifted from one state to another by a change in the gap junction coupling of one of its cell classes.

(**A**) Visual integration time is shaped, in large part, by a negative feedback loop in the outer retina: photoreceptors send signals forward to both bipolar cells and horizontal cells; the horizontal cells then, in turn, provide negative feedback to the photoreceptors (Baylor et al., 1971; Kleinschmidt and Dowling, 1975; Dowling, 1987). Note that the figure shows only one type of horizontal cell and a generic photoreceptor; this is consistent with our model system, the mouse retina, which has only one type of horizontal cell, and it acts on both rods and cones (Trumpler et al., 2008 Jul 2; Babai and Thoreson, 2009). (**B***, left*) In daylight conditions, horizontal cell feedback is strong. This cuts

photoreceptor integration time short, and the system shifts to high temporal frequency responses. At night (**B***, right*), when the system needs longer integration times, a reduction in horizontal cell feedback is needed. The opening of the gap junctions provides a mechanism for achieving this. It produces a shunting of horizontal cell current that weakens or inactivates the horizontal cells. The photoreceptor integration time then becomes longer, and the system shifts to low temporal frequency responses. The change in the gap junction coupling acts, effectively, as a knob to regulate the strength of the negative feedback. (See *Appendix 2* for a formalized version of the model.)

Panel B shows how a change in the gap junction coupling of the horizontal cells can modulate the circuit's behavior – that is, how it can change it from one state to another. The scenario is the following: In daylight conditions the gap junctions close. This strengthens the signals of the horizontal cells, so they send strong feedback to the photoreceptors. Strong feedback cuts the photoreceptors' integration time short, producing the short integration times (high temporal frequency responses) observed experimentally (Fig, 3.2B, left). In nightlight conditions, the gap junctions open. The opening produces a shunting of the horizontal cell current, which reduces or eliminates the horizontal cell signal. Without the feedback from the horizontal cells, there is no shortening of the photoreceptor integration time, and the system shifts to the observed long integration times (low temporal frequency responses)) (Fig. 3.2B, right).

The strength of the model is that it derives from well-established facts – specifically, that the integration time of photoreceptors (both rods and cones)

changes (becomes extended) as an animal moves from day to night conditions ((Kleinschmidt and Dowling, 1975; Schneeweis and Schnapf, 2000), that the strength of the horizontal cell signal changes (decreases) as the conditions move from day to night (Teranishi et al., 1983; Yang and Wu, 1989), and, finally, that there is a change in the degree of horizontal cell coupling (an increase) with the change from day to night conditions (Dong and McReynolds, 1991; Xin and Bloomfield, 1999). Put together, these facts lead to a mechanism for shifting the circuit's behavior. The novelty is the use of gap junction coupling as a shunting device (see *Discussion*) – the model makes use of the fact that coupling produces a shunt, and, therefore, has the capacity to weaken or inactivate a cell class. By casting the coupling as a shunting mechanism, the actions of the components of the circuit – the photoreceptors, the bipolar cells, the horizontal cells, and the light-dependent change in horizontal cell coupling – fall into place to explain how the system can shift from one state to another. A formalized version of the model is given in *Appendix 2*.

We test the proposal in Fig. 3.3. To do this, we used a transgenic mouse line that cannot undergo horizontal cell coupling (Hombach et al., 2004; Shelley et al., 2006; Dedek et al., 2008) (Fig. 3.3A). These mice lack the gene for the gap junction specific to the horizontal cells, connexin 57 (Cx57), so their horizontal cells are locked into the uncoupled state. We emphasize that this particular gap junction gene is not expressed anywhere in the nervous system besides the horizontal cells (Hombach et al., 2004); thus, the elimination of this gene produces a very specific perturbation. Fig. 3.3B shows

the temporal integration curves from wild-type and knockout mice in the night condition, measured both at the behavioral level and at the ganglion cell level with the three stimuli used in Fig. 3.1. In all cases, the shift to long integration times was impaired, that is, the normal increase in amplitude at low frequencies, and the normal decrease in amplitude at high frequencies did not occur (Fig. 3.3B) or was significantly hindered (Fig. 3.3C) ($p<10^{-4}$ for the behavior, $p<10^{-3}$ for the ganglion cell responses, *t*-test comparing the centers of mass of the frequency response curves for the night (scotopic) condition with those for the day (photopic) condition).

The robustness of the results is demonstrated in Fig. 3.3D. Using data that allow a direct comparison to be made between behavioral and ganglion cell results, specifically, where the results were obtained using the same stimuli – the drifting sine wave gratings – we show the complete set of individual responses. The left side of Fig. 3.3D shows the behavioral performance for all animals under day and night conditions, and the right side shows the performance for all ganglion cells under day and night conditions. As shown in the figure, by day, the performance of the knockout closely matches that of the wild-type, but at night, the two performances diverge. At night, the wild-type makes the expected shift toward longer integration times, but the knockout – which lacks horizontal cell coupling – does not.

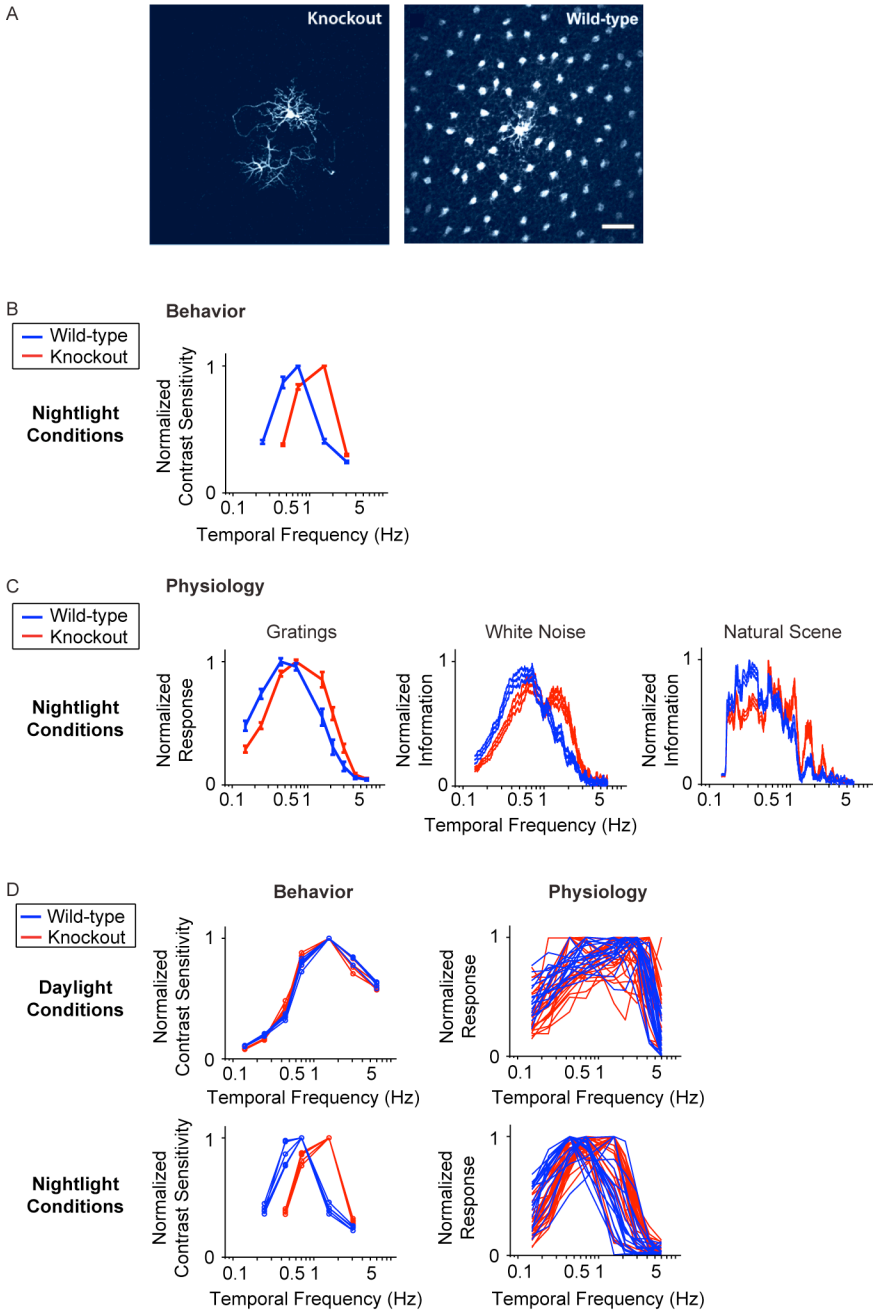

Figure 3.3 When horizontal cell coupling is prevented, the shift to long integration times is impaired at both the behavioral level and the ganglion cell level.

(**A**) Horizontal cell coupling in a retina from a Cx57 knockout versus horizontal cell coupling in a retina from a wild-type sibling control. In each retina, a single horizontal cell was injected with dye, and the extent of dye spread was measured for >1 hour. Consistent with the results in (Hombach et al., 2004; Shelley et al., 2006; Dedek et al., 2008), coupling is abolished. Scale bar = 50μm. (**B**) Behavioral performance curves measured from Cx57 knockouts and wild-type sibling controls under the night condition. The shift to long integration times (low temporal frequency responses) is significantly impaired ($p<10^{-4}$). (**C**) Ganglion cell performance curves measured from Cx57 knockout animals and wild-type sibling controls under the night condition. As in (**B**), the shift to long integration times is significantly impaired ($p<10^{-3}$). All measurements were taken as in Fig. 3.1; for the behavioral experiments, n=5 wild-type mice, 5 knockout mice, and for the ganglion cell measurements, n=20 cells from wild-type retinas, 24 cells from knockouts. (**D**) *Left*, performance for all animals shown individually. In daylight conditions, the performances of the knockouts are essentially identical to those of the wild-type animals. In night conditions, they diverge: the wild-type animals make the shift toward longer integration times, while the knockouts do not. *Right*, performance for all ganglion cells. Similar to plots on the left, the performances of the ganglion cells from the knockout and wild-type animals are the same in daytime conditions but diverge at night: the ganglion cells from the wild-type animals undergo the shift toward longer integration times, while those from the knockout are left behind.

3.3. Discussion

The nervous system faces a shifting problem. It has to shift its mode of operation from one state to another as it faces new demands (i.e., it has to shift its attention, its contrast sensitivity, its temporal integration time, etc.). How it achieves this isn't clear. Here we examined a case where it was possible to obtain an answer, and the answer was intriguingly simple: the system produced the shift by changing the gap junction coupling of one of its cell classes. The coupling acted as a way to inactivate the cell class, and, by doing so, change the system's behavior.

The findings are both surprising and exciting: surprising, because a seemingly complicated problem was solved with a simple mechanism, and exciting, because the mechanism is present not just in the retina, but throughout the brain, suggesting it might generalize to other network shifts. To be specific, gap junction coupled networks are present in visual cortex, motor cortex, frontal cortex, hippocampus, cerebellum, hypothalamus, and striatum, among many other places (Galarreta and Hestrin, 1999, 2001; Bennett and Zukin, 2004).

Furthermore, a regulator is also in place. In the retina, the regulator is a neuromodulator, dopamine: Light triggers the release of dopamine, which closes gap junctions via second messengers (McMahon et al., 1989 Oct; Dong and McReynolds, 1991; Weiler et al., 2000). Dopamine, as well as noradrenaline and histamine, have been found to open and close gap junctions in several of these brain areas (Cepeda et al., 1989; Yang and Hatton, 2002; Zsiros and Maccaferri, 2008; Onn et al., 2008 Feb 6).

The possibility for generalization to other networks is substantial and straightforward to see: **1)** While the results in this paper show the mechanism in non-spiking neurons, it readily applies to spiking cells as well and thus to networks in the brain. This is because the mechanism involves only basic biophysics – a change in cells' input resistance. Briefly, if a cell class is coupled by gap junctions, it has the potential to have its input resistance turned up and down. When the junctions are closed, the input resistance of the cells is high. This makes the cells more responsive to incoming signals and allows them to send strong signals out. When the junctions are opened, the input resistance drops. This makes the cells *less* responsive to incoming signals and allows them to send out only weak signals. In the case of spiking neurons, the signals can become so weak that the probability of firing can be reduced essentially to zero; i.e., the cells can be effectively turned off.

2) The mechanism has the potential to affect many types of network operations. While the one presented in this paper was a negative feedback loop – the gap junction coupling provided a way to turn the feedback on or off (or up or down) – one can readily imagine many other operations that could be altered by turning the activity of a pivotal cell class in a network on or off, such as alterations in feedforward signaling, lateral signaling, recurrent signaling (e.g., the stabilization of attractors), to name a few.

3) The timescale over which the mechanism operates, that is, the timescale over which the change in coupling occurs – a scale of seconds (McMahon et al., 1989 Oct; McMahon and Mattson, 1996) – is consistent with many state changes, such as changes in arousal, changes in attentional set,

shifts in decision-making strategies, e.g. shifts in the weighting of priors, shifts to speed versus accuracy (Standage and Paré, 2009), allowing it to mediate many behavioral processes.

4) Since the cellular machinery for regulation of gap junction conductances is in place, the mechanism can evolve via a change in a single gene, a gene for a gap junction protein. This makes it an easy gain from an evolutionary standpoint. A powerful selective advantage – the ability to shift a network from one state to another – could be rapidly acquired, and, in addition, acquired independently in multiple networks. (For a review of gap junction proteins, see (Bennett and Zukin, 2004).)

Fig. 3.4 emphasizes this latter point, that this gap junction coupling mechanism offers a single gene solution to a seemingly complicated set of problems, network state changes. To address this, we used, again, the horizontal cells, as an example. Specifically, we took the behavioral results from the wild-type and Cx57 knockout animals and imposed them on a predator-detection scenario. We filmed an approaching predator, restricting the movies to the temporal frequencies available to each genotype, as indicated in Fig. 3.3D left. The results are shown in Fig. 3.4. In day conditions the movies for the two genotypes are essentially the same; the predator can be seen when it is moving, i.e., when the movie is dominated by high temporal frequencies, and when it is still, i.e., when the movie is dominated by low temporal frequencies. In contrast, in night conditions, the movies diverge. In the movie filtered through the frequencies visible to the wild-type animal, the predator remains visible even when it is still; this is consistent with the wild-

type's ability to shift to low temporal frequencies. In the movie filtered though the frequencies visible to the knockout, the predator disappears. Only a ghost is present (see *Appendix 4* for the complete movies). The wild-type's maintenance of visual contact with the predator gives it an obvious selective advantage.

3.3.1 Estimating the extent to which input resistance can be reduced by coupling

As discussed above, changes in coupling can act as a dial to turn the input resistance of a cell up or down. We can estimate the range of the dial as follows: The standard experimental measure of coupling is the length constant (Xin and Bloomfield, 1999; Shelley et al., 2006). Xin and Bloomfield measured the length constant of horizontal cells under several scotopic and photopic light levels and found the maximal difference to be a factor of ~3. The maximal difference occurred when the scotopic light level was 1-1.5 log units above rod threshold and the photopic light level was >3 log units above rod threshold, levels that we matched for this paper. Since, for 2-D coupling (Lamb, 1976), input resistance is inversely proportional to the square of the length constant (detailed in *Methods* and *Appendix 2*), the input resistance of the horizontal cells at the scotopic light level is estimated to be about a factor of 9 less than that at the photopic light level.

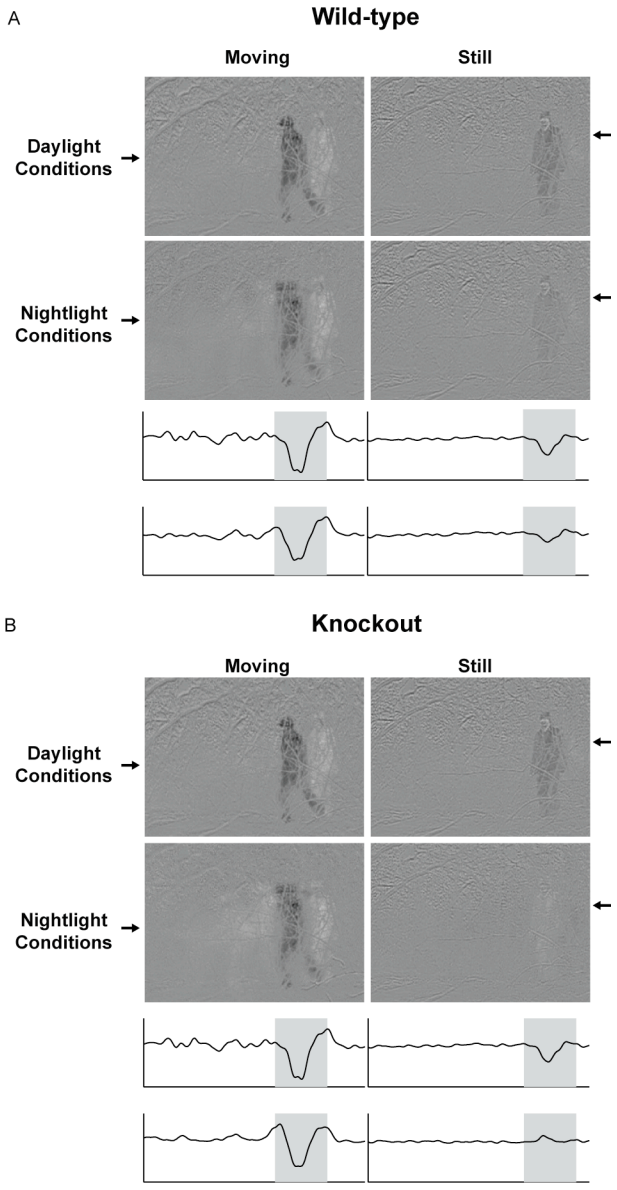

Figure 3.4 The selective disadvantage of a Cx57 gene loss.

(**A**) Movie of an approaching predator, filtered through the frequencies available to the wild-type animal, as provided by Fig. 3.3D left. In day

conditions, the predator can be seen both when it is moving (when the movie is dominated by high temporal frequencies), and when it is still (when the movie is dominated by low temporal frequencies). In night conditions, the signal is weaker, but the predator can still be seen both when moving or still. The visibility in the still condition is possible because of the shift to low temporal frequencies that occurs in the dark. The traces below the figures provide the intensity of each pixel in a horizontal slice through the image; the location of the slice is indicated by the arrow. (**B**) Same movie, filtered through the frequencies available to the knockout animal. In night conditions, the predator vanishes, see trace below figures. The wild-type's continued visual detection of the predator gives it an obvious selective advantage. (For the frequencies available to each genotype, see Fig. 3.3D left: specifically, the range of frequencies seen by the knockout at night (red curves in 3D bottom left) is a subset of the range seen by the wild-type (blue curves); the lack of low frequency sensitivity in the knockout (below ~0.3 Hz) causes the predator, when it is still, to disappear. Note that the temporal filtering was applied to the entire movie; only a representative frame from each filtered version is shown here. For the complete filtered versions, see *Appendix 4.*)

In the general case, as with horizontal cells, the extent to which gap junction coupling can shunt a cell is the ratio of the total conductances of the gap junctions that can be modulated, to the cell's baseline ("leak") conductances. Many factors – including the cell's geometry—and the complement and distribution of channels and gap junctions combine to

determine this ratio. The example of horizontal cells shows that this can be as much as an order of magnitude.

3.3.2 Linking a behavior to a neural mechanism

Following a behavioral change down to the mechanism that underlies it is often not possible experimentally. It was possible here because of a confluence of factors: the relevant network could be identified and its component cell classes are known (as shown in Figs. 3.1 and 3.2), and the protein around which the mechanism revolves, the particular gap junction protein, Cx57, is present only in one cell class (the horizontal cells) and not elsewhere in the brain (Hombach et al., 2004), allowing the circuit to be selectively disrupted. The significance of the latter is that it allowed a direct connection to be made between the disruption in the circuit and the disruption in the behavior, since no other circuits were perturbed.

3.3.3 Potential alternative models for the shift toward low temporal frequencies

As an animal moves from a light-adapted to a dark-adapted state, several changes occur in the retina other than the change in horizontal cell coupling via the Cx57 gap junctions. How can we be sure that our result – the shift toward low temporal frequencies – is not produced by these other changes? Here we systematically go through them.

The most well known change is the shift from cone to rod photoreceptors. This can't account for our results, because the knockout undergoes the same cone-to-rod shift, and it doesn't undergo the shift to low

frequencies (Fig. 3.3). In addition, it's well known that the cone-to-rod shift affects high frequencies, not low. We show this in *Appendix 1*, Fig. 3.5, specifically for our species, the mouse. As shown in the figure, the frequency response curves for the rod and cone are both flat below 0.5 Hz, meaning there is no frequency-dependent change in this region. In contrast, our results show a selective boost at frequencies below 0.5 Hz; that is, the system shifts to favor low frequencies. The shift from cones to rods can't account for this.

Another change that occurs during dark adaptation is rod-cone coupling (see Ribelayga et al., 2008, for rod-cone coupling as a result of circadian rhythms; also Wang and Mangel, 1996, Trumpler et al., 2008, and Yang and Wu, 1989b). Rod-cone coupling, though, is mediated by gap junctions formed by Cx36, Cx35, and Cx34.7 (reviewed in Li et al. (2009)), not Cx57 (Janssen-Bienhold et al., 2009). Cx57 is not present in rods and cones (Hombach et al., 2004; Janssen-Bienhold et al., 2009) and thus the knockout is not perturbing these couplings.

Similarly, gap junction coupling in the inner retina likely plays a role in dark adaptation, since the AII amacrine cells of the rod pathway are coupled by gap junctions (Bloomfield et al., 1997). However, Cx57 is not a gap junction in these cells (Janssen-Bienhold et al., 2009), so changes in inner retinal coupling can not account for our results.

Recent reports have indicated that some gap junctions act as hemichannels (Kamermans et al., 2001; Shields et al., 2007). If Cx57 acted in this fashion, it could provide for ephaptic transmission of a feedback signal. However, the possibility that Cx57 is a hemichannel has been examined at the

ultrastructural level, and ruled out (Janssen-Bienhold et al., 2009). Furthermore, feedback to photoreceptors has been shown to be intact in the Cx57 knockout by two groups (Shelley et al., 2006; Dedek et al, 2008).

Finally, a standard concern with most or all knockout experiments is that knocking out a gene could lead to secondary developmental effects. While we can't completely rule this out, there is no evidence for altered development in the Cx57 knockout: retinal anatomy appears unperturbed (Hombach et al., 2004, Shelley et al., 2006), temporal tuning by day, as measured at the ganglion cell and behavioral level, remains intact, i.e., is the same as in wild-type (Fig. 3.3D), and spatial processing, also measured at the ganglion cell and behavioral level, remains intact as well (Dedek et al., 2008). While compensatory effects are possible, the likelihood that they would lead to such close matches along all these axes is very low.

Thus, while cone-to-rod shifts, photoreceptor coupling, and other factors contribute to dark adaptation, they can't account for the results presented here, and the probability that the results could be accounted for by developmental effects, as mentioned above, is very low.

One issue that we can't completely rule out, though, is the following: even though horizontal cell feedback to photoreceptors is known to be present and can account for our results, we can't completely rule out the possibility that the shunting of horizontal cell current causes the shift in tuning through some other action. For example, if horizontal cells were to act as a mediator between multiple circuits with different kinetics (e.g., different photoreceptor readout circuits), then the shunting of the horizontal cell current could shift

tuning by causing a switch from one circuit to another. But note that any alternative model must be consistent with the known constraints: (a) the difference between wild-type and knockout is present under scotopic conditions (Fig. 3.3), where all responses are rod-driven, (b) the tuning shift involves low frequencies, (c) the mouse retina has only one kind of horizontal cell, and it serves both kinds of photoreceptors, and (d) connexin-57 is only involved in horizontal cell-to-horizontal cell coupling. We chose the horizontal cell feedback model shown in Fig. 3.2 because it is a parsimonious model that satisfies these constraints and is consistent with current known actions of horizontal cells.

We conclude by mentioning that in one species (the rabbit), when light levels are much lower, more than an order of magnitude below the scotopic level used in this study, gap junctions close (Xin and Bloomfield, 1999) with no corresponding reversal of the shift in integration times (Nakatani et al., 1991). This suggests that in this extreme range, other mechanisms must take over, mechanisms likely intrinsic to the photoreceptors, as described in Tamura et al. (1989).

3.3.4 Relation of Cx57 to spatial processing in the dark- and light-adapted conditions

Horizontal cells provide negative feedback to photoreceptors (Werblin and Dowling, 1969) and antagonistic feedforward to bipolar cells (Yang and Wu, 1991), and it has long been thought that they contribute to the receptive field surround. One might expect, therefore, that eliminating coupling in these cells

would alter spatial processing as well as temporal processing as the retina shifts from day to night vision. A previous study, though, shows that spatial tuning remains normal in the Cx57 knockout (Dedek et al., 2008). The likely basis for this is the fact that the surround is generated by circuits in more than one layer – specifically, by amacrine cell circuits in the inner retina, as well as by horizontal cells in the outer retina (Cook and McReynolds, 1998; Taylor, 1999; Roska et al., 2000; Flores-Herr et al., 2001; McMahon et al., 2004; Sinclair et al., 2004). As mentioned in Dedek et al. (2008), the lack of a change in spatial tuning in the knockout, implies that inner retinal mechanisms dominate for the problem of adjusting spatial tuning to different light-adaptation levels.

3.3.5 Coupling as a mechanism to produce synchrony

We conclude by mentioning that gap junction coupling has also been proposed as a mechanism to create synchronous firing among neurons, e.g., for creating oscillations (for review, see (Bennett and Zukin, 2004)). The idea presented in this paper – that changes in coupling serve as a way to inactivate a cell class or reduce its impact – is not mutually exclusive with this proposal. This is because the effect of coupling depends on the state of the cell. As mentioned above, when a cell becomes coupled to other cells, its input resistance drops. For spiking neurons, this means the probability of reaching threshold and firing is reduced. If, however, the cell receives strong enough input to allow it to cross threshold, its firing can produce synchronous spikes in

coupled cells. Thus, gap junction coupling can potentially mediate more than one network operation.

3.4. Methods

3.4.1 Animals

Generation of the Cx57-deficient mouse line was previously reported (Hombach et al., 2004; Dedek et al., 2008). Briefly, part of the coding region of the *Cx57* gene was deleted and replaced with the *lacZ* reporter gene (Hombach et al., 2004). Cx57-deficient mice ($Cx57^{lacZ/lacZ}$) and wild-type (littermate) controls aged 2 to 4 months were used for all experiments. After each behavioral test or recording, the genotype of the retina was confirmed with staining for β-galactosidase activity and PCR as described (Hombach et al., 2004). All experiments were conducted in accordance with the institutional guidelines for animal welfare.

3.4.2 The degree of horizontal cell coupling and light intensity

Light intensities (photopic and scotoptic) were chosen to span the range where changes in horizontal cell coupling are at, or are close to, their largest. Xin and Bloomfield (1999) showed that coupling reaches its maximum between 1 and 1.5 log units above rod threshold and its minimum at or above rod saturation (estimated at 3 log units above rod threshold. For the behavior experiments, scotopic intensity was 1.4×10^{-4} cd/m^2, which is between 0.9 and 2.1 log units above rod threshold, with mouse rod threshold estimated at 1×10^{-6} to 1.8×10^{-5} cd/m^2 (Prusky; Umino et al., 2008). Photopic intensity, 142 cd/m^2, was more

than 3 log units above rod saturation (Xin and Bloomfield, 1999). The light source was Dell, 2007FPb, Phoenix, AZ; neutral density filters were used to attenuate the monitor's output to the desired photopic and scotopic levels.

For the electrophysiology experiments, which were carried out with a different light source (Sony, Multiscan CPD-15SX1, New York, NY), the intensities were, for the scotopic, 4 x 10^{-4} cd/m^2, which is between 1.3 and 2.6 log units above rod threshold, and, for the photopic, 23 cd/m^2, which is still >3 log units above rod saturation. As above, neutral density filters were used to attenuate the monitor's output to the desired photopic and scotopic levels.

3.4.3 The relation of horizontal cell input resistance to coupling for scotopic versus photopic conditions and for wild type versus knockout animals.

As mentioned in the *Discussion*, the standard experimental measure of horizontal cell coupling is the length constant (Xin and Bloomfield, 1999; Shelley et al., 2006). Xin and Bloomfield measured length constants physiologically in the rabbit (via the dependence of the voltage response on distance from a light stimulus) under different scotopic and photopic conditions and found the maximal scotopic-to-photopic ratio to be ~3. (As indicated in the previous section, the conditions used in this paper were matched to those that produce the maximal ratio.) Given this length constant ratio and the relations below, we can find the quantity we need, the input resistance ratio due to gap junction coupling. As given in (Xin and Bloomfield, 1999),

$$\lambda = \sqrt{\frac{R_m}{R_s}}, \qquad (1)$$

where λ is the length constant, R_m is the membrane resistance, and R_s is the junctional resistance (also referred to as the sheet resistance). Rearranging in terms of R_s gives

$$R_s = \frac{R_m}{\lambda^2}. \tag{2}$$

For a 2-D cable and a point source, the input resistance, Z, is proportional to R_s. This follows from eq. 2 of Lamb (1976) (See *Appendix 2* eqs. 9-14 for details). Thus, it follows from eq. 2 that

$$Z \propto \frac{R_m}{\lambda^2}. \tag{3}$$

This indicates that a 3-fold greater value of λ, as was measured by Xin and Bloomfield, corresponds to a 9-fold smaller value of Z, assuming that R_m remains the same in the scotopic and photopic conditions. Bloomfield notes that R_m may actually be higher in the photopic, indicating that a factor of 9 may be an underestimate.

The same analysis can be used to determine the input resistance ratio for the knockout and wild-type mouse using the measurements of Shelley et al. (2006), which were taken in these animals. These measurements, however, were taken only at one light level, and thus can provide only a lower bound on the ratio. Shelley et al. report a 2.3-fold greater value for λ in wild-type as compared to knockout, which, following eq. 3, corresponds to a

2.3^2=5.29-fold lower value for Z. It should be noted that R_m, as measured in isolated horizontal cells, is 27% lower in the knockout than the wild-type. When this is taken into account in eq. 3, the wild-type-to-knockout ratio for Z is $(1-0.27)/(1/2.3^2)$=3.86. We emphasize again that this is a lower bound on the input resistance ratio, since, as mentioned above, Shelley et al. measured length constants in knockout and wild-type only at a single light level.

Note that the 27% decrease in R_m has an additional implication: the observed change in temporal tuning that results from the change in coupling constitutes a lower bound, as the decrease in R_m would have the effect of reducing the difference between knockout and wild-type.

3.4.4 Behavioral testing using a virtual optokinetic system

Behavioral responses were measured using the Prusky/Douglas virtual optokinetic system (Prusky et al., 2004; Douglas et al., 2005). Briefly, the freely-moving animal was placed in a virtual reality chamber. A video camera, situated above the animal, provided live video feedback of the testing arena. A pattern was projected onto the walls of the chamber in a manner that produced a drifting sine wave grating of fixed spatial frequency when viewed from the animal's position (0.128 cycles/degree, following the stimulus protocol of (Umino et al., 2008)). A drifting grating of a pre-selected temporal frequency at 100% contrast appeared, and the mouse was assessed for tracking behavior, as in Prusky et al. (2004). Grating contrast was systematically reduced until no tracking response was observed. The reciprocal of this threshold contrast was taken as the contrast sensitivity.

3.4.5 Stimulating and recording ganglion cell responses

Three stimuli were used: drifting sine wave gratings, a binary random checkerboard (white noise), and a spatially uniform stimulus with natural temporal statistics (natural scene). The sine wave gratings were presented at 8 temporal frequencies, ranging from 0.15 to 6 Hz, all with a spatial frequency of 0.039 cycles/degree. This spatial frequency was lower than the one used in the behavioral experiments, to ensure robust responses at the scotopic intensity. Each temporal frequency was presented for 2 minutes. The white noise stimulus was a random checkerboard at a contrast of 1, in which the intensity of each square (9 degrees x 9 degrees in mouse) was either white or black, randomly chosen every 0.067 s (large checkers were chosen to ensure stimulation of the large ganglion cell receptive fields at scotopic intensities, as indicated in (Dedek et al., 2008))**.** The natural scene stimulus was a spatially uniform movie whose intensities were taken from a time series of natural intensities (van Hateren, 1997), resampled for presentation at a 0.100 s frame period. This movie was 2 minutes long and presented 10 times, interleaved with a 2 s grey (mean intensity) screen. Measurements always started at the scotopic intensity. After all three stimuli were presented, the light intensity was increased. After 20 min of adaptation to the photopic intensity, the stimuli were presented as above.

Extracellular recordings made from central retina using a multi-electrode array, as described previously (Nirenberg et al., 2001; Sinclair et al., 2004; Dedek et al., 2008). Retina pieces were approximately 1.5 to 2 mm

across, which corresponds to 4.5-6 horizontal cell length constants under scotopic conditions and 15-20 under photopic (As indicated above, there is an estimated factor of 3 difference in length constant between the scotopic and photopic conditions used here, with the photopic condition taken from Shelley et al. (2006) Fig. 3.7B, which gives a wild-type light-adapted length constant). Spike trains were recorded and sorted into units (cells) using a Plexon Instruments Multichannel Neuronal Acquisition Processor (Dallas, TX), as described previously (Nirenberg et al., 2001; Sinclair et al., 2004; Dedek et al., 2008)

Only ON ganglion cells were used, since the optomotor response in rodents is driven exclusively by the ON pathway (Dann and Buhl, 1987; Giolli et al., 2005). With respect to cell selection, only cells with readily detectable (by eye) spike triggered averages (STAs) were included in the data set; this corresponds to cells whose STA in the center checker of the receptive field was approximately 1.5 times above background.

3.4.6 Data Analysis

Temporal tuning curves were created from ganglion cell responses to drifting sine wave gratings using standard methods (Enroth-Cugell and Robson, 1966; Purpura et al., 1990; Croner and Kaplan, 1995). Briefly, for each grating, the first harmonic of the cell's response, $R(\mathbf{f})$, was calculated as follows:

$$R(\mathrm{f}) = \left| \frac{1}{L} \sum_{j} \exp\left[-i 2\pi \mathrm{f}\, t_j\right] \right| \qquad (4)$$

where **f** is the temporal frequency of the drifting sine wave grating (cycles/s), *L* is the duration of the stimulus (s), which was always an integer multiple of 1/**f**, and t_j is the time of the *j*th spike of the cell's response to the given grating. For averaging across cells, responses were weighted by the reciprocal of the peak sensitivity, so that each cell's tuning curve contributed approximately equally to the average, independent of its absolute sensitivity.

Mutual information was estimated between the input and responses (for the white noise, the input was the stimulus intensity of the checkerboard square that produced the largest response for a given cell; for the natural scene, the input was the full-field intensity). Information was estimated at each frequency using the coherence rate, following (van Hateren and Snippe, 2001 Jun):

$$I(\mathrm{S},R) = -\log_2(1-\gamma^2(\mathrm{f})) \tag{5}$$

where γ(**f**) is the coherence between stimulus and response at temporal frequency **f**. Coherence was estimated using the multi-taper method (Chronux library for Matlab (Mitra and Bokil, 2007), available at http://chronux.org), using effective bandwidths of 0.27 Hz (white noise) and 0.33 Hz (natural scene). For averaging across cells, information curves were weighted by the reciprocal of their areas, so that each cell's information curve contributed approximately equally to the average. Note that the above estimation of information is only rigorously correct for a Gaussian linear channel, and is necessarily an underestimate of the true information. However, our focus is not on the amount of information *per se*, but on its frequency-dependence.

3.4.7 Filtered predator movies

The “predator” movie, taken with a handheld digital camera (Casio, Exilim EX-Z750, Dover, NJ), was filmed at 33 frames/s. The complete movie was filtered for each genotype, according to the behavioral data in Fig 3.3D left: 0.1 – 6 Hz for the wild-type photopic, the same for knockout photopic, 0.16 – 3.2 Hz for wild-type scotopic, and 0.38 – 3.13 Hz for knockout scotopic. Representative frames from each filtered version are shown in Fig. 3.4; the complete filtered versions are shown in *Appendix 4*.

3.5 Acknowledgements

We thank A. Molnar for helpful discussion, Y. Roudi, and K. Purpura for comments on the manuscript, and K. Willecke and colleagues for the use of the $Cx57^{lacZ/lacZ}$ mouse line. Fig. 3.3, panel A was adapted from a previous paper by our group, Dedek et al. (2008). This work was supported by funds from National Eye Institute R01 EY12978 to SN; CP was supported in part by T32-EY07138.

APPENDIX

Appendix 1: The frequency response difference between the rods and cones lies in the high frequencies, not the low

The shift to low temporal frequencies cannot be accounted for by the shift from cones to rods, as the cone-to-rod shift affects the high frequencies, not the low; see cone and rod impulse responses in Luo and Yau (2005), Nikonov et al. (2006). Here we show this explicitly in the model system we are using, the mouse. Fig. 3.5A shows the impulse responses of the two photoreceptors, and Fig. 3.5B shows the frequency responses, the latter generated by the Fourier transformation of the impulse responses. As shown in the figure, the frequency response difference lies in the high frequencies.

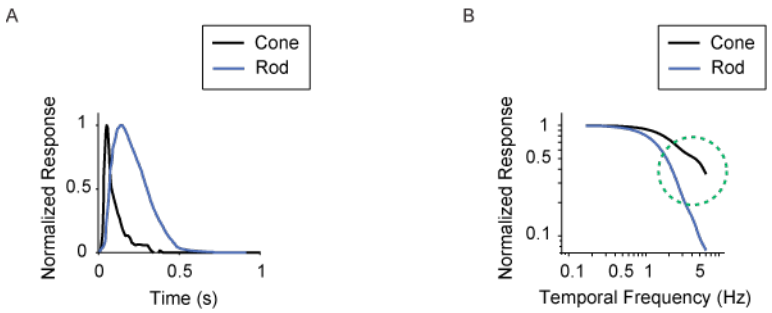

Figure 3.5 The frequency response difference between the rods and cones lies in the high frequencies, not the low.

(**A**) Impulse responses of the two photoreceptors, reproduced from Nikonov et al. (2006) for cone and Luo and Yau (2005) for rod. (**B**) Frequency responses

of the two photoreceptors, generated by Fourier transforming the impulse responses.

Appendix 2: Formal treatment of the model in Fig. 3.2: the effect of gap junction coupling on horizontal cell feedback to the photoreceptor

Section A of this Appendix formalizes the model of the photoreceptor-horizontal cell circuit to show how changing the strength of the horizontal cell feedback shapes the photoreceptor's temporal tuning, and, ultimately, the ganglion cell's temporal tuning. Section B then shows how a change in gap junction coupling modulates the strength of the horizontal cell feedback. Section C describes how these considerations apply to spatial configurations of the stimulus, and Section D briefly discusses how these considerations apply to other network geometries.

Section A

We start by briefly reiterating the model shown in Fig. 3.2. As mentioned in the main text, it builds on the well-known negative feedback between the horizontal cell and the photoreceptor, whereby the horizontal cell sends a signal to the photoreceptor that shortens the latter's integration time (Baylor et al., 1971; Kleinschmidt and Dowling, 1975; see also Smith, 1995).

To understand how the photoreceptor is able to shift its integration time from short to long as the retina is shifted from a light-adapted to a dark-adapted state, we proposed the following: In the light-adapted condition, the gap junctions of the horizontal cells close. This makes the horizontal cell

feedback signal strong and keeps the photoreceptor integration time short. In the dark, the gap junctions open. This causes a shunting of horizontal cell current, which reduces horizontal cell feedback and shifts the photoreceptors to long integration times.

The proposal is based on three established facts – that the integration time of photoreceptors increases as the retina moves from light-adapted to dark-adapted conditions (Kleinschmidt and Dowling, 1975; Daly and Normann, 1985; Schnapf et al., 1990), that the strength of the horizontal cell feedback signal decreases as the retina moves from the light-adapted to the dark-adapted condition (Teranishi et al., 1983; Yang and Wu, 1989a) and that the degree of horizontal cell coupling increases as the retina moves from the light adapted to the dark-adapted condition (Dong and McReynolds, 1991; Xin and Bloomfield, 1999; Weiler et al., 2000). Taken together, these facts led to a proposal for how the circuit shifts its behavior. The novelty was the view of gap junction coupling as a shunting device, that is, a mechanism that can turn up or down the activity of a cell class, in this case, the horizontal cells. With this view, the three facts can account for the shift from one state to another.

In the main text, we proposed this schematically. Here we formalize it and use the formalized model to determine the feedback strength required to produce the observed state change.

We start with the well-known data of Schneeweis and Schnapf (2000). The data are measurements of photoreceptor responses across a range of light-adaptation levels and show the shift in integration time that occurs as the retina moves from the dark-adapted state to states of increasing levels of light-

adaptation. We use the model to determine the change in feedback strength needed to produce the changes in photoreceptor integration time in Schneeweis and Schnapf (2000) and, ultimately, to produce the changes in ganglion cell integration time shown in this paper. (In Section B we show that the changes in feedback strength can be accounted for by the differences in horizontal cell coupling that occur in the dark- and light-adapted states.)

With these goals in mind, we use a linear systems approach. We do this for simplicity and generality, and because it allows us to focus on the essential features that lead to the shifts.

To construct the linear model, we denote the transfer function between light and the photoreceptor response in the absence of the feedback by $\tilde{P}(\omega)$, the feedback transfer function (photoreceptor output to horizontal cell, and back to photoreceptor) by $\tilde{F}(\omega)$, and the strength of the feedback by *g*. With this setup, the photoreceptor's output, $\tilde{L}(\omega, g)$, is given by the standard feedback formula (Oppenheim et al., 1997)

$$\tilde{L}(\omega, g) = \frac{\tilde{P}(\omega)}{1 + g\tilde{F}(\omega)}. \qquad (1)$$

To assign physiological values to the quantities in eq. (1), we use, as mentioned above, the measurements of Schneeweis and Schnapf (2000), who present photoreceptor responses in the dark-adapted state (i.e., the no-feedback or essentially-no-feedback state, $g = 0$) through several light-adapted states (i.e., various levels of feedback up to $g = 1$) (Fig. 3.6).

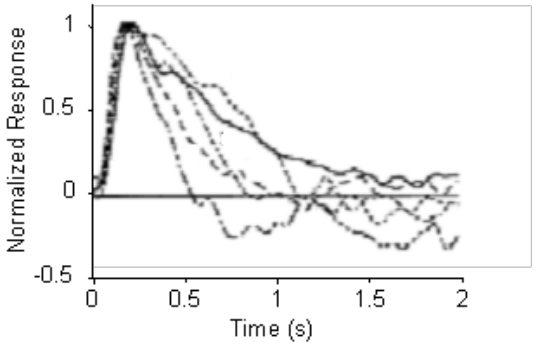

Figure 3.6 Measured photoreceptor responses at increasing levels of light adaptation.

Photoreceptor (macaque rod) responses under dark-adapted conditions (solid curve) and at increasing levels of light adaptation (dashed curves). The dark-adapted curve corresponds to the no-feedback or essentially-no-feedback condition; the light-adapted curves correspond to increasing levels of feedback. Adapted from Schneeweis and Schnapf (2000) with permission. Curves are peak-normalized and inverted so that light responses are plotted up.

We determine the photoreceptor transformation *P* directly from Schneeweis and Schnapf's dark-adapted data, since when $g = 0$, $P = L$ (see eq. (1)). Specifically, we use their fit for $P(t)$, which is a phenomenological fit, given by:

$$P(t) = (1 - w(t))At^n e^{-t/\tau_1} + w(t)Be^{-t/\tau_2}, \text{ where } w(t) = \frac{1}{1 + (\tau_3 / t)^m}, \qquad (2)$$

and $A = 3999$, $B = 1.68$, $\tau_1 = 0.063\,\text{s}$, $\tau_2 = 0.646\,\text{s}$, $\tau_3 = 0.200\,\text{s}$, $n = 3$, and $m = 4$. The corresponding transfer function $\tilde{P}(\omega)$ is then determined from the impulse response $P(t)$ by Fourier transformation. Both $P(t)$ and $\tilde{P}(\omega)$ are shown in Fig. 3.7A.

We then determine the feedback transformation *F* from the light-adapted measurements of Schneeweis and Schnapf. Since *F* was not measured directly, we proceed as follows. As mentioned above, *F* is the net result of two synapses in series: photoreceptor to horizontal cell, and horizontal cell back to photoreceptor. For simplicity, we use the same impulse response $f(t)$ for each synapse, and we use a difference of exponentials, a standard synaptic impulse response (Destexhe et al., 1995) for its functional form:

$$f(t) = e^{-(t-\delta)/\tau_a} - e^{-(t-\delta)/\tau_b} \text{ for } t \geq \delta\,, \tag{3}$$

Since the two synapses act in series, the feedback transfer function $\tilde{F}(\omega)$ is proportional to the product of the transfer functions at each synapse. We also include an overall scale factor F_0 in $\tilde{F}(\omega)$, so that we can pin the modeled response at $g = 1$ to the measured response at the highest level of light adaptation. Since we use the same transfer function $\tilde{f}(\omega)$ for the two synaptic components of *F*, the transfer function of the feedback transformation is given by

$$\tilde{F}(\omega) = F_0 \tilde{f}(\omega)^2\,. \tag{4}$$

The parameters ($\tau_a = 0.5$ s, $\tau_b = 0.01$ s, $\delta = 0.01$, and $F_0 = 10$) are chosen so that for a maximal feedback strength of $g = 1$, the photoreceptor output *L* given by eq. (1) matches the most light-adapted response obtained by Schneeweis and Schnapf. The feedback impulse response $F(t)$ is the inverse Fourier transform of $\tilde{F}(\omega)$; both are shown in Fig. 3.7B. As seen in Fig. 3.7C, without changing this feedback transformation – just changing its strength *g* – the feedback model accounts for Schneeweis and Schnapf's responses at intermediate light levels.

To summarize, then, the modeled photoreceptor responses (Fig. 3.7C) closely match the observed photoreceptor responses of Schneeweis and Schnapf (Fig. 3.6) (also reproduced in 3.7D for the reader's convenience). This enables us to obtain an estimate of the horizontal cell feedback strength needed to produce the range of changes in photoreceptor tuning. As shown in the figure, an approximate 10-fold change is needed: since $g = 0$ and $g = 0.1$ give nearly identical responses, we take $g = 0.1$ as the lower end of the range.

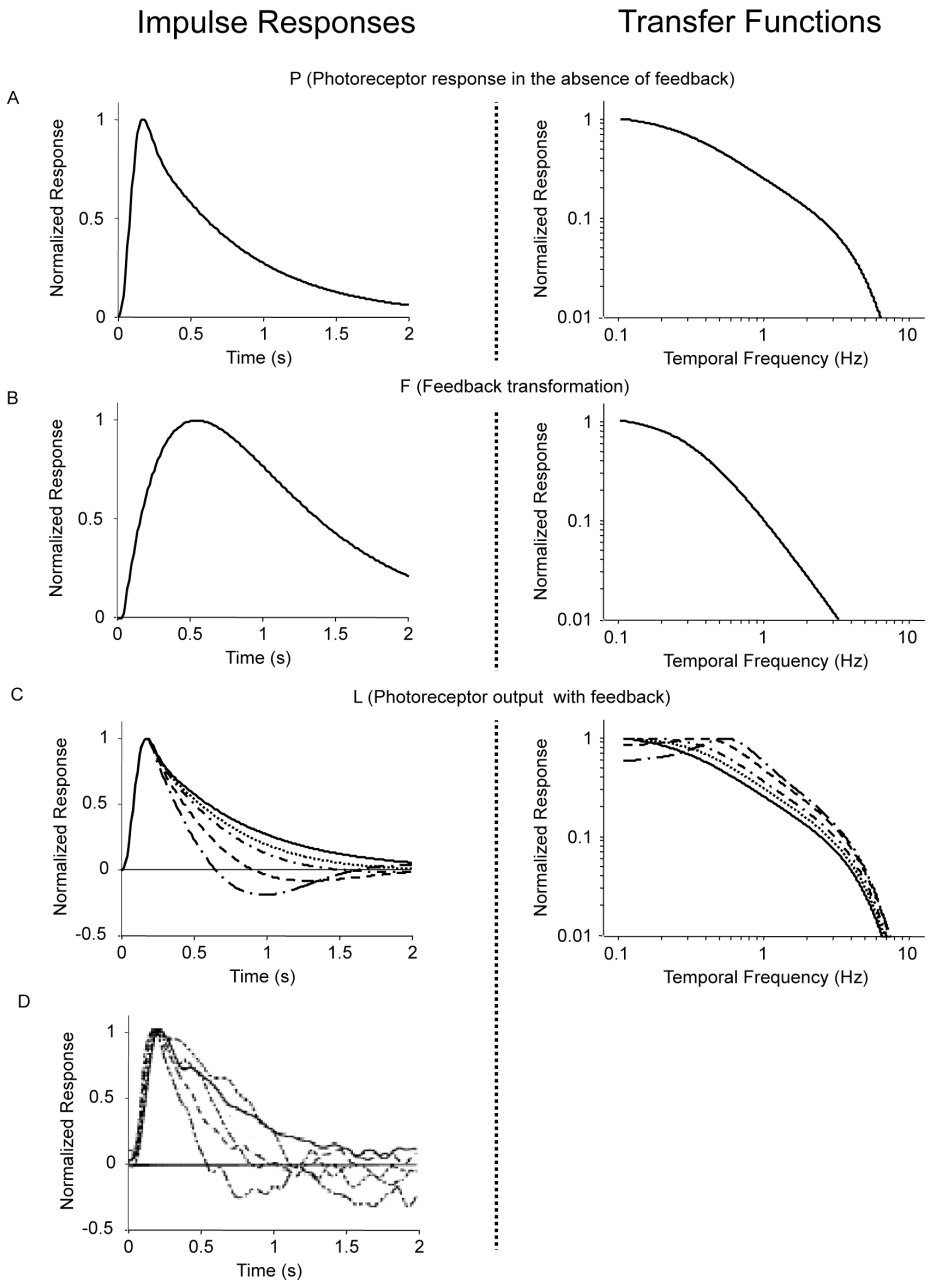

Figure 3.7 Modeled photoreceptor responses at increasing levels of light adaptation.

Impulse responses (left) and transfer functions (right) for the components of a simple feedback model of photoreceptor responses at increasing levels of light adaptation. (**A**) P, the response of the photoreceptor in the absence of feedback, corresponding to the dark-adapted state. (**B**) The feedback transformation F. (**C**) The resulting photoreceptor output, L (eq. (1)). The g=0-curve (solid) is the same as Panel A; the dashed curves correspond to g = 0.1, 0.2, 0.5, and 1. (**D**) The photoreceptor responses reported by Schneeweis and Schnapf (2000), as in Fig. 3.6. All curves are shown peak-normalized; transfer functions are plotted as a function of frequency, $f = \omega / 2\pi$.

We now relate the photoreceptor output to the ganglion cell output. Specifically, we take into account the transformations that occur in the second processing layer of the retina (the inner plexiform layer). While these transformations have many details (Werblin and Dowling, 1969; Victor, 1987; Sakai and Naka, 1988), the common denominator is that signals become more transient, i.e., high-pass filtering occurs. We represent this with a standard RC filter in feedback configuration,

$$\tilde{X}(\omega) = \frac{1 + i\omega\tau_I}{1 + k_I + i\omega\tau_I}, \qquad (5)$$

choosing the parameter values ($k_I = 4$ and $\tau_I = 6$ s) to match the dark-adapted ganglion cell response, as in Fig. 3.3C (wild type). Thus, the ganglion cell response is determined by the output of the photoreceptor-horizontal cell

feedback circuit (eq. (1)), followed by the schematic inner plexiform layer filter (eq. (5)):

$$\tilde{R}(\omega, g) = \tilde{X}(\omega)\tilde{L}(\omega, g) = \tilde{X}(\omega)\frac{\tilde{P}(\omega)}{1 + g\tilde{F}(\omega)}. \qquad (6)$$

Fig. 3.8 shows the results. Panel A recapitulates the photoreceptor output from Fig. 3.7C, and panel B shows the corresponding ganglion cell output after applying eq. (6). (Panel C shows the same result on a semilog plot, to be consistent with the main text.) As shown in Panel C, as horizontal cell feedback strength decreases, the temporal tuning of the ganglion cell response shifts to lower frequencies. The shift in the peak frequency is approximately 3-fold, from 0.6 Hz to 0.2 Hz, and can be accounted for by a factor of 10 reduction in horizontal cell feedback strength. Since the shift we observe in Fig. 3.3C is a subset of this, a 10-fold change in feedback strength more than suffices to account for the shift in tuning we observe at the ganglion cell output.

To summarize: Using the data of Schneeweis and Schnapf (2000) as the starting point, we showed that, as horizontal cell feedback strength increases, the tuning of the photoreceptor and, ultimately, the ganglion cell, shifts to higher frequencies. As shown in Fig 3.8C, the peak frequency shift is approximately 3-fold and can be accounted for by a 10-fold change in horizontal cell feedback strength. Since the shift we present in the main text (Fig. 3.3C) is a subset of this, a 10-fold change in feedback strength is more than sufficient to account for it.

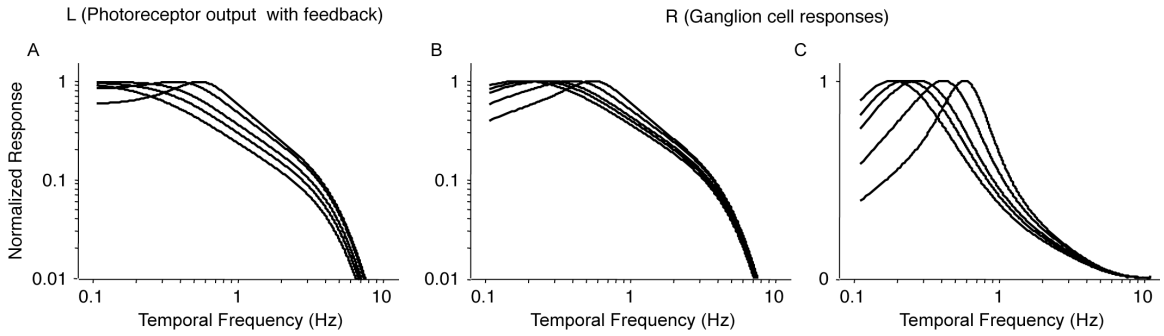

Figure 3.8 Modeled ganglion cell responses at increasing levels of light adaptation.

(**A**) Transfer functions for photoreceptor output (L, eq. (1)) at increasing levels of light adaptation (i.e., increasing levels of horizontal cell feedback), taken from Fig. 3.7C. (**B**) Transfer functions for ganglion cell responses (R, eq. (6)), obtained by high-pass filtering the curves in (**A**). (**C**) Same as (**B**), but plotted on semilog coordinates. These curves are reproduced in Fig. 3.2. From left to right within each panel, values of feedback strength are: g = 0, 0.1, 0.2, 0.5, and 1.0.

In the next section, we show how the measured changes in gap junction coupling are sufficient to produce the changes in feedback strength (an expansion of the analysis presented in Methods).

We conclude the section by mentioning that the analysis done here focused on rod conditions, that is, rod responses were shown with various levels of horizontal cell feedback. We focused on rod conditions, since these are directly compared in the main figure of the text, Fig. 3.3C. Specifically, Fig.

3.3C compares the rod condition in the high feedback state (the state in the knockout in the dark, where horizontal cells are forced to remain uncoupled) with the low feedback state (the state in the wild-type in the dark, where horizontal cells are maximally coupled).

Section B

In this section we detail the relationship between changes in gap junction coupling and horizontal cell feedback strength, an expansion of the description in Methods, Sec. 4.3. We show that the measured changes in coupling are sufficient to produce a 10-fold change in feedback strength and thus are sufficient to account for our results and also for the larger range of shifts shown in Fig. 3.8C.

As mentioned in Methods, the standard measure of horizontal cell coupling is the length constant. The strength of the horizontal cell signal, on the other hand, is determined by the cell's input resistance, since the cell's voltage response is the input resistance multiplied by the input current (Ohm's law). Thus, to determine how much the horizontal signal changes, we need to determine how much of a change in input resistance is produced by a measured change in length constant.

This is readily accomplished with a well-known model of the horizontal cell network, the two-dimensional cable (Naka and Rushton, 1967; Lamb, 1976; Xin and Bloomfield, 1999; Packer and Dacey, 2005; Shelley et al., 2006). We use the two-dimensional cable model to link horizontal cell coupling and length constant, and then to link length constant and input

resistance. As we will show, input resistance is inversely proportional to the square of the length constant (for a point source of current, but see also Section C). Xin and Bloomfield (1999) measured length constants under different degrees of coupling. Their results showed that length constant increases by a factor of 3 between the minimally- and maximally-coupled states. A 3-fold increase in length constant corresponds to a 9-fold decrease in feedback strength, nearly the 10-fold change needed to account for the complete range of shifts in Fig. 3.8C.

The following details the link between horizontal cell coupling and length constant, and then the link between length constant and input resistance. We focus on the regime in which capacitative effects can be neglected, since the phenomena of interest occur below 2 Hz. At the end of Section D, we comment on how the analysis can be extended to include capacitative effects.

As mentioned above, we start by modeling the horizontal cells as a two-dimensional sheet, as is standard (Naka & Rushton 1967; Lamb, 1976; Xin and Bloomfield, 1999; Packer and Dacey, 2005; Shelley et al 2006). Within this sheet, horizontal cell coupling determines resistance to current flow, and we denote the sheet resistance by R_s. Thus, our immediate goal is to link R_s to length constant, denoted by λ.

This linkage is well-known, and is given by the classic work of Lamb (1976). As Lamb showed (his eq. 2) the length constant of a two-dimensional sheet is given by

$$\lambda = \sqrt{R_m / R_s}\,, \tag{7}$$

corresponding to eq. 1 in the main text. Rearranging this yields

$$R_s = R_m / \lambda^2\,, \tag{8}$$

corresponding to eq. 2 in the main text. Eq. (8) demonstrates the relationship between length constant λ and horizontal cell coupling, as measured by the sheet resistance R_s.

The next step is to link input resistance to length constant. We start with a point source current, and consider other geometries in Sections C and D. For a point source current, we begin with Lamb (1976) (his eq. 8), which provides the voltage response of the sheet. At a distance *r* from the injection of a current i_0, the resulting voltage $V(r)$ is

$$V(r) = i_0 \frac{R_s}{2\pi} K_0(r/\lambda)\,, \tag{9}$$

where K_0 is a modified Bessel function of the second kind.

Input resistance is the ratio of the voltage response to the injected current. At a distance *r* from the point source, the ratio $Z_r = V(r)/i_0$ is

$$Z_r = \frac{V(r)}{i_0} = \frac{R_s}{2\pi} K_0(r/\lambda), \tag{10}$$

which follows from eq. (9).

We would like to use eq. (10) to determine Z_r at $r = 0$ (the point of injection), and how it depends on the horizontal cell parameters. Since the Bessel function in eq. (10) diverges at the origin, Z_0 is formally undefined. However, real measurements correspond to values of *r* that are small but not zero. Therefore, instead of focusing on Z_0, we focus on the limiting behavior of Z_r when *r* is small.[2]

To determine the behavior in the small-*r* limit, we approximate the Bessel function in eq. (10), whose argument is $u = r/\lambda$. When this argument is small (i.e., when $r << \lambda$), the Bessel function has an asymptotic expansion, $K_0(u) = -\ln u\left(1 + o(u)\right)$ ((Abramowitz and Stegun, 1965), eq. 9.6.54). Therefore,

$$Z_r = -\frac{R_s}{2\pi}\ln(r/\lambda)\left(1 + o(r/\lambda)\right) = \frac{R_s}{2\pi}\left(\ln(\lambda) - \ln(r)\right)\left(1 + o(r)\right). \tag{11}$$

In the small-*r* limit, the $-\ln(r)$-term grows, eventually dominating the $\ln(\lambda)$-term, Thus, Z_r has an asymptotic expansion

$$Z_r = -\frac{R_s}{2\pi}\ln r\left(1 + o(r)\right). \tag{12}$$

[2] For an alternative derivation that relies only on a dimensional analysis, see section D.

Eq. (12) shows that in the limit of a point current injection, input resistance and sheet resistance are proportional (corresponding to the comment following text equation 2). Finally, we use the relationship between sheet resistance and length constant (eq. (8)) to rewrite eq. (12) as

$$Z_r = -\frac{R_m}{2\pi\lambda^2}\ln r\left(1+o(r)\right). \tag{13}$$

Thus, in the small-*r* limit, the input resistance is proportional to R_m and inversely proportional to λ^2, as in eq. 3 in the main text:

$$Z_r \propto \frac{R_m}{\lambda^2}. \tag{14}$$

To summarize: horizontal cell coupling (sheet resistance) determines the length constant via eq. (7), and these are linked to input resistance via eqs. (12) and (13).

Section C

Above, we considered the input resistance for a point input source; we now turn to consider other spatial patterns. To do this systematically, we determine the input resistance for spatial grating pattern of spatial frequency *k*, which we denote $Z(k)$. That is, $Z(k)$ is the ratio of the voltage response to an applied grating-shaped current. We determine this voltage response by first

determining the response to a current injected along a narrow line. Then we superimpose a continuum of line sources to form the grating.

In the scenario of a current injected along a narrow line (say, along the *y*-axis) into a sheet in the (x, y)-plane, there is translational symmetry along the *y*-axis. Along the *x*-axis, the problem reduces to that of a one-dimensional cable. (This is the geometry considered by Xin and Bloomfield, 1999)). Thus, we can use standard one-dimensional cable theory to determine the resulting voltage distribution: at a distance *x* from a line of injected current I_0, the resulting voltage distribution is:

$$V_{line}(x) = I_0 Z_0 e^{-|x|/\lambda}, \tag{15}$$

where

$$Z_0 = \frac{1}{2}\sqrt{R_m R_s} \tag{16}$$

is the input resistance of the equivalent one-dimensional cable (Koch and Segev, 1998).

Next, we create a grating from these line sources. At each location x_0 along the *x*-axis, we place a source with strength $I(x_0;k) = I_0 \cos(kx_0)$; the net result of these sources is a spatial grating of current. Each of these sources yields a voltage response according to eq. (15), and they superimpose to yield the voltage response to the grating. Specifically, the contribution of the line

source at position x_0 to the voltage at position *x* is $V_{line}(x-x_0)\cos(kx_0)$, and superimposing them yields the grating response:

$$V_{grating}(x;k) = \int_{-\infty}^{\infty} V_{line}(x-x_0)\cos(kx_0)dx_0 . \qquad (17)$$

Carrying out this Fourier integral yields

$$V_{grating}(x;k) = \cos(kx)\int_{-\infty}^{\infty} V_{line}(u)e^{iku}du = \cos(kx)\frac{I_0 Z_0}{\lambda}\frac{2}{1/\lambda^2 + k^2} . \qquad (18)$$

Thus, $Z(k)$, the input resistance for a current injection patterned as a sinusoid of spatial frequency *k*, is the ratio of the voltage response to the applied current:

$$Z(k) = \frac{V_{grating}(0;k)}{I_0} = \frac{Z_0}{\lambda}\frac{2}{1/\lambda^2 + k^2} = R_m \frac{1}{1+\lambda^2 k^2} , \qquad (19)$$

where we have used eqs. (7) and (16) in the last step.

Eq. (19) shows how length constant and spatial frequency interact to determine the input resistance. At sufficiently low spatial frequencies, the shunt current has nowhere to go, so the input resistance is R_m, independent of the length constant. At sufficiently high frequencies, the shunt is very effective: input resistance is inversely proportional to λ^2, just as in the point source. For example, at $k = 3/\lambda$, $Z(k)=R_m/10$, indicating that 90% of the input resistance can be shunted away, while at $k = 1/\lambda$, $Z(k)=R_m/2$, indicating that half of the input resistance can be shunted away. Since spatial frequency *k* is

measured in radians, the latter corresponds to a spatial wavelength of $2\pi\lambda$. Thus, perhaps counterintuitively, eq. (19) shows that the shunt retains effectiveness even for a grating pattern whose period is a fairly large multiple (2π) of the length constant.

To summarize: the reduction in input resistance due to gap junction coupling diminishes at low spatial frequencies, but the falloff is gentle, as shown in eq. (19). For gratings whose period is small in comparison to $2\pi\lambda$, the shunt remains large. This was the case in the present experiments under scotopic conditions. We used gratings of 0.039 c/deg, corresponding to a spatial period of 795 μm (in the mouse retina, 1 deg = 31 μm (Remtulla and Hallett, 1985)), and a spatial frequency *k* of $2\pi/795 = 0.0079\mu\text{m}^{-1}$. Given the estimated scotopic length constant of $\lambda = 300\mu\text{m}$ (see Methods, sec. 4.5), eq. (19) yields $Z(k) = 0.15R_m$, indicating that 85% of the signal can be shunted away.

We conclude by mentioning that while the interaction of spatial pattern and gap junction coupling is a potentially interesting topic, the paper focused on temporal processing and, thus, was not set up to explore this: this is because of a limitation in the size of the retinal pieces used for the multi-electrode array recording. To test the predictions in eq. (19), retinal pieces of greater than twice the size would be needed to avoid edge effects (shunting through contact with the edge of the retinal piece) and to allow sampling of sufficiently low spatial frequencies. We included the above discussion of the theoretical effects of spatial pattern in any case, because it makes predictions for future work, both in retina and other brain areas where gap junction

coupled networks are present.

Section D

Because the gap-junction switch has the potential to operate in a wide range of neural networks, here we briefly note how the above considerations generalize to geometries not directly related to the horizontal cell network of the retina.

First, we mention that the notion that gap junction conductance modulates input resistance is not limited to situations in which the gap-junction-coupled cells form part of a feedback loop. That is, opening the gap junctions of a group of neurons is simply a general way to reduce their gain and thus remove them functionally from a network, whatever their role.

For networks within the brain parenchyma, a three-dimensional space-filling network may be a more appropriate caricature than a two-dimensional syncytial sheet. (We have in mind a scenario in which each neuron is connected to its neighbors in all three spatial dimensions, but that only a part of the volume is occupied by these neurons.) In this case, the dependence of input resistance on gap junction coupling is $Z \propto R_s^{3/2}$, an even stronger dependence than the proportionality which holds in two-dimensional case, eq. (12).

To see this, we apply a dimensional analysis. In three dimensions, the resistance R_m to the bath (i.e., extracellular space) has units of ohm-cm^3, and the internal resistance, R_s, has units of ohm-cm. Thus, the input resistance for a point source must be proportional to $\sqrt{R_s^3 / R_m}$, since this is the only

parameter combination that has units of ohms. The length constant λ is still $\sqrt{R_m / R_s}$, so the input resistance is also proportional to R_m / λ^3.

There is a simple intuition behind this result and the corresponding ones results in the earlier sections: for a point source, the input resistance decreases in proportion to the number of neurons to which an input current spreads. In a "cable" of effective dimension *D* and length constant λ, this number is proportional to λ^D.

Finally, we mention that in all of the above analyses, we have considered the gap-junction-coupled network to be purely resistive. This is a reasonable approximation for the experiments considered here: the phenomena of interest occur below 2 Hz. These frequencies are much slower than the estimated RC time constant for the horizontal cell, which is 20 ms, based on membrane resistance and capacitance values provided by Smith et al. (1995). Nevertheless, our treatment immediately generalizes to scenarios in which capacitive effects become relevant, by replacing the resistance parameters R_m, R_s, and Z by corresponding frequency-dependent impedances (Koch and Poggio, 1985). The cable formalism still applies, but now, the effective length constant will be frequency-dependent, and the shunt may be associated with a phase shift.

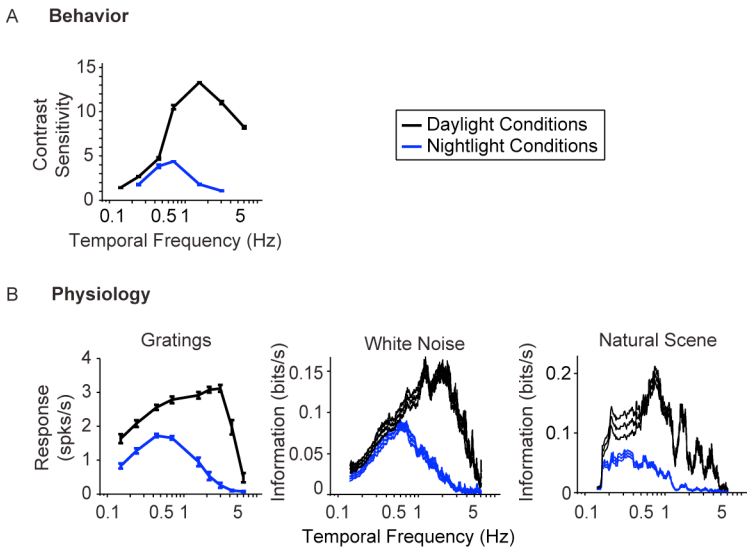

Figure 3.9 The visual system undergoes a shift in integration time as it shifts from day to night (photopic to scotopic) conditions.

This figure reproduces the data in Fig. 3.1, but un-normalized. Note that in the un-normalized plots, the shift in tuning to low temporal frequencies is superimposed on an overall decrease in sensitivity, as is well-known at the behavioral level (Kelly, 1961 (human), Umino et al., 2008 (mouse)) and at the ganglion cell level (Purpura et al., 1990).

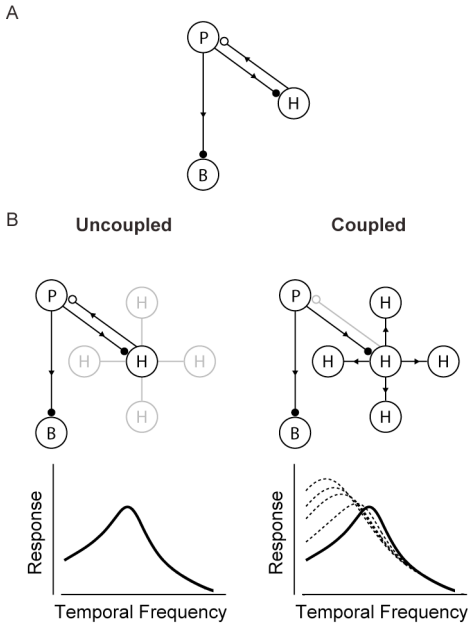

Figure 3.10 The circuit that controls visual integration time can be shifted from one state to another by a change in the gap junction coupling of one of its cell classes.

This figure reproduces the model shown in the main text, but with the response curves un-normalized (see Fig. 3.2 or Fig. A2.8C).

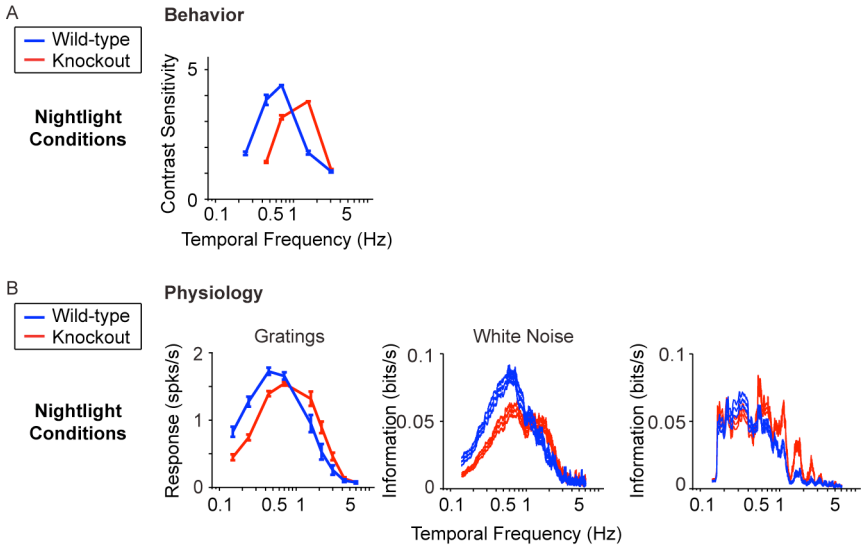

Figure 3.11 When coupling is prevented, the shift to long integration times is impaired at both the behavioral level and the ganglion cell level. This figure reproduces the data in Fig. 3.3, but un-normalized. As in the main text, the knockout response fails to make the normal shift in tuning to low temporal frequencies, because the feedback signal is not reduced by the shunt. Note that the un-normalized plots show that at low temporal frequencies, the wild-type response is higher, while at high temporal frequencies, the knockout response is higher. This is predicted by the model (Fig. 3.10, which shows the un-normalized model predictions; lower right of figure). Note also that this crossover (the higher response in the no-feedback state at low frequencies, and the higher response in the high-feedback state at high frequencies) is a well-known phenomenon in light adaptation (Purpura et al. 1990).

Appendix 4: The selective disadvantage of a Cx57 gene loss, demonstrated using a natural movie

As indicated in the main text, we filmed an approaching predator and restricted the movies to the temporal frequencies available to each genotype, using the data from Fig. 3.3D left. In Fig. 3.4 we showed single frames from the movies; here we show the movies in total. As indicated in the main text, in daytime conditions, the movies for the two genotypes are essentially the same – see Video 1, Wild-type by Day, and Video 2, Knockout by Day. In nighttime conditions, though, the two movies diverge. In the movie filtered through the frequencies visible to the wild-type animal, the predator is visible both when it is moving, i.e., when the movie is dominated by high frequencies, and when it is still, i.e., when the movie is dominated by low frequencies. In the movie filtered though the frequencies visible to the knockout, the predator disappears in the still condition. Only a ghost remains – see Video 3, Wild-type at Night, and Video 4, Knockout at Night.

The videos are available as Supplemental Material in the original article, published in the open access journal *Frontiers in Computational Neuroscience*:

http://www.frontiersin.org/computationalneuroscience/paper/10.3389/fncom.2010.00002

REFERENCES

Abramowitz M, Stegun IA (1965) Handbook of mathematical functions: with formulas, graphs, and mathematical tables: Courier Dover Publications.

Babai N, Thoreson WB (2009) Horizontal cell feedback regulates calcium currents and intracellular calcium levels in rod photoreceptors of salamander and mouse retina. J Physiol 587:2353-2364.

Baylor DA, Fuortes MG, O'Bryan PM (1971) Receptive fields of cones in the retina of the turtle. J Physiol 214:265--294.

Bennett MVL, Zukin RS (2004) Electrical coupling and neuronal synchronization in the Mammalian brain. Neuron 41:495--511.

Bonin V, Mante V, Carandini M (2006) The statistical computation underlying contrast gain control. J Neurosci 26:6346--6353.

Cepeda C, Walsh JP, Hull CD, Howard SG, Buchwald NA, Levine MS (1989) Dye-coupling in the neostriatum of the rat: I. Modulation by dopamine-depleting lesions. Synapse 4:229--237.

Croner LJ, Kaplan E (1995) Receptive fields of P and M ganglion cells across the primate retina. Vision Res 35:7--24.

Dann JF, Buhl EH (1987) Retinal ganglion cells projecting to the accessory optic system in the rat. J Comp Neurol 262:141--158.

De Valois RL, De Valois KK (1990) Spatial Vision. New York, NY: Oxford University Press.

Dedek K, Pandarinath C, Alam NM, Wellershaus K, Schubert T, Willecke K, Prusky GT, Weiler R, Nirenberg S (2008) Ganglion cell adaptability: does the coupling of horizontal cells play a role? PLoS ONE 3:e1714.

Desimone R, Duncan J (1995) Neural mechanisms of selective visual attention. Annu Rev Neurosci 18:193--222.

Dong CJ, McReynolds JS (1991) The relationship between light, dopamine release and horizontal cell coupling in the mudpuppy retina. J Physiol 440:291--309.

Douglas RM, Alam NM, Silver BD, McGill TJ, Tschetter WW, Prusky GT (2005) Independent visual threshold measurements in the two eyes of freely moving rats and mice using a virtual-reality optokinetic system. Vis Neurosci 22:677--684.

Dowling JE (1987) The retina: an approachable part of the brain. Cambridge, MA: Belknap Press.

Enroth-Cugell C, Robson JG (1966) The contrast sensitivity of retinal ganglion cells of the cat. J Physiol 187:517--552.

Galarreta M, Hestrin S (1999) A network of fast-spiking cells in the neocortex connected by electrical synapses. Nature 402:72--75.

Galarreta M, Hestrin S (2001) Electrical synapses between GABA-releasing interneurons. Nat Rev Neurosci 2:425--433.

Giolli RA, Blanks RHI, Lui F (2005) The accessory optic system: basic organization with an update on connectivity, neurochemistry, and function. Prog Brain Res 151:407--440.

Hombach S, Janssen-Bienhold U, Sohl G, Schubert T, Bussow H, Ott T, Weiler R, Willecke K (2004) Functional expression of connexin57 in horizontal cells of the mouse retina. Eur J Neurosci 19:2633--2640.

Kelly DH (1961) Visual response to time-dependent stimuli. I. Amplitude sensitivity measurements. J Opt Soc Am 51:422--429.

Kleinschmidt J, Dowling JE (1975) Intracellular recordings from gecko photoreceptors during light and dark adaptation. J Gen Physiol 66:617--648.

Maunsell JHR, Treue S (2006) Feature-based attention in visual cortex. Trends Neurosci 29:317--322.

McMahon DG, Mattson MP (1996) Horizontal cell electrical coupling in the giant danio: synaptic modulation by dopamine and synaptic maintenance by calcium. Brain Res 718:89--96.

McMahon DG, Knapp AG, Dowling JE (1989 Oct) Horizontal cell gap junctions: single-channel conductance and modulation by dopamine. Proc Natl Acad Sci U S A 86:7639--7643.

Mitra P, Bokil H (2007) Observed brain dynamics. New York, NY: Oxford University Press.

Nirenberg S, Carcieri SM, Jacobs AL, Latham PE (2001) Retinal ganglion cells act largely as independent encoders. Nature 411:698--701.

Ohzawa I, Sclar G, Freeman RD (1982) Contrast gain control in the cat visual cortex. Nature 298:266--268.

Onn S-P, Lin M, Liu J-J, Grace AA (2008 Feb 6) Dopamine and cyclic-AMP regulated phosphoprotein-32-dependent modulation of prefrontal cortical input and intercellular coupling in mouse accumbens spiny and aspiny neurons. Neuroscience 151:802--816.

Peskin CS, Tranchina D, Hull DM (1984) How to see in the dark: photon noise in vision and nuclear medicine. Ann N Y Acad Sci 435:48--72.

Prusky GT Personal communication; Prusky is a co-author on this paper.

Prusky GT, Alam NM, Beekman S, Douglas RM (2004) Rapid quantification of adult and developing mouse spatial vision using a virtual optomotor system. Invest Ophthalmol Vis Sci 45:4611--4616.

Purpura K, Tranchina D, Kaplan E, Shapley RM (1990) Light adaptation in the primate retina: analysis of changes in gain and dynamics of monkey retinal ganglion cells. Vis Neurosci 4:75--93.

Reynolds JH, Heeger DJ (2009) The normalization model of attention. Neuron 61:168--185.

Schneeweis DM, Schnapf JL (2000) Noise and light adaptation in rods of the macaque monkey. Vis Neurosci 17:659--666.

Shapley RM, Victor JD (1978) The effect of contrast on the transfer properties of cat retinal ganglion cells. J Physiol 285:275--298.

Shelley J, Dedek K, Schubert T, Feigenspan A, Schultz K, Hombach S, Willecke K, Weiler R (2006) Horizontal cell receptive fields are reduced in connexin57-deficient mice. Eur J Neurosci 23:3176--3186.

Sinclair JR, Jacobs AL, Nirenberg S (2004) Selective ablation of a class of amacrine cells alters spatial processing in the retina. J Neurosci 24:1459--1467.

Standage D, Paré M (2009) Flexible control of speeded and accurate decisions afforded by temporal gain modulation of decisional

processes. In: 39th Society for Neuroscience Annual Meeting. Chicago, IL.

Teranishi T, Negishi K, Kato S (1983) Dopamine modulates S-potential amplitude and dye-coupling between external horizontal cells in carp retina. Nature 301:243--246.

Trumpler J, Dedek K, Schubert T, de Sevilla Muller LP, Seeliger M, Humphries P, Biel M, Weiler R (2008 Jul 2) Rod and cone contributions to horizontal cell light responses in the mouse retina. J Neurosci 28:6818--6825.

Umino Y, Solessio E, Barlow RB (2008) Speed, spatial, and temporal tuning of rod and cone vision in mouse. J Neurosci 28:189--198.

van Hateren JH (1997) Processing of natural time series of intensities by the visual system of the blowfly. Vision Res 37:3407--3416.

van Hateren JH, Snippe HP (2001 Jun) Information theoretical evaluation of parametric models of gain control in blowfly photoreceptor cells. Vision Res 41:1851--1865.

van Nes FL, Koenderink JJ, Nas H, Bouman MA (1967) Spatiotemporal modulation transfer in the human eye. J Opt Soc Am 57:1082--1088.

Weiler R, Pottek M, He S, Vaney DI (2000) Modulation of coupling between retinal horizontal cells by retinoic acid and endogenous dopamine. Brain Res Brain Res Rev 32:121--129.

Xin D, Bloomfield SA (1999) Dark- and light-induced changes in coupling between horizontal cells in mammalian retina. J Comp Neurol 405:75--87.

Yang QZ, Hatton GI (2002) Histamine H1-receptor modulation of inter-neuronal coupling among vasopressinergic neurons depends on nitric oxide synthase activation. Brain Res 955:115--122.

Yang XL, Wu SM (1989) Effects of background illumination on the horizontal cell responses in the tiger salamander retina. J Neurosci 9:815--827.

Zsiros V, Maccaferri G (2008) Noradrenergic modulation of electrical coupling in GABAergic networks of the hippocampus. J Neurosci 28:1804--1815.

CHAPTER 4

Symmetry breakdown in the ON and OFF pathways of the retina at night: functional implications

Chethan Pandarinath[1], Jonathan D. Victor[2], and Sheila Nirenberg[1]

[1]Department of Physiology and Biophysics and [2]Department of Neurology and Neuroscience, Weill Medical College of Cornell University, New York, NY 10065

Abstract

Several recent studies have shown that the ON and OFF channels of the visual system are not simple mirror images of each other, that their response characteristics are asymmetric (Chichilnisky and Kalmar, 2002; Sagdullaev and McCall, 2005). How the asymmetries bear on visual processing is not well understood. Here we show that ON and OFF ganglion cells show a strong asymmetry in their temporal adaptation to photopic (day) and scotopic (night) conditions and that the asymmetry confers a functional advantage. Under photopic conditions, the ON and OFF ganglion cells show similar temporal characteristics. Under scotopic conditions, the two cell classes diverge – ON cells shift their tuning to low temporal frequencies, while OFF cells continue to

respond to high. This difference in processing corresponds to an asymmetry in the natural world, one produced by the Poisson nature of photon capture and persists over a broad range of light levels. This work characterizes a previously unknown divergence in the ON and OFF pathways and its utility to visual processing. Furthermore, the results have implications for downstream circuitry and thus offer new constraints for models of downstream processing, since ganglion cells serve as building blocks for circuits in higher brain areas. For example, if simple cells in visual cortex rely on complementary interactions between the two pathways, such as push-pull interactions (Alonso et al., 2001; Hirsch, 2003), their receptive fields may be radically different under scotopic conditions, when the ON and OFF pathways are out of sync.

4.1 Introduction

The ON and OFF pathways are among the most well-known examples of parallel processing in the visual system (Wassle, 2004). The division into these streams begins in the retina at the very first synapse – bipolar cells contain either sign-inverting or sign-conserving glutamate receptors, which determine whether they depolarize or hyperpolarize to light. The depolarizing and hyperpolarizing bipolar cells constitute two general classes of cells, termed ON and OFF bipolar cells. The ON and OFF bipolar cells send their axon terminals to separate sublaminae in the inner-plexiform layer, where they synapse with ganglion cell dendrites and shape ganglion cell responses. Thus, the split into cells that respond to ON and OFF signals in the retina is carried forth from the first synapse to the ganglion cell output.

Initially, the working hypothesis was that this ON and OFF output was essentially "equal and opposite," that is, the ON and OFF cells were thought to respond to the same features of the visual scene, just with opposite polarity. Evidence has begun to accumulate, though, that this description is too simple, that ON and OFF cells carry at least partially different information. Specifically, at the level of the retinal circuitry, studies have shown that the two pathways receive distinct inhibitory input (Pang et al., 2003; Zaghloul et al., 2003; Murphy and Rieke, 2006; Eggers et al., 2007; Molnar and Werblin, 2007). Further, at the level of retinal output, ON and OFF cells of the same class have been shown to have 10-20% differences in receptive field size and kinetics (Chichilnisky and Kalmar, 2002, but cf. Benardete and Kaplan, 1999, with respect to the kinetics), and additional differences in the degree of nonlinearity (Sagdullaev and McCall, 2005). The significance of these differences for visual processing is not well-understood. While a proposal has been made for the functional role of the difference in receptive field size (a spatial aspect) (Balasubramanian and Sterling, 2009), the roles of the differences in dynamics have yet to be determined.

Here we show that ON and OFF cells show a substantial difference in their temporal adaptation to day and night, and, further, that this difference has a functional advantage. We characterized the temporal responses of mouse ON and OFF ganglion cells using gratings and white-noise stimuli under photopic and scotopic conditions. Our results show that under photopic conditions, the pathways are, in fact, largely symmetric: their responses differ in sign, but their temporal characteristics are similar. Under scotopic

conditions, though, the pathways diverge – the tuning of the ON cells shifts to low temporal frequencies, whereas the tuning of the OFF cells remains high. Using a model for signal detection, we then address the issue at the functional level, showing how this difference corresponds to a natural asymmetry in the visual world.

These results show a new divergence in the ON and OFF pathways and its potential value for processing visual information. The results also have implications for downstream circuitry, specifically, for receptive field models that depend on ON and OFF interactions.

4.2 Materials & Methods

4.2.1 Experiments

Recording Ganglion cell spike trains were recorded from the central retina of C57BL/6J mice using a multi-electrode array, as described previously (Nirenberg et al., 2001; Sinclair et al., 2004; Dedek et al., 2008). Spikes were sorted into units (cells) using a Plexon Instruments Multichannel Neuronal Acquisition Processor (Dallas, TX). Five retinas were used in these studies. Retina pieces used for the recordings were approximately 1.5 to 2 mm across.

Stimulation The light source for these experiments was a Sony Multiscan CPD-15SX1 computer monitor. Neutral density filters were used to attenuate the monitor's output to the desired scotopic and photopic levels. The scotopic intensity was 2.8×10^{-5} mW/cm^2; the photopic was 0.25 mW/cm^2. Following (Lyubarsky et al., 2004) and using the spectrum of our monitor (Bohnsack et al., 1997), these radiometric units can be converted to photoreceptor

equivalent photons/mm^2/s: The scotopic intensity converts to 0.3 rod-equivalent-photons/mm^2/s, 0.3 M-cone-equivalent-photons/mm^2/s (in mouse, the rod and the M-cone have very closely matching absorption spectra (Lyubarsky et al., 1999, Nirenberg et al., 2001)), and 0.01 S-cone-equivalent-photons/mm^2/s, the photopic, to 2.7 x 10^3 rod-equivalent-photons/mm^2/s, 2.7 x 10^3 M-cone-equivalent-photons/mm^2/s, and 120 S-cone-equivalent-photons/mm^2/s. This gives a rate of 0.2 R*/rod/s, 0.1 R*/M-cone/s, and 5 x 10^{-3} R*/S-cone/s for scotopic, and 1.8 x 10^3 R*/rod/s, 900 R*/M-cone/s, and 40 R*/S-cone/s for photopic, assuming an effective collecting area (i.e., collecting area/ funneling factor) from (Lyubarsky et al., 1999; Lyubarsky et al., 2004) of 0.67 mm^2 for rods and 0.34 mm^2 for cones. Note that recordings were made in central retina, where most cones co-express both opsins (Applebury et al., 2000; Nikonov et al., 2006). Thus the numbers 900 R*/cone/s and 40 R*/cone/s constitute the range of photoisomerizations at the higher light intensity. See also *Appendix 3* for experiments with 2-amino-4-phosphonobutyric acid (APB) that show that responses to the low light level condition are mediated through the rod bipolar pathway.

Two stimuli were used: drifting sine wave gratings and a binary random checkerboard (white noise). The sine wave gratings were presented at 9 temporal frequencies, ranging from 0.15 to 6 Hz, all with a spatial frequency of 0.039 cycles/degree. Each temporal frequency was presented for 2 minutes. The white noise stimulus was a random checkerboard at a contrast of 1, in which the intensity of each square was either white or black, randomly chosen every 0.067 s. The size of the squares was 9 degrees x 9 degrees; this size

was chosen to elicit responses in the low light (scotopic) condition. The white noise stimulus was presented for 10 minutes. Note that the update rate of the white noise stimulus, 1/0.067=15 Hz, which would be considered low for some species, is appropriate for the mouse, whose ganglion cells' responses fall off rapidly above 5 Hz. The frequency range focused on in this paper is 3 Hz to 0.5 Hz (or lower). With a noise update rate of 15 Hz and a corresponding Nyquist frequency of 7.5 Hz, this range is well-covered. After both stimuli were presented, the light intensity was increased. After 20 min of adaptation to the photopic intensity, the stimuli were presented again, as above. All animals were dark-adapted for 1 hour prior to recording.

Assessing potential rundown due to bleaching Response rundown can occur due to bleaching during the photopic condtion. To assess this, we measured the firing rate in the responses to a periodic flashing stimulus at the beginning and end of the photopic condition. Firing rates between the beginning and end differed by less than 10% on average, and this was not significantly different between ON and OFF cells ($p > 0.5$, Student's *t*-test comparing the mean firing rate change of ON cells with that of the OFF cells).

4.2.2 Data Analysis

Designation of ON and OFF cells Cells were designated as ON or OFF using the spike triggered average to the checkerboard stimulus (see above). If the sign of the initial deflection was positive, the cells were designated as ON; if negative, then OFF.

Analysis of responses to drifting gratings For the drifting sine wave gratings, temporal tuning curves were created from ganglion cell responses using standard methods (Enroth-Cugell and Robson, 1966; Purpura et al., 1990; Croner and Kaplan, 1995). Briefly, for each grating, the first harmonic of the cell's response, $R(\mathbf{f})$, was calculated as follows:

$$R(\mathbf{f}) = \left| \frac{1}{L} \sum_j \exp\left[-i 2\pi \mathbf{f} t_j \right] \right|$$

where **f** is the temporal frequency of the drifting sine wave grating (cycles/s), L is the duration of the stimulus (s), which was always an integer multiple of 1/**f**, and t_j is the time of the jth spike of the cell's response to the given grating.

Analysis of responses to the white noise stimulus For the white noise stimulus, spike-triggered averages were computed using reverse correlation (reviewed in Chichilnisky, 2001). When calculating temporal frequency responses, for a given cell, the input stimulus was the intensity of the checkerboard square that produced the largest response for that cell. Temporal frequency responses were then taken as the transfer function between that stimulus and the cell's response, calculated as:

$$R(\mathbf{f}) = \left| \frac{\mathbf{W}_{\mathbf{XY}}}{\mathbf{W}_{\mathbf{XX}}} \right|$$

where **f** is the temporal frequency of interest, $\mathbf{W_{XY}}$ is the cross-spectrum between the stimulus and response, and $\mathbf{W_{XX}}$ is the power spectrum of the stimulus. Spectra were estimated using the multi-taper method (Chronux library for Matlab (Mitra and Bokil, 2007), available at http://chronux.org), using an effective bandwidth of 0.27 Hz.

Generation of confusion matrices Confusion matrices were used to quantify and visualize the extent to which different stimuli could be distinguished based on the ganglion cell responses. The vertical axis of a confusion matrix gives the presented stimulus (*i*), while the horizontal axis gives the decoded stimulus (*j*). Each element (*i,j*) of the confusion matrix indicates the probability that when stimulus *i* is presented, it will be decoded as stimulus *j*. The matrices were constructed using the responses to the drifting sine wave grating stimuli at the 7 highest temporal frequencies, ranging from 0.45 to 6 Hz (the extreme low frequency gratings did not provide a sufficient number of repeats for estimating probability distributions, and thus were not included in the construction of the matrices).

On each trial of the task, a stimulus, *s*, was presented (a grating of a particular temporal frequency), and a response, ***r***, was recorded. The response was then decoded by choosing the stimulus most likely to have produced it. The probability that a recorded response ***r*** is produced by the stimulus s_j, namely, $p(s_j|\mathbf{r})$, can be calculated by Bayes rule:

$$p(s_j \mid \mathbf{r}) \propto p(\mathbf{r} \mid s_j) p(s_j).$$

Thus, to decode a response ***r***, we need to find the stimulus s_j for which $p(\mathbf{r}|s_j)$ is maximal. (This is because all stimuli were equally likely, i.e., all $p(s_j)$ are identical).

To calculate the response distribution for each stimulus, $p(\mathbf{r}|s_j)$, we proceeded as follows. First, the 34 trials at each frequency were split into interleaved sets: one set to build the response distributions (the training set), and the other set to be decoded (the test set). For each stimulus, the response distribution was assumed to be an inhomogenous Poisson process spanning 1.2 sec, and constant in 133-ms bins. The firing rate in each bin was estimated by binning each spike train at this resolution, and averaging over all training trials of a given stimulus. To calculate $p(\mathbf{r}|s_j)$ for a response in the test set, we binned responses in the same manner. Since we assumed that the conditional response distribution is an inhomogeneous Poisson process, the probability $p(\mathbf{r}|s_j)$ was the product of the Poisson probabilities for each bin. This process was repeated for each response in the test set, and results were tallied into the confusion matrix. Results similar to those shown in Figs. 4.5 and 4.6 were obtained with a range of bin sizes (75 to 170 ms) and random assignments to training and test sets.

4.2.3 Animals

Animals were from a C57BL/6J background. All experiments were conducted in accordance with the institutional guidelines for animal welfare. Mice were dark-adapted for one hour prior to the start of an experiment.

4.3 Results

To assess differences in the temporal response properties of ON and OFF ganglion cells, we recorded the cells' spiking activity in response to drifting sine wave gratings of different temporal frequencies and a white noise stimulus. Measurements were carried out under both photopic and scotopic conditions.

Fig. 4.1 shows the results for the grating stimulus under the photopic conditions. The left panel shows the responses of several individual ON cells (top) and OFF cells (bottom), and the right panel shows the average temporal frequency tuning curves for the ON and OFF populations (n=20 ON cells, n=31 OFF cells). Consistent with previous studies (Kremers et al., 1993; Benardete and Kaplan, 1999; Keat et al., 2001; Zaghloul et al., 2003), both cell classes responded similarly, that is, they both responded to a broad range of temporal frequencies (0.15 to 6 Hz) (p>0.05, Student's t-test comparing the mean center of mass of the ON cell tuning curves with those of the OFF cells).

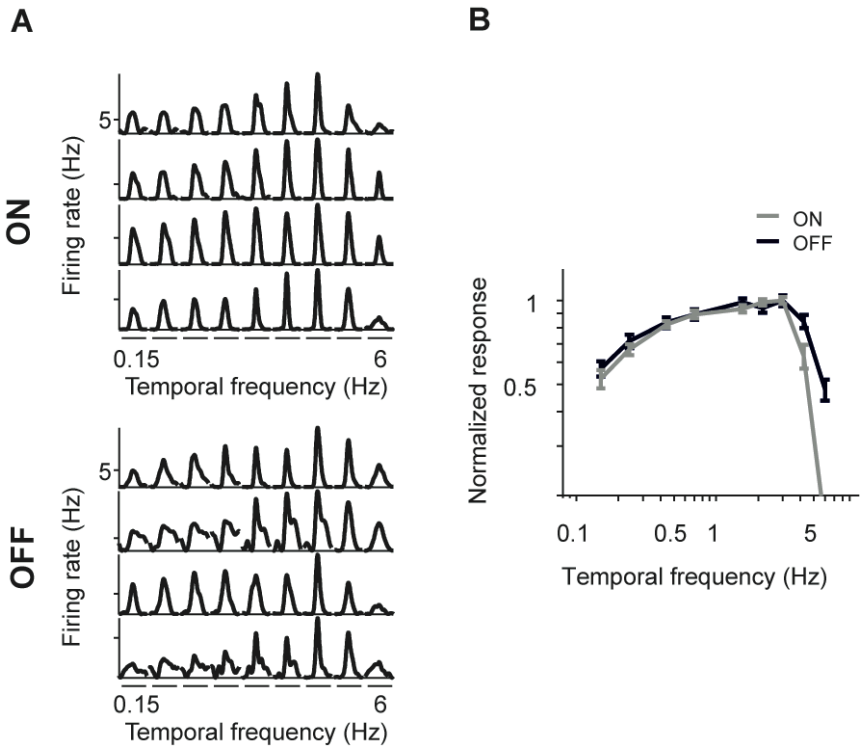

Figure 4.1 ON and OFF cells show similar temporal frequency tuning in response to sine wave gratings under photopic conditions.

(**A**) Representative responses for four ON and four OFF ganglion cells to drifting sine wave gratings of increasing temporal frequency. Each segment of the traces shows the average firing rate over one period of the drifting grating for a given frequency. (**B**) Average tuning curves (mean +/- SEM) for all ON and OFF cells, normalized to the peak (n=20 ON cells, 31 OFF cells). Temporal tuning curves were calculated by Fourier analyzing the responses and extracting the amplitude of the first harmonic response at each frequency. ON and OFF cells respond to a similar range of temporal frequencies (p>0.05,

Student's *t*-test comparing the mean center of mass of the ON cell tuning curves with that of the OFF cells).

The results for the same cells under scotopic conditions are shown in Fig. 4.2. As in Fig. 4.1, the left panel shows responses for several individual ON and OFF cells, and the right panel shows the average tuning curves. In contrast to the photopic condition, there was a clear difference in tuning: ON cells showed tuning to low temporal frequencies, peaking near 0.5 Hz, while OFF cells continued to respond to high temporal frequencies. The difference in tuning between the ON and OFF populations was highly significant ($p<10^{-3}$, Student's *t*-test comparing the mean center of mass of the tuning curves of the two populations).

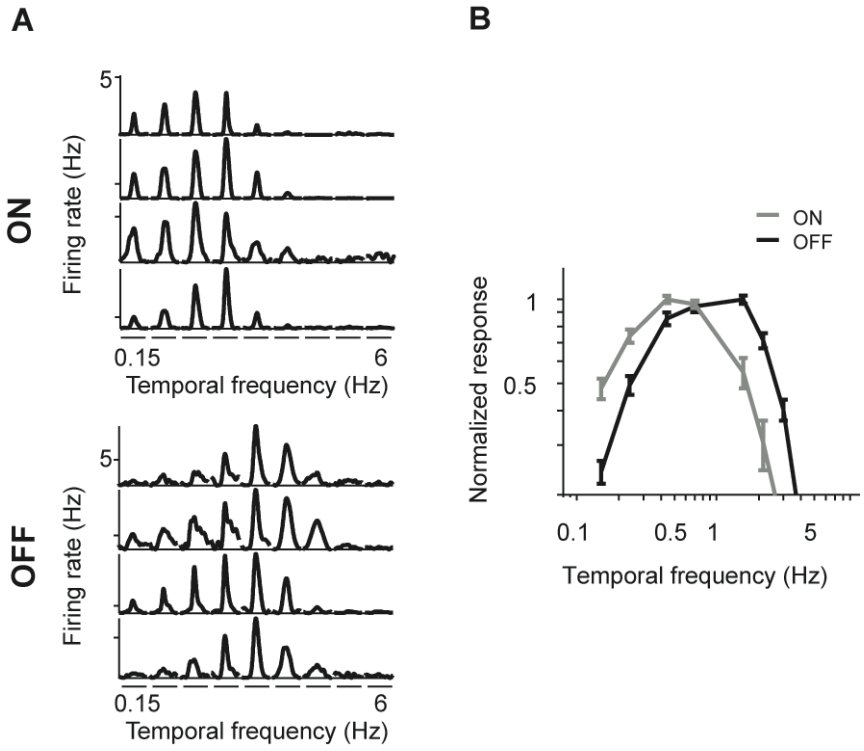

Figure 4.2 Frequency tuning of ON and OFF cells diverges under scotopic conditions.

(**A**) Representative responses of four ON and four OFF ganglion cells to drifting sine wave gratings of increasing temporal frequency. (**B**) Average tuning curves (mean +/- SEM) for all ON and OFF cells, normalized to the peak (n=20 ON cells, 31 OFF cells). On average the ON cells shifted to low frequencies, while the OFF cells continued to respond to high frequencies ($p<10^{-3}$, Student's t-test comparing the mean center of mass of the two populations). Note that under scotopic conditions, both ON and OFF cells fail to respond to the extreme high frequencies.

Similar results occurred for the white noise stimulus (Figs. 4.3 and 4.4). Fig. 4.3 shows the responses from the two cell classes under photopic conditions. The left panel shows the time course of the spike triggered average (STA) for several ON cells and OFF cells, and the right panel shows the average temporal frequency responses for both cell classes (n=20 ON cells, 31 OFF cells). As with the grating stimulus, both cell types responded similarly over a broad range of temporal frequencies (p>0.05, Student's t-test comparing the mean center of mass of the ON cell temporal frequency responses with those of the OFF cells). Fig. 4.4 shows the responses to the same stimulus under scotopic conditions. Again, the left panel shows STA time courses for individual ON and OFF cells, and the right panel shows the average temporal frequency responses across all cells for the two populations. The same divergence in tuning observed with the grating stimulus – that ON cells were tuned to low frequencies, while OFF cells continued to respond to high frequencies – was also seen with the white noise stimulus ($p<10^{-3}$, Student's t-test comparing the mean center of mass of the temporal frequency responses of the two populations).

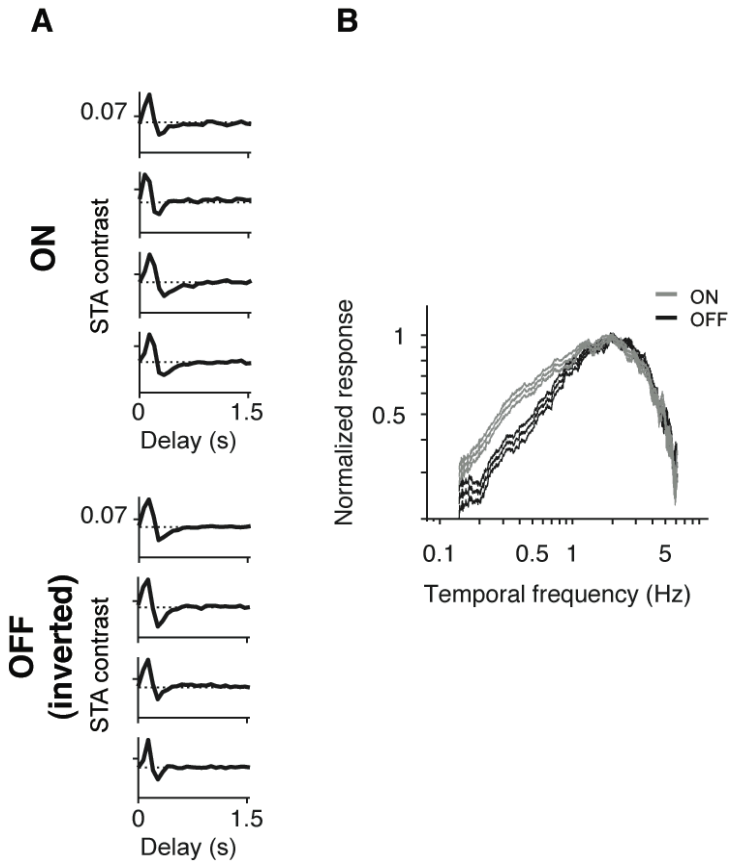

Figure 4.3 ON and OFF cells show similar temporal response properties to white noise under photopic conditions.

(**A**) Representative STA time courses for four ON and four OFF ganglion cells in response to a white noise (random checkerboard) stimulus. Note that OFF STAs are inverted so that the similarity of the short peaks is easy to observe. (**B**) Average temporal frequency responses (mean +/- SEM) for all ON and OFF cells (*n*=20 ON cells, *n*=31 OFF cells), normalized to the peak. Temporal frequency responses were calculated by Fourier analyzing the STA at the checkerboard square that produced the largest response for each cell. ON and OFF cells showed similar temporal response profiles ($p>0.05$, Student's *t*-test

comparing the mean center of mass of ON cell temporal frequency responses with that of the OFF cells).

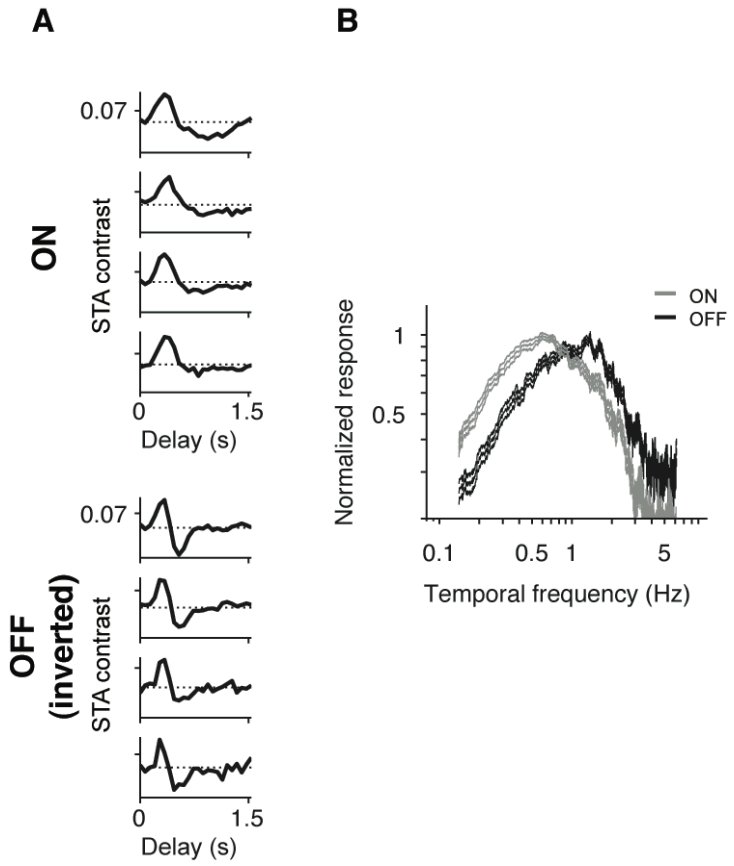

Figure 4.4 The divergence under scotopic conditions was also observed for the white noise stimulus.

(**A**) Representative STA time courses for four ON and four OFF ganglion cells in response to a white noise (random checkerboard) stimulus. (**B**) Average temporal frequency responses (mean +/- SEM), normalized to the peak (*n*=20 ON cells, *n*=31 OFF cells). As with the grating stimulus, the ON cells shifted to

low frequencies, while the OFF cells continued to respond to high frequencies ($p<10^{-3}$, Student's *t*-test comparing the mean center of mass the two populations).

These differences in temporal frequency characteristics show that there is an ON cell/OFF cell asymmetry with respect to *encoding* stimuli at low light levels. To assess the effects of this on *decoding* stimuli, we used an ideal observer approach (Barlow, 1978; Geisler, 1989). Specifically, we measured the extent to which different stimuli can be distinguished given responses from each cell class.

The decoding results were then quantified and visualized via confusion matrices (Figs. 4.5 and 4.6) (Hand, 1981). A confusion matrix indicates the probability that the neural response to a presentation of a stimulus will be decoded as that stimulus, or whether it will be confused with another stimulus. Specifically, the element in position (*i,i*) of the matrix indicates the probability that stimulus *i* is decoded correctly, and the element in position (*i,j*) indicates the probability that stimulus *i* is decoded incorrectly as stimulus *j*.

Fig. 4.5 shows the confusion matrices generated from responses taken under photopic condtions. The stimuli were drifting gratings of different temporal frequencies. As shown in the figure, both ON and OFF cells decoded the gratings correctly over the range of frequencies; this is indicated by the prominent diagonal line in each confusion matrix. As in the previous figures, results for individual ON and OFF cells are shown on the left, and the average for the population is shown on the right. The results are summarized in panel

B, which shows the average of the diagonals of the matrices for each population, i.e., the average probability that stimuli will be correctly decoded. Under photopic conditions, no statistically significant difference between the classes was observed ($p>0.1$ for all frequencies, Student's *t*-test, adjusted for multiple comparisons).

Fig. 4.6 shows the same analysis for these cells under scotopic conditions. Here, there is a clear difference in the decoding: the ON cells showed accurate decoding at low frequencies and poor decoding at high frequencies; this is indicated by the bright squares along the diagonal line at the low frequencies that dissolve as high frequencies are approached. In contrast, the OFF cells showed accurate decoding at high frequencies; here, the bright squares are shifted toward the midde and high frequencies of the matrices. As summarized in panel B, which shows the average of the diagonals of the matrices for each population, the ON cells were more accurate at low frequencies, while the OFF cells were more accurate at high frequencies ($p<0.01$, Student's *t*-test, adjusted for multiple comparisons, $n=20$ ON cells, $n=31$ OFF cells). (All individual grating responses, tuning curves, and confusion matrices for both light conditions are provided in *Appendix 2* for the interested reader (Fig. 4.9 for ON cells and Fig. 4.10 for OFF cells).)

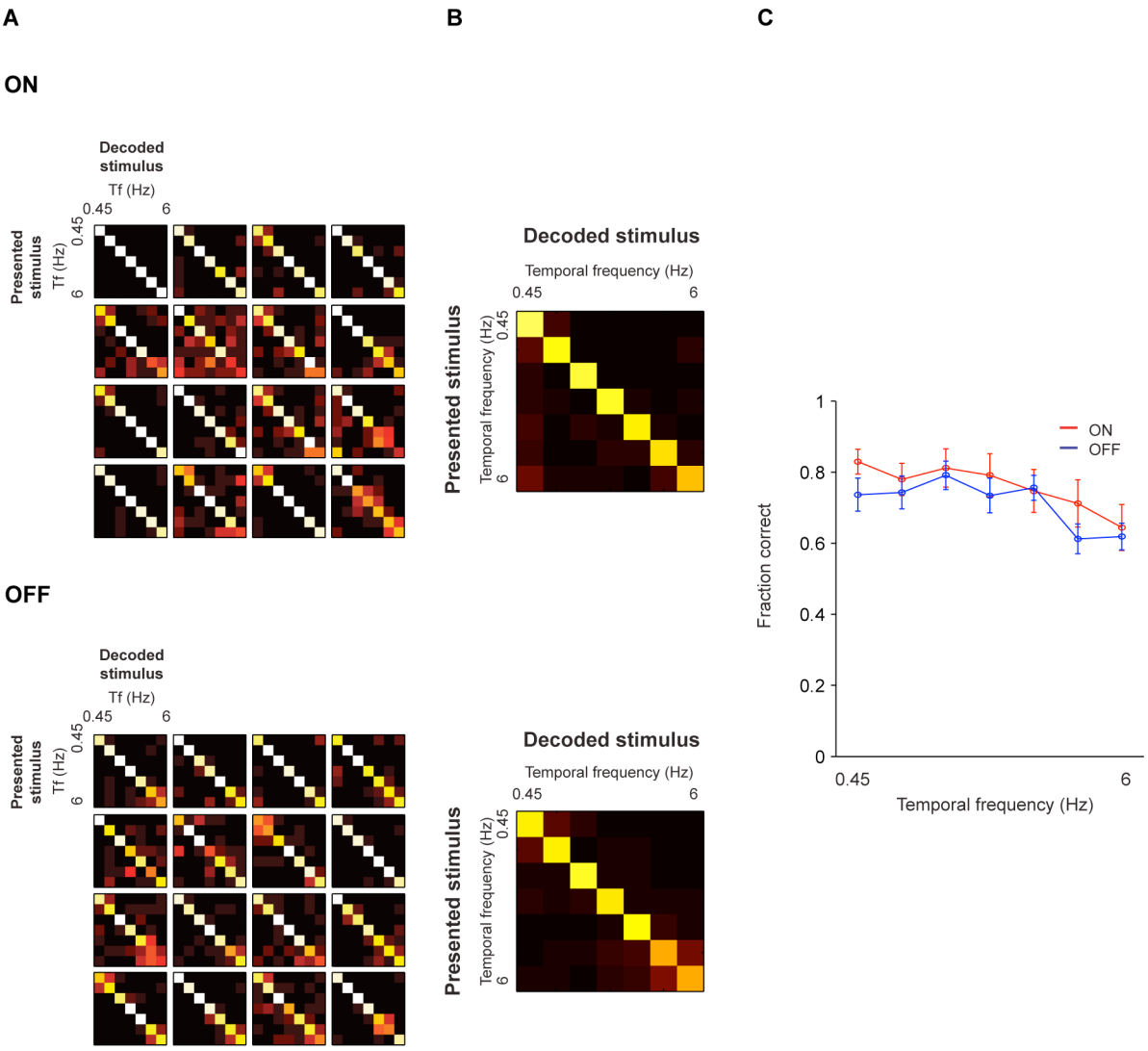

Figure 4.5 Under photopic conditions, it is possible to decode across the entire range of temporal frequencies using responses of ON or OFF cells.

(**A**) Representative confusion matrices for sixteen ON and sixteen OFF cells calculated using responses to drifting gratings. The vertical axis gives the presented stimulus (*i*), and the horizontal axis gives the decoded stimulus (*j*). Each element of a confusion matrix plots the probability of decoding stimulus *j* when presented with stimulus *i* (see text). Decoders based on both ON and OFF responses show little confusion over the range of temporal frequencies, as indicated by the prominent diagonal lines in the confusion matrices. (**B**) Average confusion matrices over *all* ON and OFF cells (*n*=20 ON cells, *n*=31 OFF cells). (**C**) The average of the diagonals of the matrices (mean +/- SEM) for all ON (red) and OFF (blue) cells (*n*=20 ON cells, *n*=31 OFF cells). ON and OFF cells perform equally well over the full range of temporal frequencies ($p>0.1$ for all frequencies, Student's *t*-test, adjusted for multiple comparisons).

The above finding – that ON cells but not OFF cells shift to low temporal frequencies in the dark – indicates that, as light level decreases, the retina processes increments and decrements differently. Interestingly, this difference in processing corresponds to an asymmetry in the physical world, one produced by the Poisson nature of photon capture. In a Poisson process, the variance is proportional to the mean. This means that there is more dispersion in the distribution of counts when the event rate increases (i.e., when light increments occur) than when the event rate decreases (when light decrements occur). Due to this asymmetry, more time is needed to detect increments than decrements.

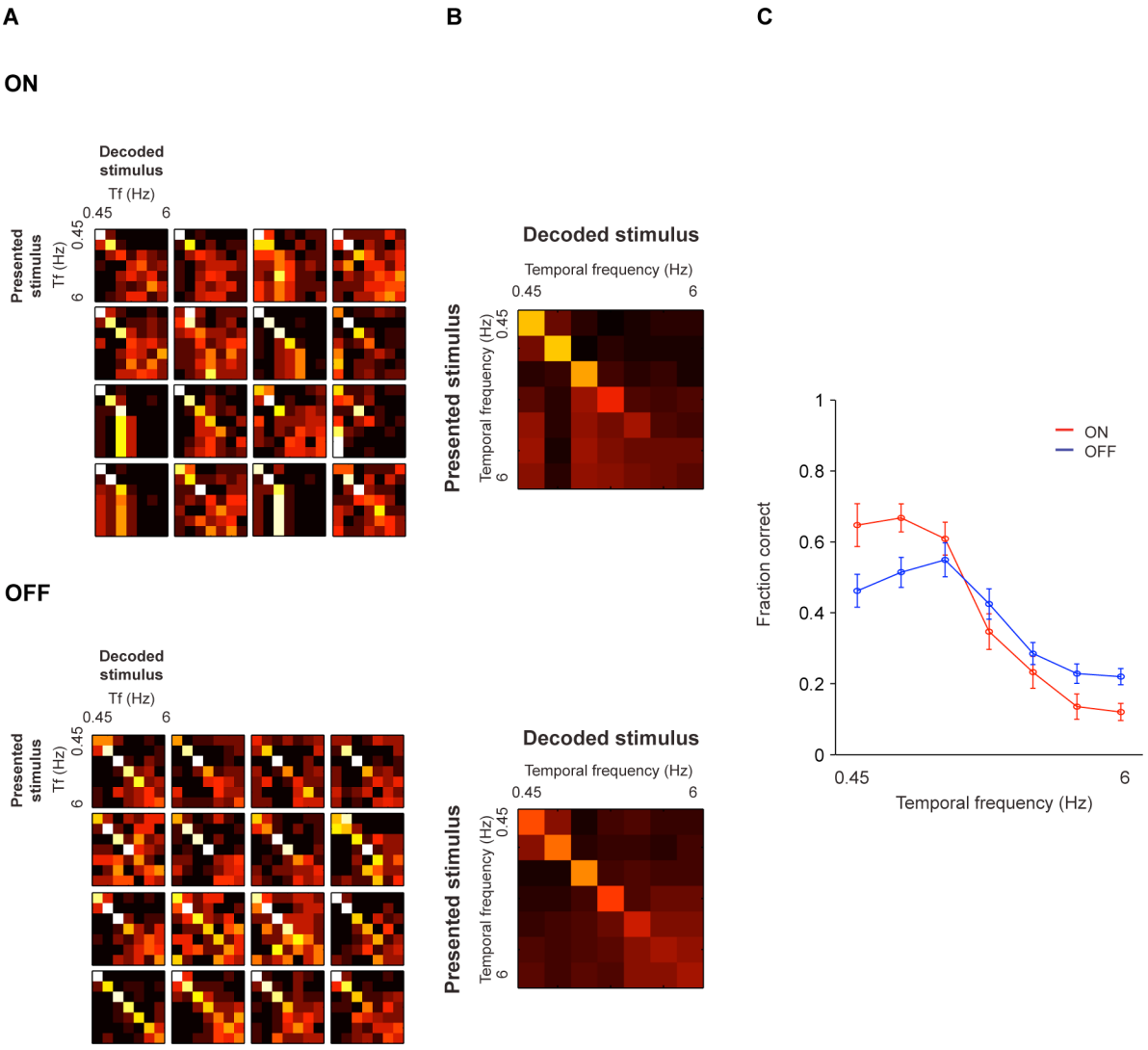

Figure 4.6 Under scotopic conditions, there is a divergence in performance – ON cells perform better at low frequencies, while OFF cells perform better at high.

(**A**) Representative confusion matrices calculated using the responses of sixteen ON and sixteen OFF cells to drifting gratings. ON cells show better

performance at low frequencies, as indicated by the bright squares along the diagonal at low frequencies, which break down at middle and high frequencies. In contrast, for OFF cells, performance is shifted toward high frequencies. (**B**) Average confusion matrices over all ON and OFF cells show the same trend (n=20 ON cells, n=31 OFF cells). (**C**) The average of the diagonals of the matrices (mean +/- SEM) for ON (red) and OFF (blue) populations (n=20 ON cells, n=31 OFF cells). ON cells perform significantly better at the lowest two frequencies tested (p<0.01), while OFF cells perform significantly better at the highest frequency (p<0.01, Student's t-test, adjusted for multiple comparisons).

The effect of this asymmetry is shown in Fig. 4.7A. We consider the discrimination of positive and negative fluctuations around a background luminance. As mentioned above, Poisson statistics dictate that increments are associated with broader count distributions, and decrements with narrower ones. Consequently, there is more overlap among the increments, making them harder to distinguish. As shown in panel B, an ideal observer in a discrimination task, who chooses stimuli based on the maximum *a posteriori* probability over the set of stimuli, will be less accurate in discriminating between increments than between decrements. Changing the event count (either by changing the integration time or the photon rate) changes performance for both increments and decrements, but the difference between decrements and increments persists – for at least three orders of magnitude,

as shown in the figure. (*Appendix 1* provides an information-theoretic analysis of this asymmetry.)

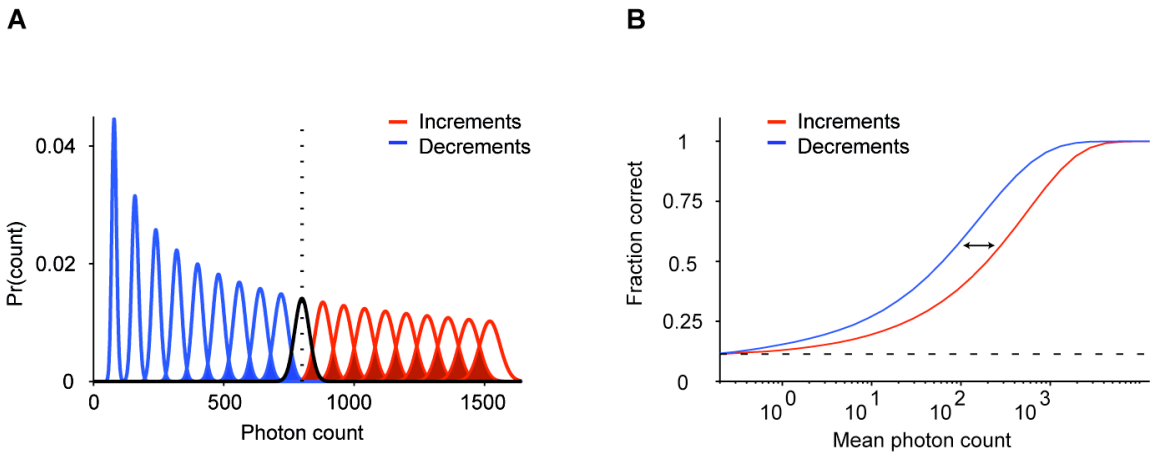

Figure 4.7 At low light levels, increments become harder to discriminate than decrements of equal magnitude, due to asymmetries in the Poisson distribution.

(**A**) Distributions of photon counts are shown for increments (grey) and decrements (black) in steps of 10% contrast around a mean rate (dotted line). For increments, the distributions are broader and show much greater overlap than for decrements, making increments harder to detect. (**B**) Performance for an ideal observer in the discrimination task for increments (grey) or decrements (black) over a range of mean photon counts. For each mean photon count, stimuli at steps of ±10% contrast around the mean are simulated (as in **A**), and the observer chooses stimuli based on the maximum a posteriori probability over the set of stimuli. Over a broad range of photon

counts, performance is better for decrements than for increments. Arrows indicate separation between increment and decrement performance, i.e. the factor by which an increment detector needs to observe more photons to match the performance of the decrement detector. The dotted line indicates performance at chance. We note that this aspect of Poisson processes – that it is more difficult to detect increments than to detect decrements – might seem counterintuitive, since signal-to-noise ratio (SNR) increases with mean rate increases. But SNR is not the relevant statistic here. An increase in SNR means that it is easier to detect the same fractional change around a high mean rate than around a low mean rate. In our case, we are asking whether, given a constant mean rate (e.g., the rate under night conditions), it is easier to detect an increment or a decrement. Since the variability of a Poisson process is proportional to its rate, an increment leads to a more variable signal than a decrement, and, therefore, is harder to detect. The suggestion in this paper, then, is that ON cells compensate for the higher variability by integrating their input over a longer period of time, i.e, by shifting toward low temporal frequencies.

4.4 Discussion

It is well known that the signals in the first stages of visual processing segregate into ON and OFF channels. The working hypothesis for many years was that these channels are symmetric, but recent observations suggest that this notion needs modification, that the two pathways show differences (DeVries and Baylor, 1997; Demb et al., 2001; Chichilnisky and Kalmar, 2002;

Pang et al., 2003; Zaghloul et al., 2003; Sagdullaev and McCall, 2005; Murphy and Rieke, 2006; Eggers et al., 2007; Molnar and Werblin, 2007). The significance of the differences in conveying visual information has been unclear.

Here we showed a case where the symmetry breakdown between the ON and OFF channels is very apparent, and functional significance can be attributed. By day, that is, under photopic conditions, the temporal tuning of ON and OFF ganglion cells in the mouse retina is very similar, but, at night it diverges: ON cells shift to low temporal frequencies, that is, they increase their gain at low temporal frequencies and reduce it at high. Fig. 4.2 and 4.4 show the changes in gain, and Fig. 4.6 shows an example of the functional consequences: the changes in gain correspond to changes in signal-to-noise ratio, which directly affect performance on a temporal frequency discrimination task. Fig 4.7 then shows that this result is predicted by an asymmetry in the physical world, specifically, the asymmetric detection of light increments and decrements due to the Poisson nature of photon capture.

This breakdown of symmetry between the two pathways in the dark is unlikely to be specific to the mammalian visual system. Armstrong-Gold & Rieke (2003) recorded from ON and OFF bipolar cells under scotopic conditions in the tiger salamander retina and noted that OFF bipolar cells responded to higher frequency stimuli than ON bipolar cells. While the salamander appears to have significant differences in the circuitry that mediates rod-driven signals (Yang and Wu, 1997), their findings suggest that

the asymmetries in the ON and OFF pathways at low light levels generalizes to non-mammals as well.

4.4.1 Functional implications of the differences in visual processing

The results in this paper represent an example of a neural system evolving to match a fundamental property of the natural world – the intrinsic asymmetry in the detection of light increments and decrements that arises from the Poisson nature of photon capture. That there is an asymmetry has been previously noted (Cohn, 1974; Thibos et al., 1979; Hornstein et al., 1999), but the studies considered only the implications for photoreceptor responses, and only in the regime of low photon counts (<10 per discrimination window). Here we show that the retina exploits this asymmetry after photoreceptor signals are partitioned into ON and OFF channels. Moreover, we demonstrate that this asymmetry is relevant to much higher photon counts, up to thousands of photons per window in our discrimination task (see Fig. 4.7B).

Two factors make the asymmetry relevant to high counts. First, the asymmetry is greater for large deviations from the mean than for small ones. For example, in Fig. 4.7A, the signals near threshold (the distributions of counts closest to the mean) only show a slight difference between increment and decrement distributions, and thus would be nearly equally challenging to discriminate. In contrast, for supra-threshold signals (deviations further from the mean), the increment distributions become broader (less discriminable), while the decrement distributions become narrower (more discriminable). (Formally, the intrinsic difference in discriminability of increments and

decrements depends in an accelerating fashion on distance from the mean – detailed in *Appendix 1*.) Second, the effects of the asymmetry are compounded when one considers not just the detection of a single increment or decrement, but instead the discrimination of multiple increments or decrements around a mean photon count. This latter task is much more closely related to the task the animal's visual system is performing – that is, cells in the retina do not simply signal the presence of an increment or decrement, but their response increases with larger magnitude increments or decrements, and therefore the cells must be able to discriminate multiple levels. Because these levels overlap with one another (more so for increments than decrements, as shown in Fig. 4.7A), the task becomes harder as multiple contrasts are considered, which makes the asymmetry relevant to higher photon counts.

The results of the simple discrimination task, presented in Fig. 4.7B suggest that ON cells would need to observe more photons, by approximately a factor of 3, in order to match the performance of OFF cells (shown by the separation between the grey and black curves). (This is similar to the factor of 2.5 found in *Appendix 1* using a formal information theoretic analysis.) This factor of 3 approximates the shift of the tuning curves along the frequency axis seen in the observed data in Figs. 4.2 and 4.4. Note, though, that the discriminability of increments and decrements will not always differ by this ratio. This is because Poisson fluctuations in photon count are not the only source of noise. As the signals travel through multiple levels of processing other noise sources are added. To the extent that these noise sources corrupt

increments and decrements equally, they will dilute the intrinsic difference in detectability.

An additional point worth mentioning is that the impact of the increment/decrement asymmetry on signaling by ON and OFF ganglion cells depends on the presence of a nonlinearity, specifically, the well-known rectification in the output of ganglion cells in many species, including mouse. If, for example, ON cells and OFF cells were not rectified, they could each signal both increments and decrements. In this scenario, the increment/decrement asymmetry would not have a differential effect on the two classes.

Finally, the results in this paper have implications for downstream circuitry, since retinal outputs serve as building blocks for circuits in higher brain areas. For example, some models of simple cell receptive fields in visual cortex hold that cortical cells are activated in a push-pull manner, with ON and OFF subregions driven by complementary ON and OFF retinal ganglion cell input, relayed through the LGN (J. M. Alonso et al., 2001; J. A. Hirsch, 2003). Our findings predict that if simple cell receptive fields rely on complementarity of ON and OFF input, their receptive field structure may be radically different at night, when the two pathways are out of sync; alternatively, assuming this model is correct, these cells may have some plasticity, e.g. the ability to differentially filter ON and OFF input, which would allow the cells to preserve their receptive field structure with the shift to scotopic vision.

4.4.2 Relating the differential filtering properties of ON and OFF ganglion cells to retinal circuitry

Our results show, at the level of the ganglion cell output, that ON and OFF pathways have filtering properties that diverge in the dark. This requires elements in retinal circuitry that act separately on ON and OFF signals. Under the scotopic conditions used in this paper, signal transmission to ON and OFF ganglion cells is dominated by the rod bipolar pathway (see *Appendix 3*; for review of the pathway, see Bloomfield and Dacheux, 2001, also Volgyi et al., 2004 and Murphy and Rieke, 2006, 2008). Along this pathway, ON and OFF signals first diverge at the output from the AII amacrine cell, which connects to ON cone bipolar cells, OFF cone bipolar cells, and OFF ganglion cells. Here, ON signals are mediated by gap junctions, while OFF signals (both to the bipolar and ganglion cells) are mediated by chemical synapses (Kolb and Famiglietti, 1974; Strettoi et al., 1992; Volgyi et al., 2004; Murphy and Rieke, 2008). It has been shown recently that under these conditions, the synaptic input to ON and OFF ganglion cells is correlated (Murphy and Rieke, 2006, 2008), creating an expectation that the ON and OFF responses would be similar. However, it has also been shown that the two ganglion cell types undergo different filtering with respect to their inputs (Murphy and Rieke, 2006, 2008). In ON cells, excitation is followed by delayed inhibition, in a feed-forward manner, whereas in OFF cells, excitation and inhibition occur simultaneously, but with opposite polarity; in this case, the cell is driven to fire in a push-pull manner by a combination of excitation and disinhibition. These different filtering mechanisms are potential mediators of the differences in the

output properties between the two pathways. We emphasize, though, that since the ON and OFF pathways have not been completely delineated, it is possible that there are other processes as well that shape response dynamics. Interestingly, under photopic conditions, where ON and OFF signals diverge at an earlier point in the circuitry, i.e., at the level of the photoreceptor output to the bipolar cells, one might expect greater divergence between ON and OFF ganglion cell responses. This was not the case for the filtering properties we examined. However, differences between the ON and OFF pathways under photopic conditions have been reported by others in studies of adaptation, specifically, contrast adaptation (Chander and Chichilnisky, 2001; Kim and Rieke, 2001; Wark et al., 2009).

4.5 Acknowledgements

We thank I. Bomash and Z. Nichols for helpful discussion. This work was supported by National Eye Institute Grants EY012978 to S.N., by National Eye Institute Grants EY07977 and EY09314 to J.D.V., and by the Tri-Institutional Training Program in Vision Research.

APPENDIX

Appendix 1: Discriminability of increments and decrements in the rate of a Poisson process: an information-theoretic perspective

Here we analyze the asymmetry in detecting increases and decreases in the rate of a Poisson process, viewed from an information-theoretic perspective. This asymmetry has previously been analyzed from the point of view of signal detection theory and asymptotic expressions for receiver operating curve characteristics (Thibos et al., 1979). The information-theoretic perspective used here leads to a simple, exact result (eq. 2) that indicates how much more quickly an ideal observer can detect a decrement, vs. an increment, in a Poisson process. This ratio depends in an accelerating fashion on the fractional size of the change (i.e., the contrast), and, perhaps surprisingly, is independent of the baseline event rate.

To reach our result, we first need a measure of the discriminability of two Poisson processes, one with rate λ_P from one with rate λ_Q. We will then compare the discriminability of a fractional increase in rate by an amount *c* (i.e., $\lambda_P = \lambda_Q(1+c)$) to the discriminability of a fractional decrease by the same amount (i.e., $\lambda_P = \lambda_Q(1-c)$).

The first step is to define a natural measure of discriminability per unit time. We do this by taking the Kullback-Leibler divergence, which is a standard measure of discriminability for discrete distributions, and extending it to continuous processes. For discrete distributions *P* and *Q*, the Kullback-Leibler divergence is given by

$$D_{KL}(P \| Q) = \sum_i p_i \log \frac{p_i}{q_i}.$$

This is a natural measure of discriminability because it has the following interpretation: given a random draw from the *P*-distribution, $D_{KL}(P \| Q)$ is the log likelihood ratio that this observation arises from the *P*-distribution, vs. that it arises from the *Q*-distribution (Latham and Nirenberg, 2005; Cover and Thomas, 2006).

To apply this notion to Poisson processes, we note that for a sequence of independent samples, log likelihood ratios combine by simple addition. In a Poisson process discretized in small intervals of size Δt, each time step is independent. So the discriminability per unit time, which we denote $R_{KL}(P \| Q)$, is given by the number of time steps $(1/\Delta t)$ multiplied by the discriminability within a time step of size Δt. Since this holds for infinitesimal time steps as well as finite ones, we can write

$$R_{KL}(P \| Q) = \lim_{\Delta t \to 0} \frac{D_{KL}(P_{\Delta t} \| Q_{\Delta t})}{\Delta t},$$

where $P_{\Delta t}$ and $Q_{\Delta t}$ indicate the Poisson processes P and Q, discretized in time steps of size Δt.

We now calculate this single-time-step discriminability, $D_{KL}(P_{\Delta t} \| Q_{\Delta t})$. With time discretized in steps of size Δt, a Poisson process of rate λ can be approximated as a discrete symbol sequence: the symbol 0 occurs with

probability $1-\lambda\Delta t$ and the symbol 1 occurs with probability $\lambda\Delta t$. Thus, in a discretization interval Δt, the discriminability of a Poisson sequence with rate λ_P from one with rate λ_Q is

$$D_{KL}(P_{\Delta t} \| Q_{\Delta t}) = p_0 \log \frac{p_0}{q_0} + p_1 \log \frac{p_1}{q_1} + O\left((\Delta t)^2\right),$$

where $p_0 = 1-\lambda_P \Delta t$, $p_1 = \lambda_P \Delta t$, $q_0 = 1-\lambda_Q \Delta t$, $q_1 = \lambda_Q \Delta t$. The final term in the above equation represents the contribution of bins with two or more events; their contribution is negligible as the step size Δt approaches zero.

With these substitutions, we find

$$D_{KL}(P_{\Delta t} \| Q_{\Delta t}) = (1-\lambda_P \Delta t) \log \frac{1-\lambda_P \Delta t}{1-\lambda_Q \Delta t} + \lambda_P \Delta t \log \frac{\lambda_P \Delta t}{\lambda_Q \Delta t} + O\left((\Delta t)^2\right)$$

or

$$D_{KL}(P_{\Delta t} \| Q_{\Delta t}) = (\lambda_Q - \lambda_P)\Delta t + \lambda_P \Delta t \log \frac{\lambda_P}{\lambda_Q} + O\left((\Delta t)^2\right).$$

Here we have used the approximation $\log(1+u) = u + O(u^2)$ because we are interested in the limit of a small discretization interval, Δt.

From this it follows that

$$R_{KL}(P \,||\, Q) = \lim_{\Delta t \to 0} \frac{D_{KL}(P_{\Delta t} \,||\, Q_{\Delta t})}{\Delta t} = (\lambda_Q - \lambda_P) + \lambda_P \log \frac{\lambda_P}{\lambda_Q}, \qquad (1)$$

which is the discriminability per unit time of a Poisson process with rate λ_P from one with rate λ_Q.

Finally, we want to compare the discriminability of a decrement by a fractional contrast *c* from the background, with the discriminability of an increment by a fractional contrast *c* from the same background. We represent the background signal as a Poisson process *Q* with rate λ, and we represent the decrements and increments as Poisson processes Q^- and Q^+, with rates $\lambda^- = \lambda(1-c)$ and $\lambda^+ = \lambda(1+c)$.

The answer we seek, the ratio of discriminabilities, is $\frac{R_{KL}(Q^- \,||\, Q)}{R_{KL}(Q^+ \,||\, Q)}$. Substituting the above expressions for λ^+ and λ^- in eq. (1) yields

$$\frac{R_{KL}(Q^- \,||\, Q)}{R_{KL}(Q^+ \,||\, Q)} = \frac{\lambda c + \lambda(1-c)\log(1-c)}{-\lambda c + \lambda(1+c)\log(1+c)} = \frac{c + (1-c)\log(1-c)}{-c + (1+c)\log(1+c)}. \qquad (2)$$

The numerator and denominator of $\frac{R_{KL}(Q^- \,||\, Q)}{R_{KL}(Q^+ \,||\, Q)}$ are proportional to the baseline event rate λ, so the ratio of discriminabilities is independent of λ. That is, the ratio of discriminabilities depends only on contrast and the relative photon rates, but not on the absolute photon rate. This gives the ratio eq. (2) a universal interpretation: it indicates how much more quickly an ideal observer can reach the same certainty in detecting a decrement of a given contrast, vs. detecting an increment.

To understand the qualitative behavior of eq. (2), we consider its Taylor expansion. This begins

$$\frac{R_{KL}(Q^- \| Q)}{R_{KL}(Q^+ \| Q)} = 1 + \frac{2}{3}c + \frac{2}{9}c^2 + O(c^3).$$

Thus, the asymmetry between detection of increments and decrements an accelerating function of the contrast *c* (see Figure 4.8): it is progressively more prominent in the suprathreshold range. At the extreme ($c = 1$), we find $\frac{R_{KL}(Q^- \| Q)}{R_{KL}(Q^+ \| Q)} = \frac{1}{2\log 2 - 1}$, approximately 2.589. That is, abrupt extinction of a light can be detected about 2.5 times faster than abrupt doubling.

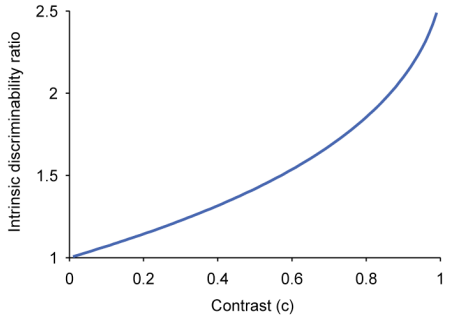

Figure 4.8 Decrements can be detected more readily than increments, and the asymmetry is an accelerating function of contrast.

To compare intrinsic discriminability, we use the ratio of Kullback-Leibler distances between a baseline Poisson process, and one whose rate changes by a factor of (1+*c*) or (1-*c*). This ratio (eq. (2)) has a value of 1 for equal

discriminability. Values > 1 indicate that decrements are more readily discriminated.

Appendix 2: Data from individual cells

For the interested reader, all individual grating responses, tuning curves, and confusion matrices for both light conditions are provided below.

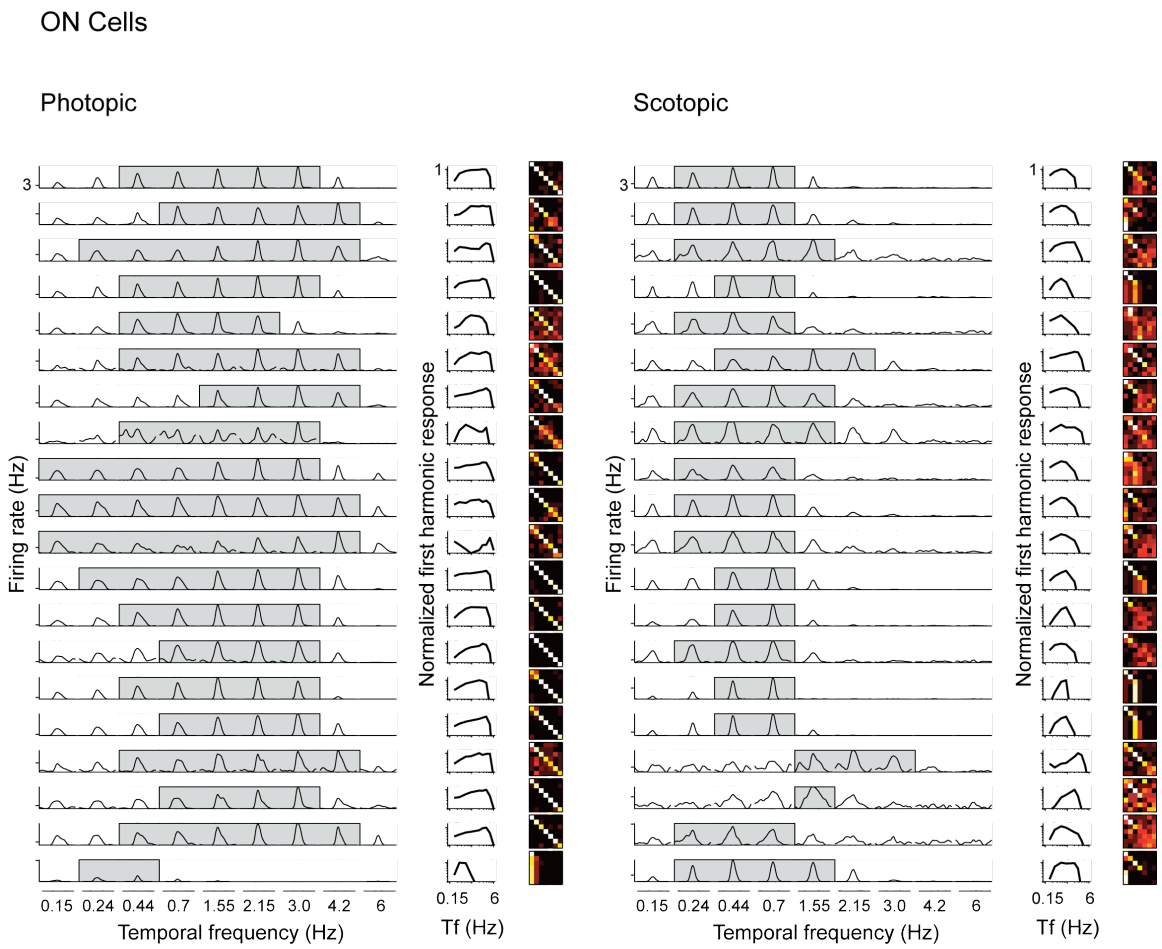

Figure 4.9 All individual ON cell grating responses, tuning curves, and confusion matrices for both light conditions.

As indicated in the main text, ON cells shift their tuning toward low temporal frequencies under scotopic conditions. In each row, the first column shows the set of PSTHs for the cell: each segment shows the average firing rate over one period for each temporal frequency. Responses shaded in grey represent the range of frequencies in the cell's passband, that is, the frequencies for which the response is above the 3dB cutoff, estimated from the tuning curves.

The second column shows the normalized tuning curve, calculated from the amplitude of the first harmonic response at each frequency of the grating. The final column shows the confusion matrix for the given cell.

Figure 4.10 All individual OFF cell grating responses, tuning curves, and confusion matrices for both light conditions.

As described in the main text, OFF cells do not make the shift to low temporal frequencies under scotopic conditions; their tuning favors the middle of the frequency range tested. Note that both ON and OFF cells lose responses to the highest temporal frequencies in scotopic conditions (consistent with behavioral measurements for the mouse (Umino et al., 2008)), but ON cells shift to the lower end of the frequency range, while OFF cells continue to respond to the middle of the range. As in Fig. 4.9, the first column in each row shows the set of PSTHs for the cell: with each segment showing the average firing rate over one period for each temporal frequency. The second column shows the normalized tuning curve, calculated from the amplitude of the first harmonic response at each frequency of the grating, and the final column shows the cell's confusion matrix.

OFF Cells

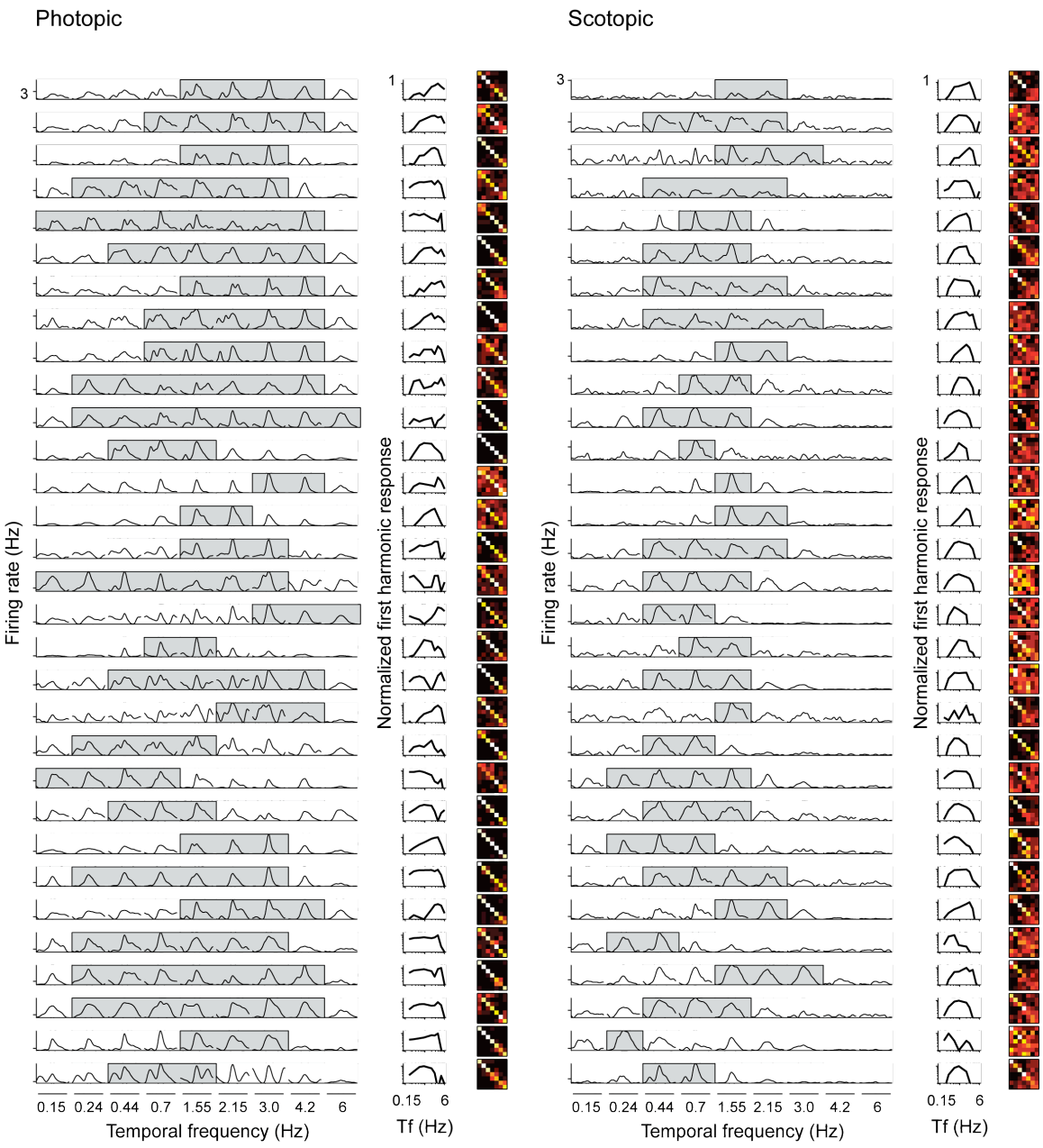
Photopic
Scotopic
Firing rate (Hz)
3
Normalized first harmonic response
1
0.15 0.24 0.44 0.7 1.55 2.15 3.0 4.2 6
Temporal frequency (Hz)
0.15 6
Tf (Hz)

Appendix 3: Scotopic responses are driven by the rod bipolar pathway

To verify that signaling under the scotopic condition was driven by the rod bipolar pathway, we tested whether responses of the OFF pathway under scotopic conditions were sensitive to the mGluR6 agonist APB. APB causes a blockade of synaptic signaling between rods and rod bipolar cells, as well as between cones and cone ON bipolar cells (Murphy and Rieke, 2006). Thus APB should selectively block OFF responses through the rod bipolar pathway, but OFF responses through alternate pathways should be resistant to APB blockade.

Fig. 4.11 shows the results of this experiment for 5 example OFF cells. As expected, APB abolished light driven responses in the scotopic condition. Switching to the photopic condition, where pathways alternate to the rod bipolar pathway become available, produces a recovery of the responses.

Fig. 4.12 then shows the results of this experiment for 5 example ON-OFF cells. As in Fig. 4.11, APB abolished light driven responses in the scotopic condition, again showing that the responses are mediated by the rod bipolar pathway. Transitioning to the photopic condition, where alternate pathways become available, leads to response recovery. Here only OFF responses recover, as APB, in addition to blocking the rod bipolar pathway, blocks the cone ON bipolar pathway as well.

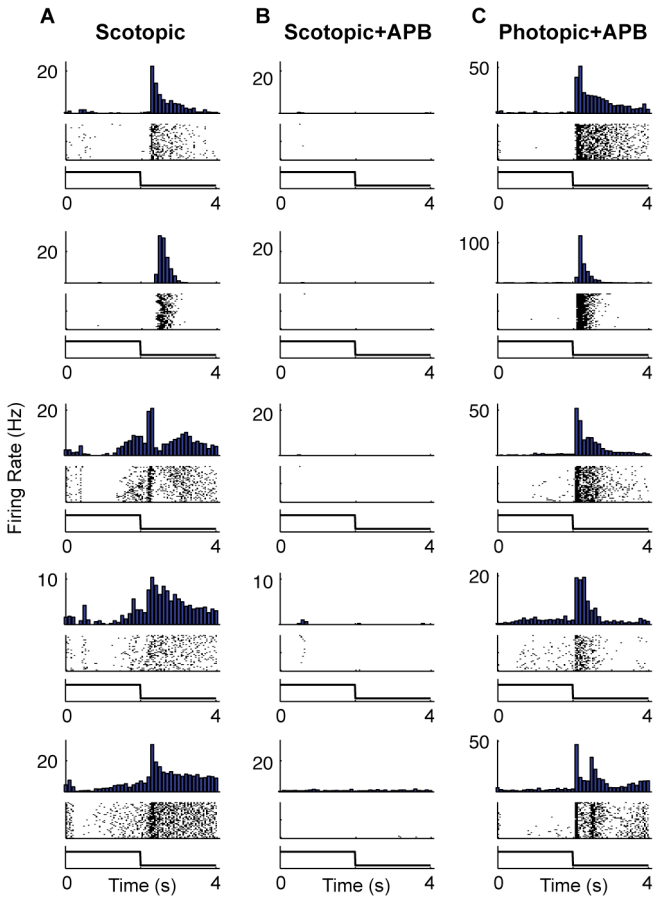

Figure 4.11 Responses in the scotopic condition are driven by the rod bipolar pathway.

(**A**) Responses to a flashing full-field stimulus recorded from 5 example OFF cells under scotopic conditions. (**B**) Under these conditions, addition of 20 μM APB abolishes nearly all light responses, showing that the responses are driven by the rod bipolar pathway. (**C**) Transitioning to the photopic intensity causes the recovery of the responses, as pathways alternate to the rod bipolar pathway become utilized.

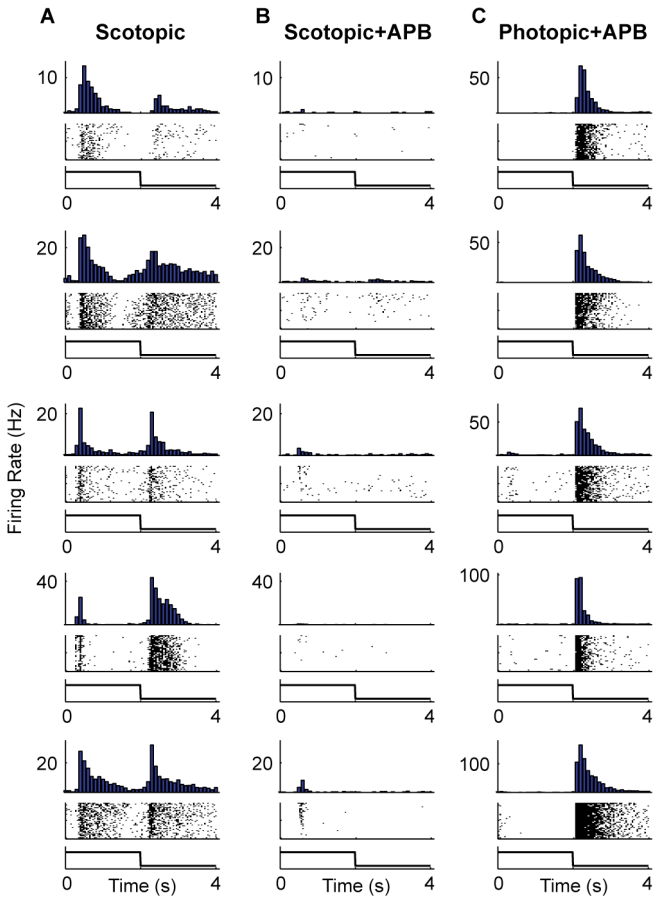

Figure 4.12 Recovery of responses in the photopic condition was specific to OFF responses.

(**A**) Responses to a flashing full-field stimulus were recorded for 5 example ON-OFF cells under scotopic conditions. (**B**) Under these conditions, addition of 20 μM APB abolishes nearly all light responses, showing that the responses are driven by the rod bipolar pathway. (**C**) Transitioning to the photopic intensity causes the recovery of OFF responses, but not ON responses.

REFERENCES

Alonso JM, Usrey WM, Reid RC (2001) Rules of connectivity between geniculate cells and simple cells in cat primary visual cortex. J Neurosci 21:4002--4015.

Applebury ML, Antoch MP, Baxter LC, Chun LL, Falk JD, Farhangfar F, Kage K, Krzystolik MG, Lyass LA, Robbins JT (2000) The murine cone photoreceptor: a single cone type expresses both S and M opsins with retinal spatial patterning. Neuron 27:513-523.

Armstrong-Gold CE, Rieke F (2003) Bandpass filtering at the rod to second-order cell synapse in salamander (Ambystoma tigrinum) retina. J Neurosci 23:3796-3806.

Balasubramanian V, Sterling P (2009) Receptive fields and functional architecture in the retina. J Physiol 587:2753-2767.

Barlow HB (1978) The efficiency of detecting changes of density in random dot patterns. Vision Res 18:637-650.

Benardete EA, Kaplan E (1999) Dynamics of primate P retinal ganglion cells: responses to chromatic and achromatic stimuli. J Physiol 519 Pt 3:775-790.

Bloomfield SA, Dacheux RF (2001) Rod vision: pathways and processing in the mammalian retina. Prog Retin Eye Res 20:351-384.

Bohnsack DL, Diller LC, Yeh T, Jenness JW, Troy JB (1997) Characteristics of the Sony Multiscan 17se Trinitron color graphic display. Spatial Vision 10:345--351.

Chander D, Chichilnisky EJ (2001) Adaptation to temporal contrast in primate and salamander retina. J Neurosci 21:9904-9916.

Chichilnisky EJ (2001) A simple white noise analysis of neuronal light responses. Network 12:199--213.

Chichilnisky EJ, Kalmar RS (2002) Functional asymmetries in ON and OFF ganglion cells of primate retina. J Neurosci 22:2737--2747.

Cohn TE (1974) A new hypothesis to explain why the increment threshold exceeds the decrement threshold. Vision Res 14:1277--1279.

Cover TM, Thomas JA (2006) Elements of information theory. New York: Wiley.

Croner LJ, Kaplan E (1995) Receptive fields of P and M ganglion cells across the primate retina. Vision Res 35:7--24.

Dedek K, Pandarinath C, Alam NM, Wellershaus K, Schubert T, Willecke K, Prusky GT, Weiler R, Nirenberg S (2008) Ganglion cell adaptability: does the coupling of horizontal cells play a role? PLoS ONE 3:e1714.

Demb JB, Zaghloul K, Haarsma L, Sterling P (2001) Bipolar cells contribute to nonlinear spatial summation in the brisk-transient (Y) ganglion cell in mammalian retina. J Neurosci 21:7447-7454.

DeVries SH, Baylor DA (1997) Mosaic arrangement of ganglion cell receptive fields in rabbit retina. J Neurophysiol 78:2048-2060.

Eggers ED, McCall MA, Lukasiewicz PD (2007) Presynaptic inhibition differentially shapes transmission in distinct circuits in the mouse retina. J Physiol 582:569-582.

Enroth-Cugell C, Robson JG (1966) The contrast sensitivity of retinal ganglion cells of the cat. J Physiol 187:517--552.

Geisler WS (1989) Ideal observer theory in psychophysics and physiology. Physica Scripta 39:153--160.

Hand DJ (1981) Discrimination and classification. Chichester, UK: Wiley.

Hirsch JA (2003) Synaptic physiology and receptive field structure in the early visual pathway of the cat. Cereb Cortex 13:63-69.

Hornstein EP, Pope DR, Cohn TE (1999) Noise and its effects on photoreceptor temporal contrast sensitivity at low light levels. J Opt Soc Am A Opt Image Sci Vis 16:705--717.

Keat J, Reinagel P, Reid RC, Meister M (2001) Predicting every spike: a model for the responses of visual neurons. Neuron 30:803--817.

Kim KJ, Rieke F (2001) Temporal contrast adaptation in the input and output signals of salamander retinal ganglion cells. J Neurosci 21:287--299.

Kolb H, Famiglietti EV (1974) Rod and cone pathways in the inner plexiform layer of cat retina. In: Science, pp 47-49.

Kremers J, Lee BB, Pokorny J, Smith VC (1993) Responses of macaque ganglion cells and human observers to compound periodic waveforms. Vision Res 33:1997--2011.

Latham PE, Nirenberg S (2005) Synergy, redundancy, and independence in population codes, revisited. J Neurosci 25:5195--5206.

Lyubarsky AL, Daniele LL, Pugh ENJ (2004) From candelas to photoisomerizations in the mouse eye by rhodopsin bleaching in situ

and the light-rearing dependence of the major components of the mouse ERG. Vision Res 44:3235--3251.

Lyubarsky AL, Falsini B, Pennesi ME, Valentini P, Pugh ENJ (1999) UV- and midwave-sensitive cone-driven retinal responses of the mouse: a possible phenotype for coexpression of cone photopigments. J Neurosci 19:442--455.

Mitra P, Bokil H (2007) Observed brain dynamics. New York, NY: Oxford University Press.

Molnar A, Werblin F (2007) Inhibitory feedback shapes bipolar cell responses in the rabbit retina. J Neurophysiol 98:3423-3435.

Murphy GJ, Rieke F (2006) Network variability limits stimulus-evoked spike timing precision in retinal ganglion cells. Neuron 52:511-524.

Murphy GJ, Rieke F (2008) Signals and noise in an inhibitory interneuron diverge to control activity in nearby retinal ganglion cells. Nat Neurosci 11:318-326.

Nikonov SS, Kholodenko R, Lem J, Pugh ENJ (2006) Physiological features of the S- and M-cone photoreceptors of wild-type mice from single-cell recordings. J Gen Physiol 127:359--374.

Nirenberg S, Carcieri SM, Jacobs AL, Latham PE (2001) Retinal ganglion cells act largely as independent encoders. Nature 411:698--701.

Pang J-J, Gao F, Wu SM (2003) Light-evoked excitatory and inhibitory synaptic inputs to ON and OFF alpha ganglion cells in the mouse retina. J Neurosci 23:6063--6073.

Purpura K, Tranchina D, Kaplan E, Shapley RM (1990) Light adaptation in the primate retina: analysis of changes in gain and dynamics of monkey retinal ganglion cells. Vis Neurosci 4:75--93.

Sagdullaev BT, McCall MA (2005) Stimulus size and intensity alter fundamental receptive-field properties of mouse retinal ganglion cells in vivo. Vis Neurosci 22:649--659.

Sinclair JR, Jacobs AL, Nirenberg S (2004) Selective ablation of a class of amacrine cells alters spatial processing in the retina. J Neurosci 24:1459--1467.

Strettoi E, Raviola E, Dacheux RF (1992) Synaptic connections of the narrow-field, bistratified rod amacrine cell (AII) in the rabbit retina. In: J Comp Neurol, pp 152-168.

Thibos L, Levick W, Cohn T (1979) Receiver operating characteristic curves for Poisson signals. Biological Cybernetics 33:57--61.

Umino Y, Solessio E, Barlow RB (2008) Speed, spatial, and temporal tuning of rod and cone vision in mouse. J Neurosci 28:189--98.

Volgyi B, Deans MR, Paul DL, Bloomfield SA (2004) Convergence and segregation of the multiple rod pathways in mammalian retina. J Neurosci 24:11182--11192.

Wark B, Fairhall A, Rieke F (2009) Timescales of inference in visual adaptation. Neuron 61:750--761.

Wassle H (2004) Parallel processing in the mammalian retina. Nat Rev Neurosci 5:747--757.

Yang XL, Wu SM (1997) Response sensitivity and voltage gain of the rod- and cone-bipolar cell synapses in dark-adapted tiger salamander retina. J Neurophysiol 78:2662-2673.

Zaghloul KA, Boahen K, Demb JB (2003) Different circuits for ON and OFF retinal ganglion cells cause different contrast sensitivities. J Neurosci 23:2645-2654.